ANALYSIS OF THE BIOMARKERS DETECTABLE TITANIUM DIOXIDE NANOTUBES BASED SENSING PLATFORMS

by

Younghwan Kim

A thesis submitted to the faculty of
The University of Utah
in partial fulfillment of the requirements for the degree of

Master of Science

Department of Metallurgical Engineering

University of Utah

December 2013

The University of Utah Graduate School

STATEMENT OF THESIS APPROVAL

The thesis of **Younghwan Kim**

has been approved by the following supervisory committee members:

Manoranjan Misra	, Chair	**07/18/2013** Date Approved
Swomitra K. Mohanty	, Member	**07/18/2013** Date Approved
Raj K. Rajamani	, Member	**07/18/2013** Date Approved

and by **Manoranjan Misra** , Chair of

the Department of **Metallurgical Engineering**

and by David B. Kieda, Dean of The Graduate School.

ABSTRACT

Titanium dioxide nanotubes (TiO_2-NTs) is such an attractive material because of photocatalysis, semiconductivity, biocompatibility, self-organization, and extremely large surface area. This thesis introduces several structural characteristics of TiO_2-NTs synthesized by the electrochemical method. Although the research of biosensing platform using TiO_2-NTs is not studied well, two types of biosensing platform systems will be discussed. At first, Tuberculosis (TB) detectable volatile biomarkers sensing platform using exhaled breath is studied. TB is easily cured at initial stage, thus the early diagnosis is a key point of fighting against TB. Breath analysis method is easier, faster, and cheaper while recent diagnosis methods require complicated conditions. Cobalt is functionalized on the nanotubes surface to detect the biomarker molecules in breath. The other application is the glutathione molecule detectable sensing platform. Glutathione protein is the scavenger of reactive oxygen species (ROS) which causes several diseases. The ratio of concentration of oxidized form and reduced form of glutathione molecules is served as a sign of the oxidative stress in body. Copper is loaded on the TiO_2-NTs in order to hold glutathione molecules in liquid. From these experiments, the metal functionalized TiO_2-NTs sensing platforms successfully detect their target biomarkers at vapor based and liquid based systems.

TABLE OF CONTENTS

LIST OF TABLES

ACKNOWLEDGMENTS

I would like to express my appreciation to my supervisor, Professor M. Misra, whose expertise, understanding, and patience added considerably to my graduate experience. Also I would like to thank Professor S. Mohanty for their expert advice and instructions. I appreciate their vast knowledge and skill in many areas and their assistance in writing my publications in addition to this thesis.

I appreciate Professor K. S. Raja for his technical advice.

My special thanks to Professor H. Sohn, Professor M. S. Moats, Professor M. Free, and Professor S. Guruswami for their academic guidance.

Last, I am grateful to my parents and sister for the constant support they provided to me from the opposite side of the earth.

CHAPTER 1

SYNTHESIS AND ANALYSIS OF TITANIUM DIOXIDE NANOSTRUCTURES

1.1 Introduction

Nanotube became one of the most studied nanomaterials after Iijima reported on the carbon nanotube in 1991.[1] Fullerene and graphene are other types of carbon nanomaterials that have special characteristics of: strength, flexibility, conductivity, elasticity, and so on. The discovery of these nanomaterials inspired the research of nanotechnology. Nowadays, this nanotechnology stimulates the development of related academic fields, biology, chemistry, physics, and other engineering fields to harmonize and synchronize together in order to produce improved new research areas.

These carbon-based nanomolecules (nanorods, nanowires, and nanotubes) have the ability of high efficient electron transport and excitation. While the carbon nanotube is studied for various purposes, it has been triggered to look for other materials, for other nanostructures having similar properties as carbon nanotubes. Therefore, other materials (silica, cobalt, copper, alumina, titania, etc.) have been found and studied as noncarbon nanomaterials.

Titanium, among these materials, has superior optical, thermal, mechanical,

electrical properties, and biological nontoxicity. Also, it can be used as basic building blocks for nanotechnology such as biosensors, chemical sensors, gas sensors, solar cell, and drug delivery.[2] Thus, titanium dioxide (TiO_2) is an attractive noncarbon nanostructure among many transition metal oxides.

The research of TiO_2 has been accelerated after the findings of Fujishima and Honda. TiO_2 shows interesting properties of excellent biocompatibility, semiconductivity with 3.2 eV of wide band gap, electrical resistance, high chemical stability, and high electron drift mobility.[3] In addition, it has the special characteristics of self-cleaning, super-hydrophilicity, self-sterilization, self-deodorizaion, hydrogen generation, low temperature sensitivity, and easiness of manipulation.

TiO_2 nanotubes structure (TiO_2-NTs) became one of the biggest research fields because of its numerous potential applications. There are several methods of titanium nanostructure synthesis: hydrothermal synthesis methods,[4] electrospinning method,[5] solvothermal process in organic solvent,[6, 7] hydrothermal method using NaOH,[8] KOH method,[9] and direct heating method.[10] These TiO_2 nanomaterials are applied to scientific research, industries, cosmetics, biomedicines, and sensors. Especially, the applications related with biotechnology have the benefit of biocompatibility. For example, TiO_2 is used for dental or bone materials[11, 12] or biosensors.[13-15] The synthesis of TiO_2-NTs using electrochemical method will be introduced in Chapter 2. Nanograss and nanolace will be discussed together.

Glucose sensor is one of the famous biosensors. This sensor detects the amount of glucose in blood and indicates the increase or decrease of sugar content in blood

quickly. This kind of sensor is easily operated by non-expert people at home whenever they want to test themselves and is called point-of-care (POC) kit.

The importance of biosensors has increased and diverse types of POC diagnosis kits are invented and produced for the general population and also specialized workers in limited and critical situations. For example, airplane pilots or astronauts work in limited circumstances, and the change of their vital signs are directly related to their life safety. In these cases, the real-time indication of their health status is highly important and required. Thus, specific biosensors for individuals in high risk environments can prevent unexpected and unwanted accidents.

Biosensors can detect specific target molecules from humans or animals. The main targets of biosensor are DNA fragments,[16] proteins,[17] or specific chemicals like glucose. The target molecules usually indicate any signal of diseases. Disease is the other name of the uncontrolled situation of biomechanism caused by infection, contamination, malfunction of cell cycle, loss of immune system, and other unexpected causes. When people get disease, specific enzymes are usually over produced against the diseases in order to control the situation. Therefore, the changed quantity of specific enzymes (proteins) becomes the signal of diseases. These enzymes flow to the destination organs through blood and limp fluid. So, these biomarker samples can be obtained from urine, saliva, and blood. Also, DNA and RNA are the precursors of proteins and they are also kinds of biomarkers even though their detection is difficult.

Pathogen infection is one of the causes of diseases, take for example, cholera, Tuberculosis, septicemia, typhoid fever, Lyme disease, diphtheria, and pertussis. These diseases are diagnosed by detection of increased enzymes, as explained previously. It is

also analyzed by detection of specific molecules released from pathogens. Tuberculosis (TB) occurs by the pathogen named *Mycobacteria tuberculosis*. Pathogens have their own molecule-exchange systems through membrane to environment. Thus, the unique molecules released from TB pathogen are the biomarkers of TB disease. TB pathogen usually infects the lung at first. In the lung, therefore, specific volatile organic molecules are released from *M. tuberculosis* pathogens and mixed with the breath of patients. The volatile molecules are called volatile organic compounds (VOCs), or volatile biomarkers. The exhaled breath (gas) is the sample containing biomarkers, in this case. This is a good example of easy sampling, instead of drawing blood. This kind of breath analysis is not studied well so far since it is quite new. Chapter 3 will discuss the development of the TB pathogen detection system using volatile biomarkers TiO_2-NTs.

The human body and most all living things want to keep their metabolism in stable status, in other words, safe status. This characteristic of living things is generally called homeostasis. When some molecules are overproduced by disease and it breaks the homeostasis, special mechanisms begin to return it to stable. Oxidative stress is one of the reasons for the breakdown of homeostasis. The oxidative stress is caused by, among many factors, severe muscular exercise without rest, chemicals from smoke, side effects from diabetes, contaminations, hypoxia, and ingestion of burnt foods. These factors trigger the overproduction of the reactive oxygen species (ROS) which is originally a necessary molecule for stable metabolism in the body. The excess amount of ROS also causes other diseases to occur. Glutathione is an organic molecule and it can remove the excess ROS. Glutathione is not a volatile molecule but it is dissolved in fluid such as saliva. Thus, the level of glutathione molecules in body fluid is considered an alarm of

oxidative stress. The study for detection of glutathione molecule using TiO_2-NTs is introduced in Chapter 4.

CHAPTER 2

EXPERIMENTAL SETUP FOR TITANIUM DIOXIDE NANOTUBES SYNTHESIS

2.1 Mechanism of tube growth

There are mainly three types of TiO_2 in nature: anatase, rutile, and brookite. It also has been reported that five more types of TiO_2 are synthesized from specific conditions such as temperature and pressure: TiO_2-B, TiO_2-R, TiO_2-H, TiO_2-II, and TiO_2-III.[18, 19] Anatase and rutile are the most common phases even though the stability of anatase is arguable.[19-21] The various methods of TiO_2 nanotubes (TiO_2-NTs) synthesis are manufactured such as electrochemical anodization method, sol-gel method, and high temperature solvothermal synthesis method.[22]

Among them, the fluoride containing ethylene glycol (EG) electrolyte anodization method is applied for this thesis research because of its convenience. TiO_2-NTs anodization is affected by many experimental conditions such as temperature, applied voltage, anodization time, water concentration in electrolyte, and mechanical shearing. TiO_2-NTs anodization using EG and sodium fluoride show high strength, regularity, and homogeneity of TiO_2-NTs.[23, 24]

The electrolyte anodization method is usually performed using platinum as

cathode electrode and titanium foil as anode electrode (Figure 2-1). The solution is continuously stirred with 90 rpm using a magnetic bar. Cathode and anode electrodes are dipped in electrolyte connected to a power supply. Platinum is commonly used as the cathode because of its superior conductivity.

Self-organized TiO_2-NTs arrays are generated through several steps of anodization process.[19] The initial step of titanium dioxide anodization process without fluoride reaction begins like below:

$$2H_2O \rightarrow O_2 + 4e^- + 4H^+ \quad (1)$$

$$Ti \rightarrow Ti^{4+} + 4e^- \quad (2)$$

$$Ti + 2H_2O \rightarrow TiO_2 + 4H + 4e^- \quad (3)$$

$$Ti^{4+} + 4H_2O \rightarrow Ti(OH)_4 + 4H^+ \quad (4)$$

$$Ti(OH)_4 \rightarrow TiO_2 + 2H_2O \quad (5)$$

The next step is pit formation on the titanium dioxide layer. Fluoride (F^-) in electrolyte binds to Ti^{4+} from Ti metal to make a soluble $[TiF_6]^{2-}$ species from the pits. These dimple structures on the TiO_2 layer are expanded over all the Ti metal surface and are the initial point of the nanotube. The overall reaction is like:

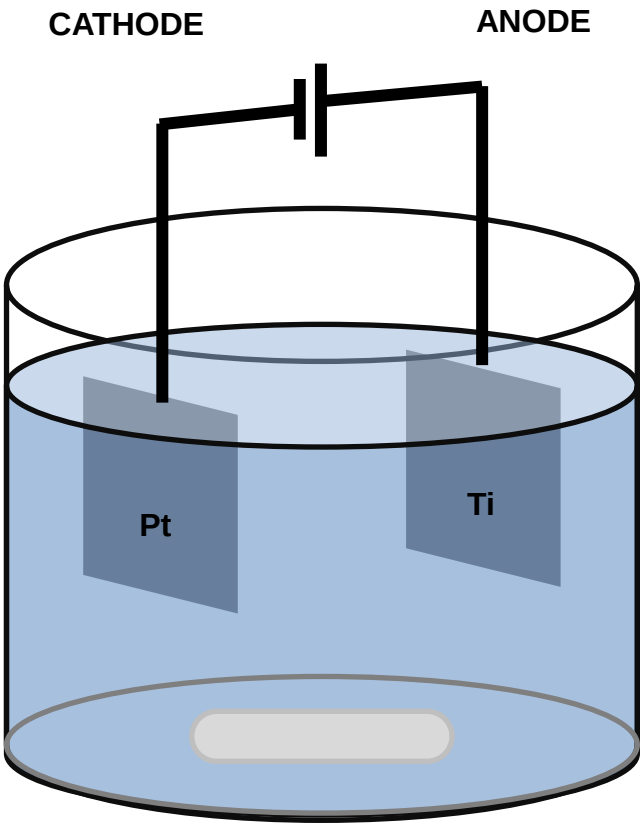

Figure 2-1. Conceptual image of electrolyte anodization method.

$$Ti^{4+} + 6F^{-} \rightarrow [TiF_6]^{2-} \quad (6)$$

$$TiO_2 + 6F^{-} \rightarrow [TiF_6]^{2-} + 2H_2O \quad (7)$$

The fluorides form water soluble $[TiF_6]^{2-}$ species during anodization, and the amount of $[TiF_6]^{2-}$ is decided by the rate of nanotube synthesis.[25] After the initiation phase, the tubes elongate until the etching action at the tube top area by fluoride has occurred.[26] The main functions of fluorides are: 1) maintaining a thinner bottom oxide layer by etching and 2) controlling the solvatization of Ti^{4+} ions.[27] Also, the fluoride competes with O^{2-} migration to the bottom of TiO_2. Since the rate of migration of fluoride is faster than O^{2-}, a fluoride-rich layer is made at the TiO_2 interface.[28]

Figure 2-2 shows the steps of nanotube generation. A) Ti^{4+} ions are solvated in the electrolyte and it is continuously dissolved, corroded, or electropolished. B) A compact oxide (TiO_2) layer is generated on the metal surface. C), D) The porous TiO_2 is growing under specific electrolyte conditions. The shape of porous TiO_2 is changed by modified electrolyte conditions. E) The metal oxide porous expands its length and thickness using Ti^{4+} dissolved from the oxide layer.[19]

Figure 2-3 shows a simple concept of the structure of TiO_2-NT. The inner oxide shell grows as a V-shape because of the continuous fluoride etching. The outer oxide layer (OST) is relatively dense and thick with pure TiO_2, and the inner oxide layer (IST) is less dense with incorporated electrolyte components.

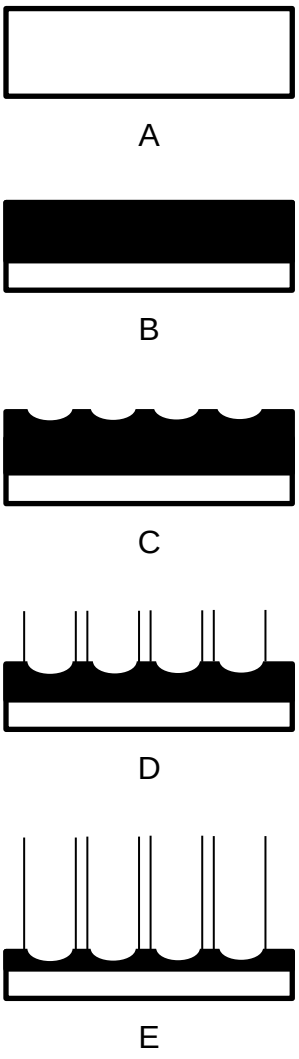

Figure 2-2. Conceptual image of titanium dioxide nanotubes growing. (A) Pure Ti foil, (B) Oxide layer generation, (C) Pit formation, and (D, E) Nanotube growth.

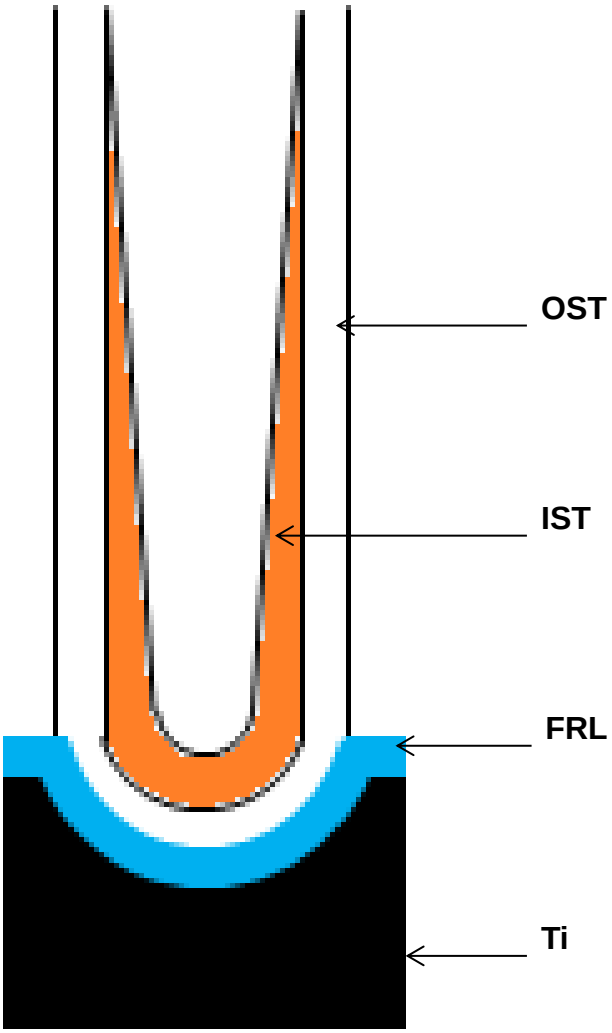

Figure 2-3. The conceptual image of a TiO_2-NT anodized in organic electrolyte. IST: inner oxide shell, OST: outer oxide shell, FRL: fluoride-rich layer, and Ti: titanium.

2.2 Anodization of TiO_2-NTs

In this thesis research, most of anodization is done using 30 volts DC for 1h with cathode and anode connections (Figure 2-1). Electrolyte is composed of 0.5 w/v% of sodium fluoride in 3 wt% water and filled up with EG. Electrolyte is mixed for 3 h on a stirring plate and an additional 2 h in ultrasonic bath. Ti foil is cut as 10 mm × 10 mm and polished using sand paper. Then samples are rinsed with 1:1 mixture of isopropanol and acetone solution by ultrasonication for 10 minutes. After anodization, samples are rinsed by ultrasonication in DI water for 3-5 seconds to remove all EG and then dried up in 110° C chamber for at least 1 day. Overall set up is shown in Figure 2-4.

2.3 Annealing of TiO_2-NTs

The as-anodized sample has an amorphous structure. Therefore annealing under O_2-rich circumstance is required for anatase crystallization.[19, 23, 29] The annealing process is done using a gas tube furnace at 500 ° C for 2 h with 1.5 ° C/m as ramp rate. Gas directly flows from an oxygen gas tank into a tube furnace and is then exhaled into the fume hood (Figure 2-5).

2.4 SEM analysis of TiO_2-NTs structure

The scanning electron microscope (SEM) images of TiO_2-NTs are shown in Figure 2-6. The surface of the nanotube sample is scratched to break the nanotube structure and to be able to observe inside the nanotubes. In Figure 2-6, A is the top view with different levels of depth of nanotubes shown in (1), (2) and (3). The double wall structure of the nanotube is observed at the lower part and is a lateral view (Figure 2-6,

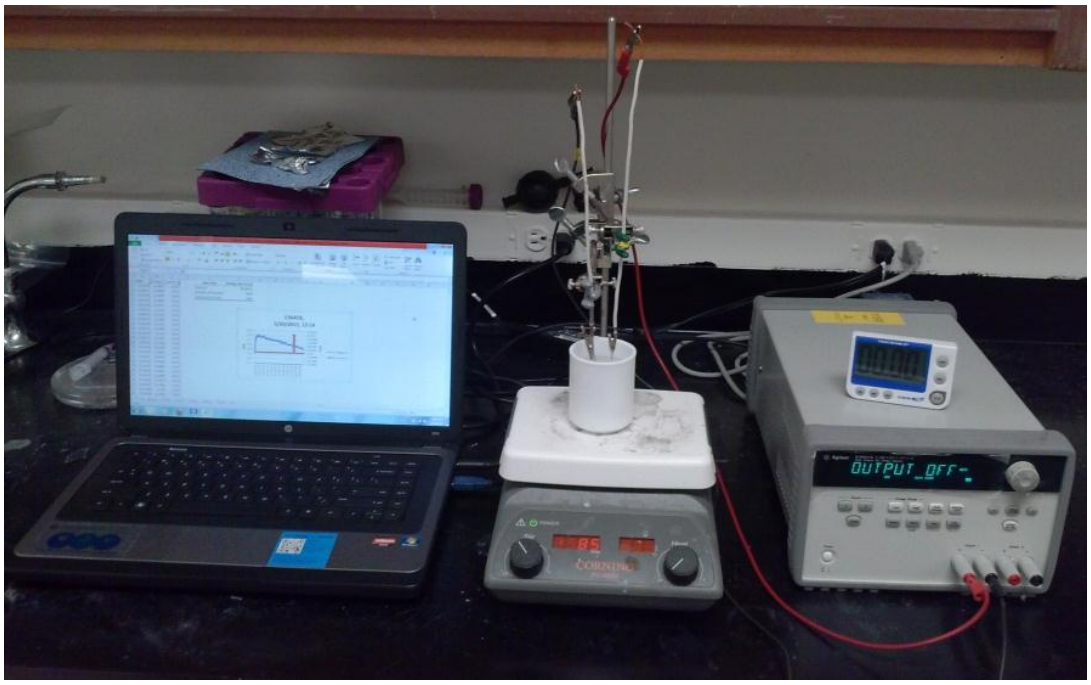

Figure 2-4. Overall setup of anodization system of I/O measurement system computer (left), anodization setting with cathode and anode (middle), and DC power supply (right).

Figure 2-5. Gas furnace system setup. Nitrogen gas flows in from left and flows out to right.

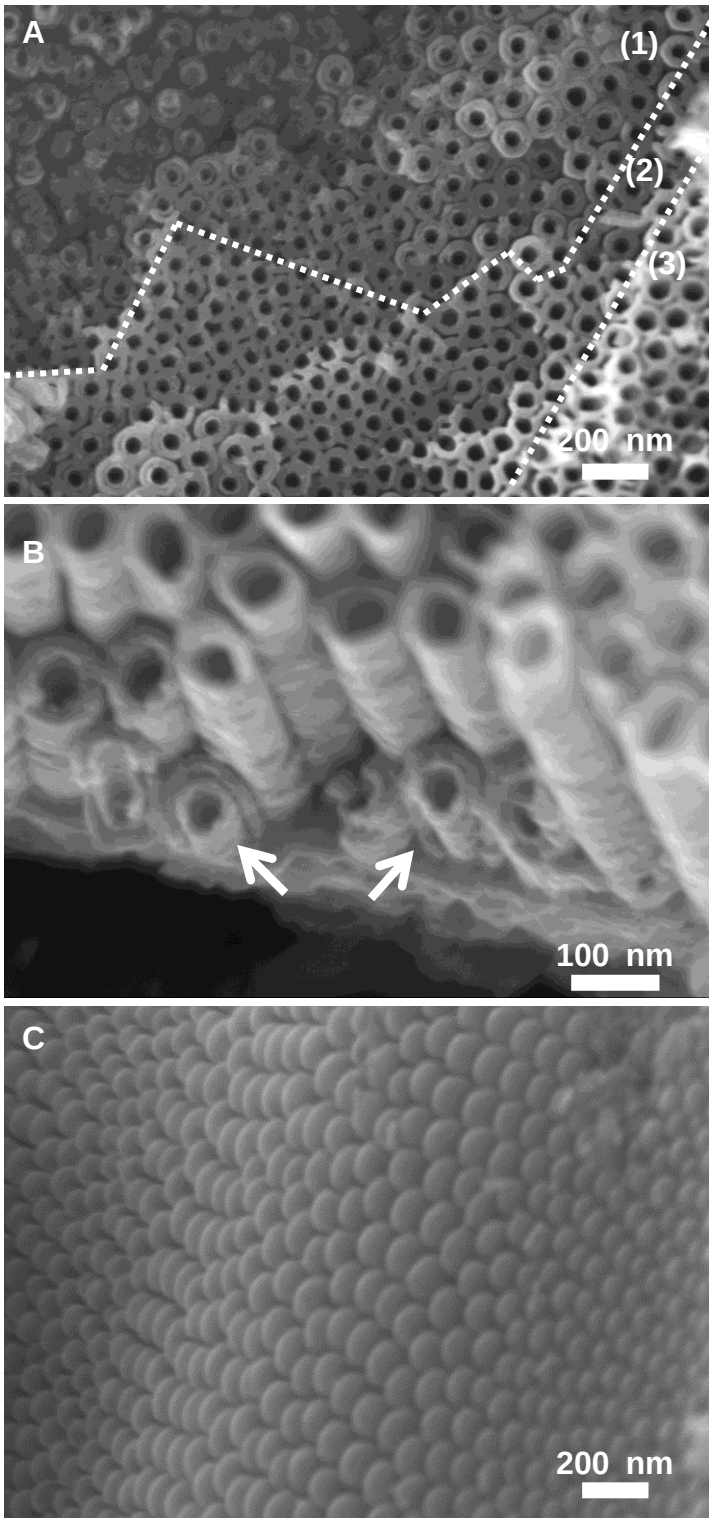

Figure 2-6. The scanning electron microscope (SEM) images of TiO_2-NTs. (A), (1): lower part, (2): middle part, (3): upper part of nanotubes. (B), double layer of nanotubes at arrows. (C), FRL layer at bottom of the nanotubes.

B). The well-organized fluoride rich layer (FRL) at the bottom of the tube is also shown in Figure 2-6, C.

2.5 Variable structures of TiO_2-NTs growth by conditions

The solution-based anodization method is greatly affected by conditions such as time, temperature, water concentration in electrolyte, and applied potential.[11, 16] The relationship between the shape of a nanotube and anodization conditions are observed and organized in Figure 2-7. The length of TiO_2-NTs is decided by the potential for anodization and the concentration of ethylene glycol electrolyte. Two variables of anodization are tested: applied voltage (30 V, 40 V, and 50 V) and EG concentration (90 wt%, 95 wt%, and 97 wt%). Lower EG concentration and higher potential make for larger diameter nanotubes. The averaged diameter at each condition is shown in Table 2-1.

The distribution of length of nanotube is observed at the same condition. Figure 2-8 shows a well-distributed pattern of the length of nanotubes that higher EG concentration and higher voltage make. The average length of each condition is shown in Table 2-2. The distribution of nanotube growth is tested using 1, 1.5, 2, 2.5, and 3 h anodization with constant 30 volts. The length is increased by time (Figure 2-9).

In addition, Figure 2-10 is the SEM image under 350,000 magnification with 7 kV of beam energy, which is good for surface observation. The thickness of wall is around 4-5 nm.

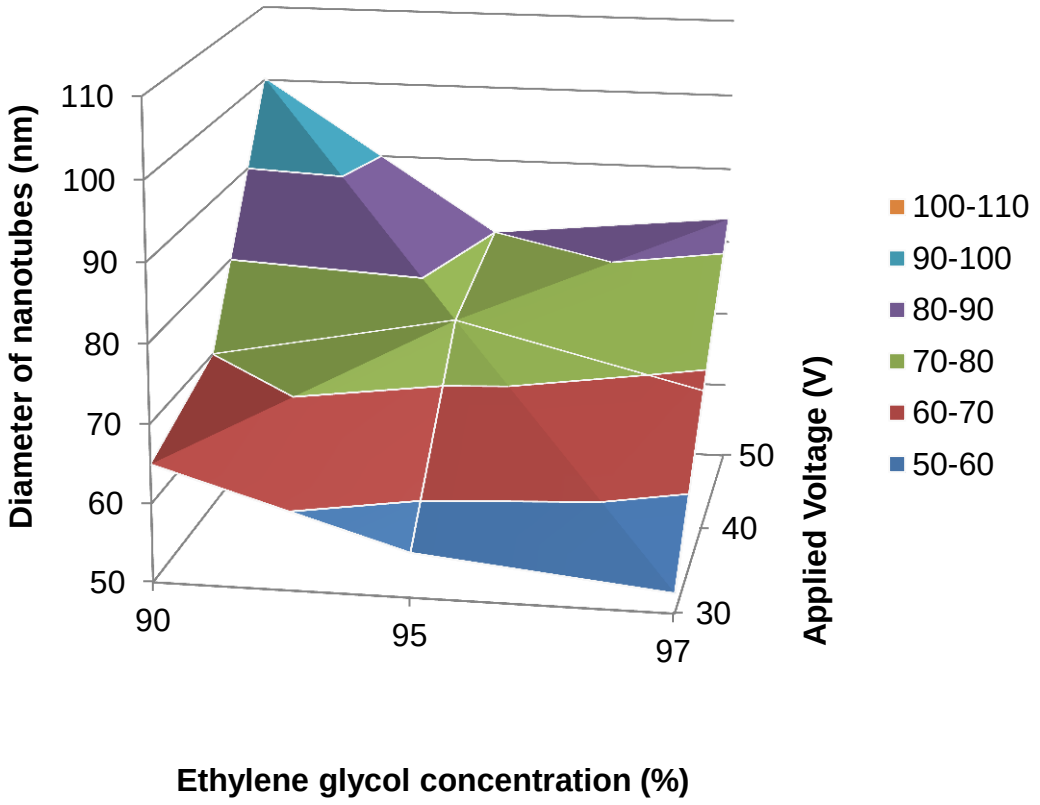

Figure 2-7. The pattern of diameter of nanotubes by anodization condition.

Table 2-1. The average diameter at each anodization condition.

	Diameters of nanotubes (nm)		
Volts / EG (%)	**30**	**40**	**50**
90	65.00	70.00	100.26
95	55.67	76.01	80.00
97	52.53	68.28	83.16

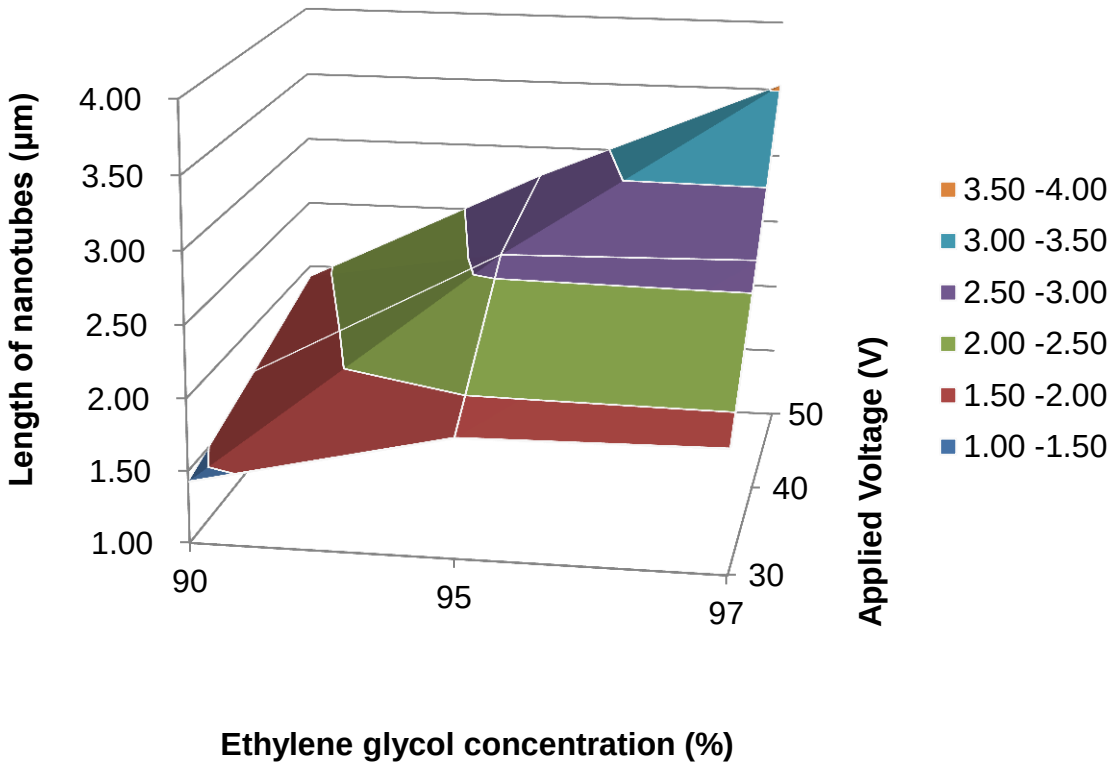

Figure 2-8. The pattern of length of nanotubes by anodization condition.

Table 2-2. The average length at each anodization condition.

	Lengths of nanotubes (um)		
Volts / EG (%)	**30**	**40**	**50**
90	1.43	1.83	1.86
95	1.67	2.61	2.65
97	1.92	2.78	3.53

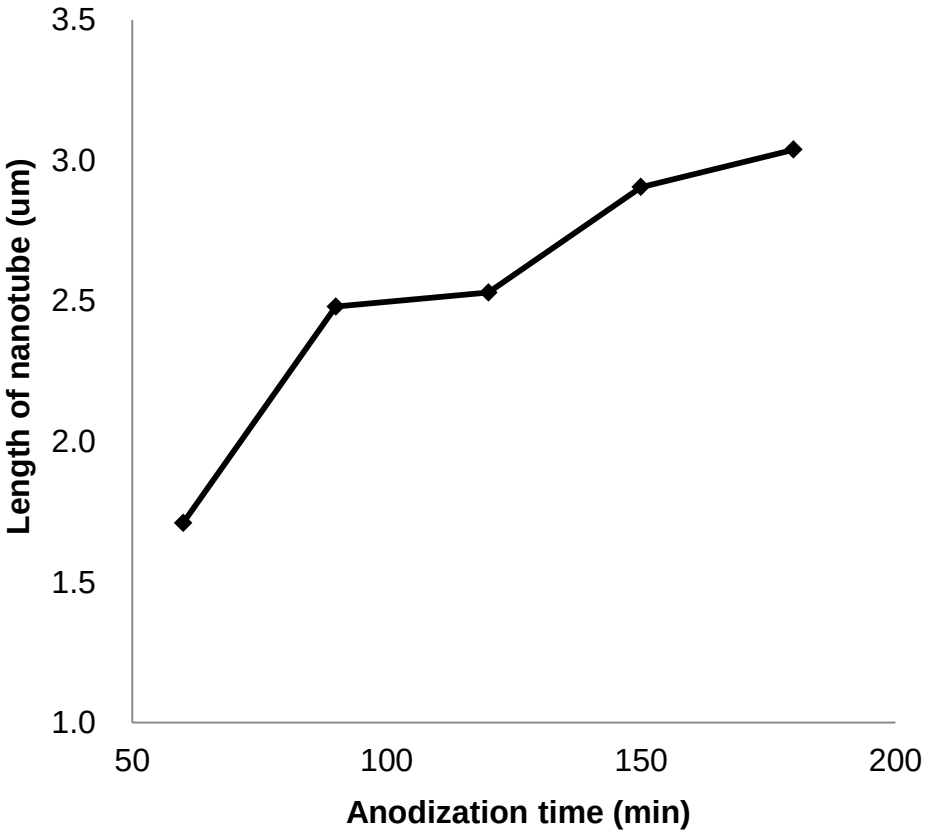

Figure 2-9. The pattern of nanotubes length depending on anodization time under 30 volts of applied potential and 25 ºC of electrolyte temperature.

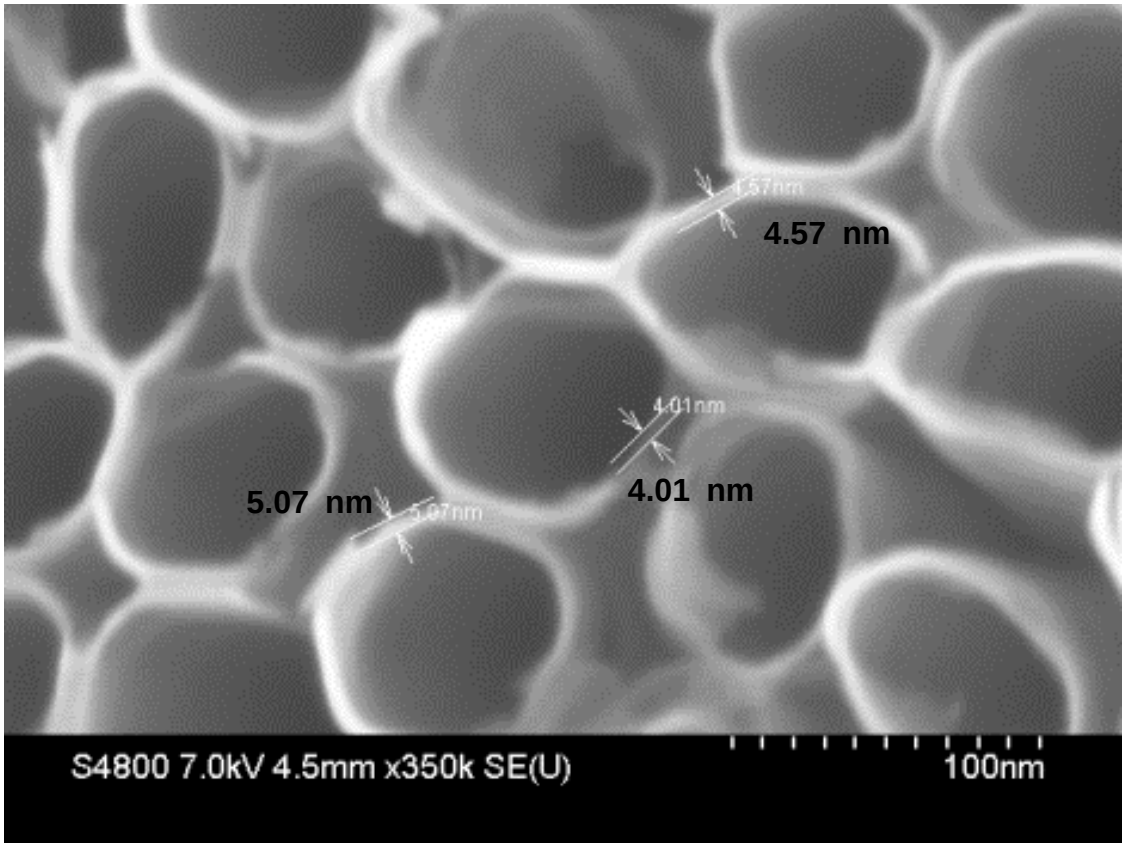

Figure 2-10. The thickness of wall (~4 nm) of individual nanotubes.

2.6 Corrosion of TiO_2-NTs by reused electrolyte

The anodization of TiO_2-NTs is composed via oxide layer formation step, pit formation step, and nanotube growth step. The current of each step during anodization is measured and plotted. Figure 2-11 shows the conceptual plot of current change during anodization of TiO_2-NTs. The current dramatically drops at the oxide layer formation in the initial step. Then a small hill appears on the plot when pit formation is beginning. Finally, a stabilized plot is shown for nanotube growth until the end of the reaction.

The anodization of TiO_2-NTs in used electrolyte shows a different pattern of current plot. This is thought to be a change in the electrolyte component. Therefore, one series of test is designed to discover what changed in the electrolyte component during repeated anodization. Basically, the 1000 ml of bulk electrolyte is composed with 0.5 g of sodium fluoride (NaF) dissolved in 30 ml water (H_2O) and 970 ml of ethylene glycol ($C_2H_6O_2$). A brand new 100 ml EG electrolyte is repeatedly used for 1 h anodization 13 times. All Ti foils for these tests are brand new samples (5 mm × 10 mm). Potential is constantly flowed as 30 volts during all experiments. The TiO_2-NTs samples from the 1^{st}-4^{th} experiments are not shown here because they are normal. From the 5^{th} sample (5 h reused), some corrosion is observed at the edge of the nanotube sample (Figure 2-12) and later samples have more corrosion.

Figure 2-13 shows the plot of current change during anodization for the 1^{st} (fresh electrolyte), 5^{th} and 13^{th} TiO_2-NTs samples. The pit formation hill appeared at the plot of the 1^{st} sample, but the plot for 5^{th} and 13^{th} do not have the pit formation peak. The plot for the 13^{th} sample especially has severe noise current for overall anodization with slower decrease at the beginning of the anodization process. The diameter and length of 13^{th}

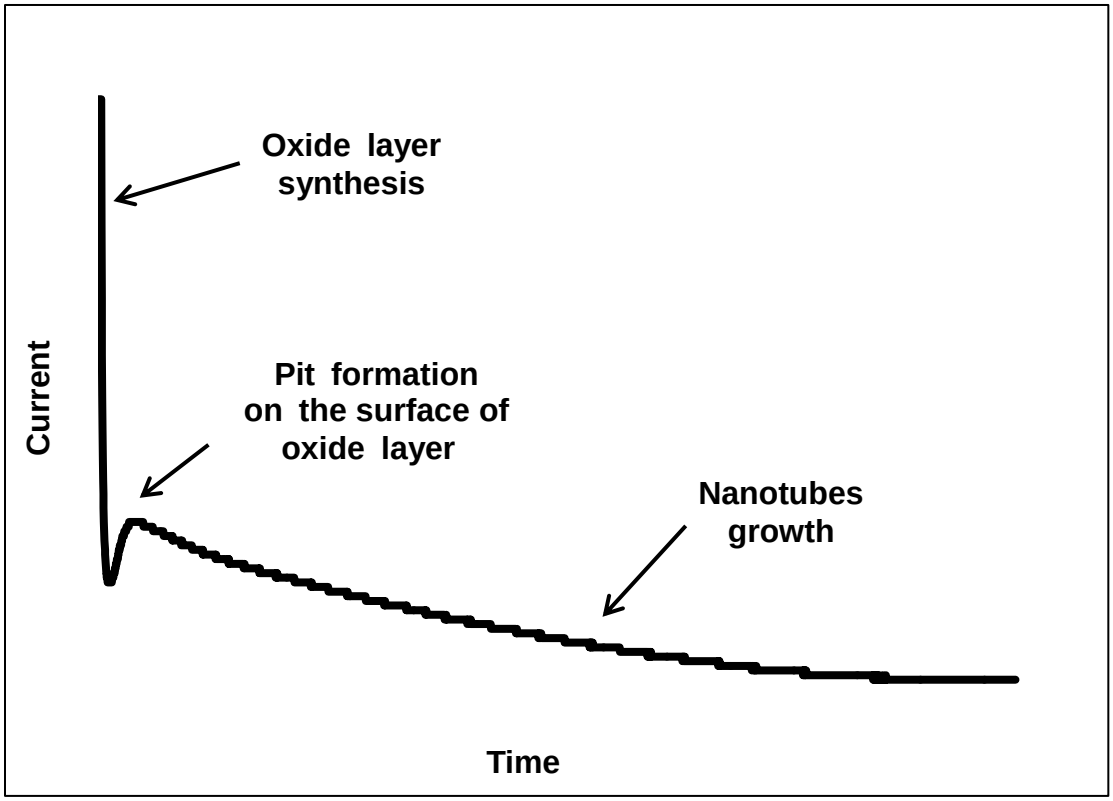

Figure 2-11. The current measurement of TiO_2-NTs sample during anodization under constant 30 volts.

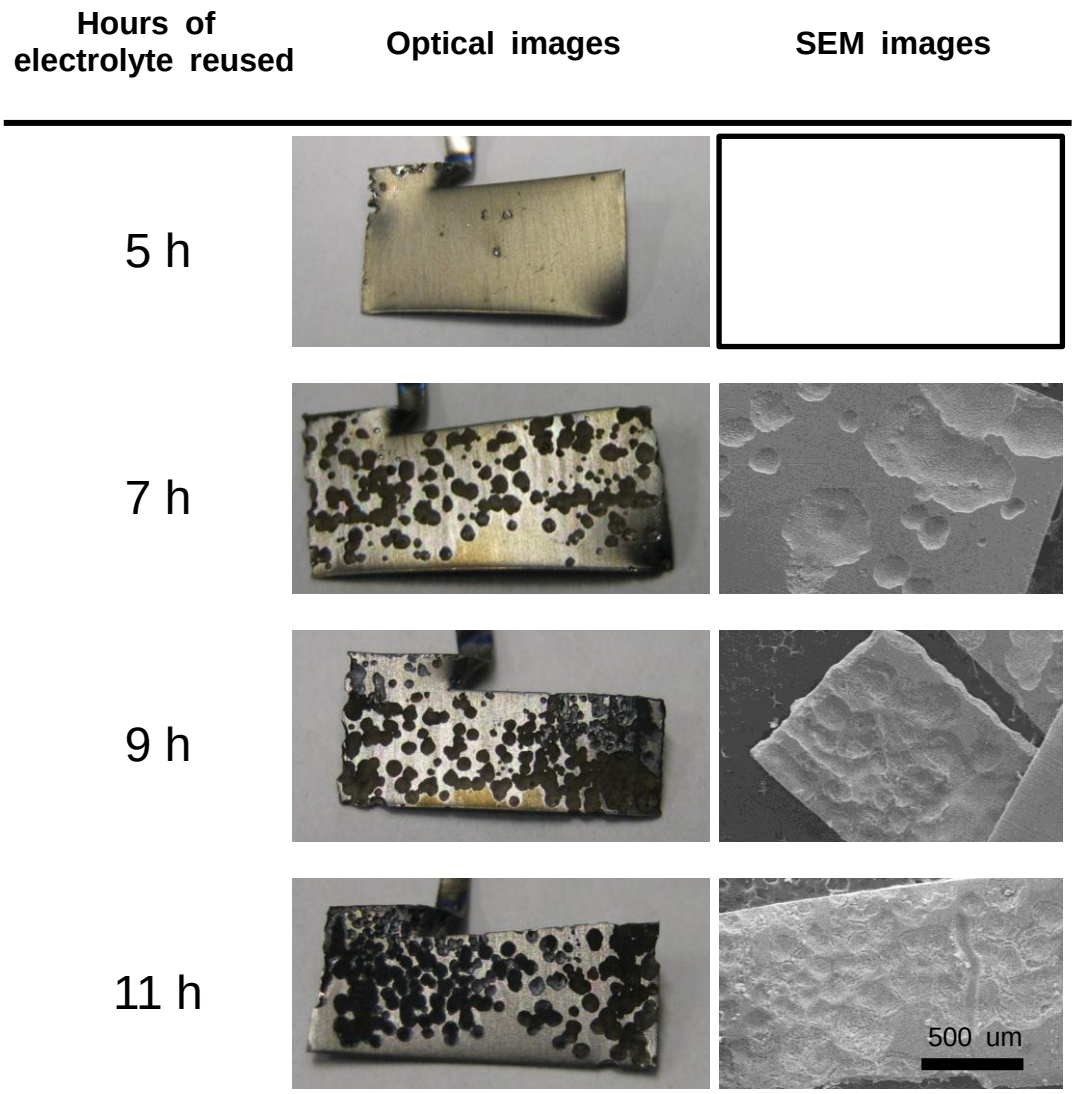

Figure 2-12. The optical images and SEM images from brand new TiO_2-NTs samples anodized for 5, 7, 9, and 11 h used electrolyte.

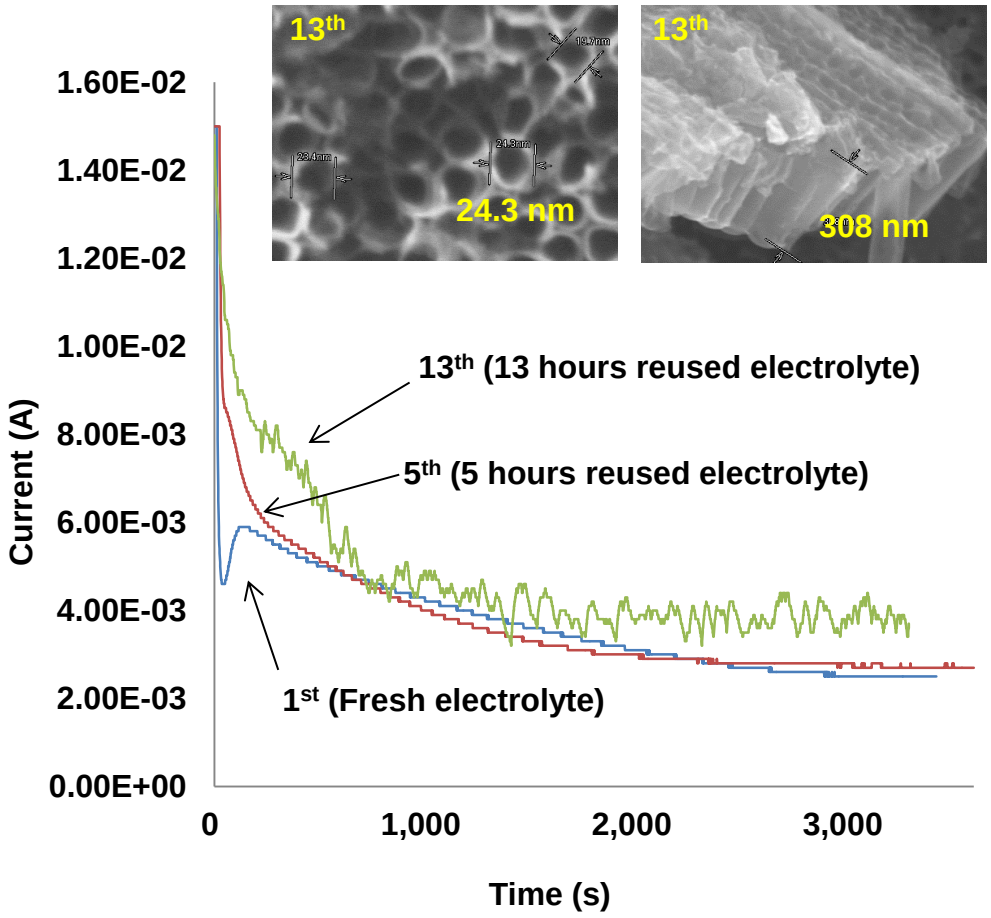

Figure 2-13. The current changes of the TiO_2-NTs anodization using brand new Ti foil from fresh EG electrolyte, 5 h reused electrolyte, and 13 h reused electrolyte.

sample are around 20 nm and 300-400 μm that is smaller than normal nanotube (Table 2-1).

The wt% of fluoride is decreased and pH is increased, although the wt% of carbon, titanium, and oxygen are constant (Figure 2-14 and 2-15). From these results, the corrosion of TiO_2-NTs is related with fluoride depleted by time. Still, it requires more research to clearly reveal the relationship of corrosion and pH, temperature, and other factors.

2.7 TiO_2-NTs nanograss

Nanograss is an unexpected structure on nanotubes that does have some beneficial applications.[30-33] The reasons for nanograss generation are thought to be the amount of water content, pH, temperature during anodization, and corrosive molecules such as fluoride. Nanograss covers the top surface of a nanotube layer, interrupts fluid flow to the inside of nanotubes, and disturbs the diffusion of small size molecules such as nano-level metal particles, small proteins, or large amino acids. Thus, nanograss free TiO_2-NTs anodization is required to prevent unexpected failure of nanotube's properties. But, many cases of TiO_2-NTs show nanograss. Therefore, it is necessary to know how to improve anodization conditions and eliminate nanograss.

2.7.1 Temperature effect

As discussed in section 2.6, the temperature of electrolyte was increased during 1 h anodization even though it was not measured. Thus, a simple test was performed using cooled EG electrolyte and warmed EG electrolyte. In the same anodization method,

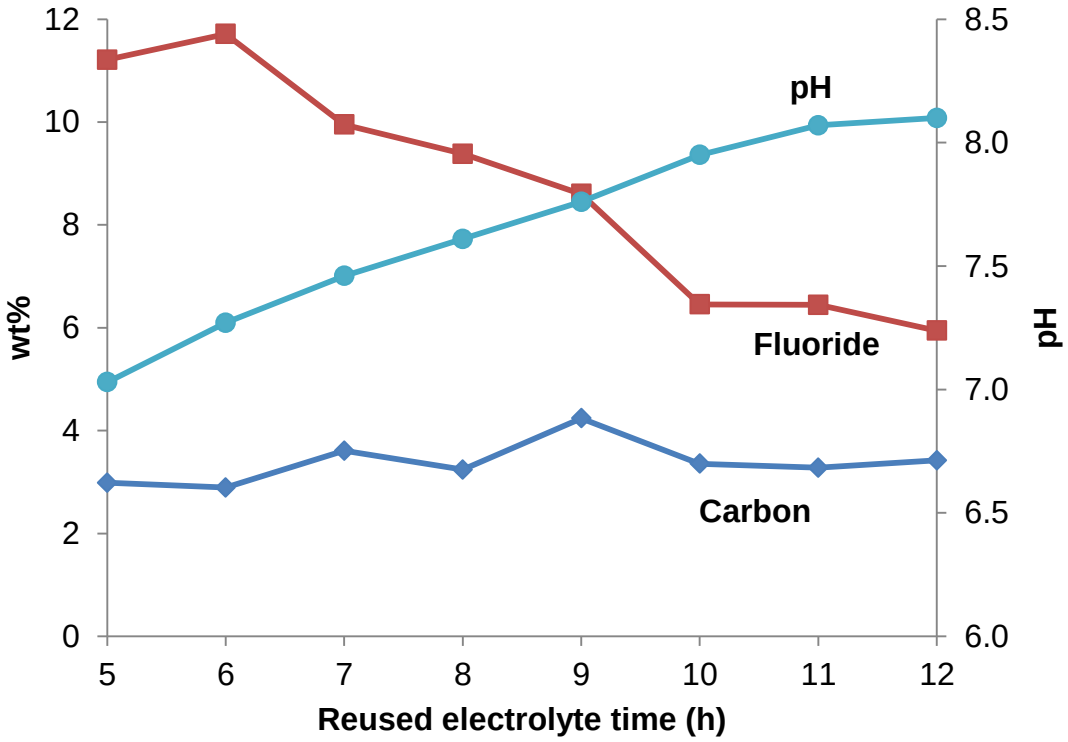

Figure 2-14. The plots of wt% of fluoride and carbon from TiO_2-NTs samples by EDX analysis, and pH change.

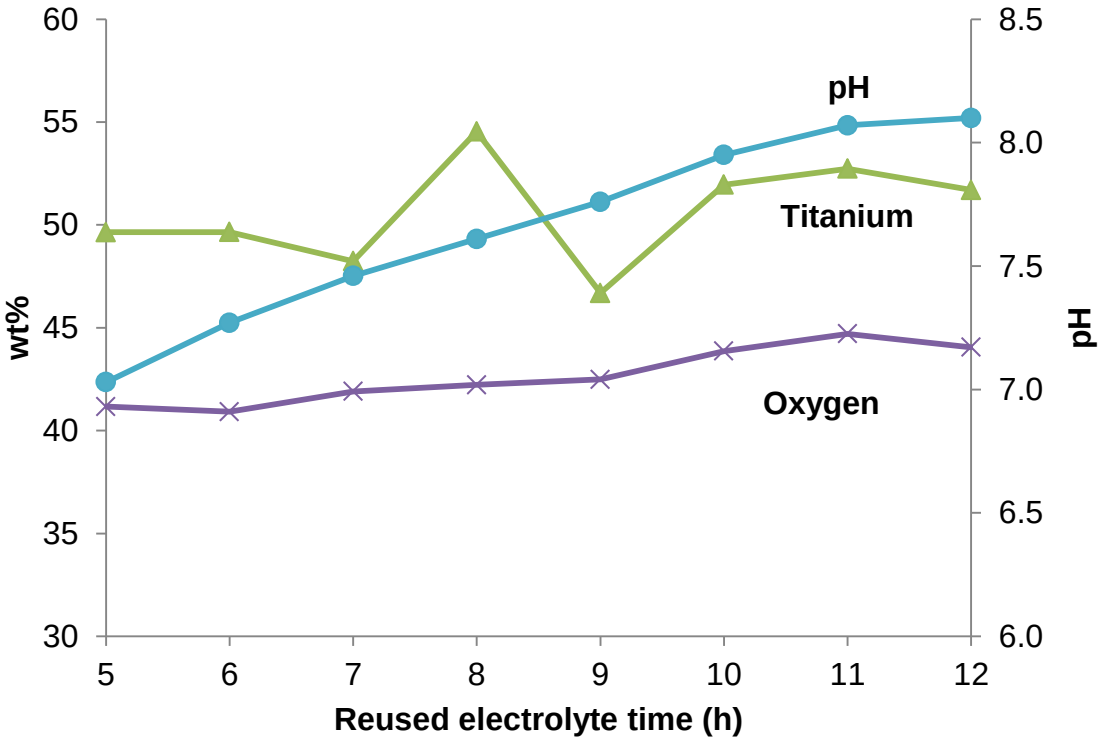

Figure 2-15. The plots of wt% of titanium and oxygen from TiO_2-NTs samples by EDX analysis, and pH change.

the same Ti foil was anodized at 30 volts for 1h with 90 rpm stirring. The SEM image shows small and fine white lines anodized in cold EG and shows longer and thicker white lines from warm EG at the same magnification (Figure 2-16).

More detail experiments were performed at 65 °, 40 °, 25 °, and 1 °C to compare the morphology of nanograss (Figure 2-17). As results, more nanograss was generated at higher temperature. Therefore, the nanotube growth was directly affected by temperature. It also implied that the chemical reactions for nanotube growth such as $[TiF_6]^{2-}$ generation or pit formation are faster at higher temperature. Thus, the etching process might be faster at higher temperature.

In addition, the anodization times are calculated for each temperature for 2 μm. For example, growth rate at 1 °C is 0.179 μm/h and it requires 11 h anodization for 2 μm length. Interestingly, the nanotubes anodized at lower temperature has the unexpected characteristic being of easily broken. The rate of nanotube growth is shown in Figure 2-18 as having 0.983 of R^2 value.

2.7.2 Nanograss morphology

Nanograss has quite a long length compared to its nanotube length. For example, one nanograss length is over 1 μm at 30 volts, and 1h of TiO_2-NTs anodization (Figure 2-19, left); and the average length of a nanotube is ~1.7 μm (Figure 2-9). The ratio of total length of one nanotube and its nanograss is almost 1:1, and this is arguable because the nanograss is considered the remnant of etching the nanotube. In here, however, it is suggested that the nanograss generation is not the etching of existing nanotube walls, but has its own growth mechanism.

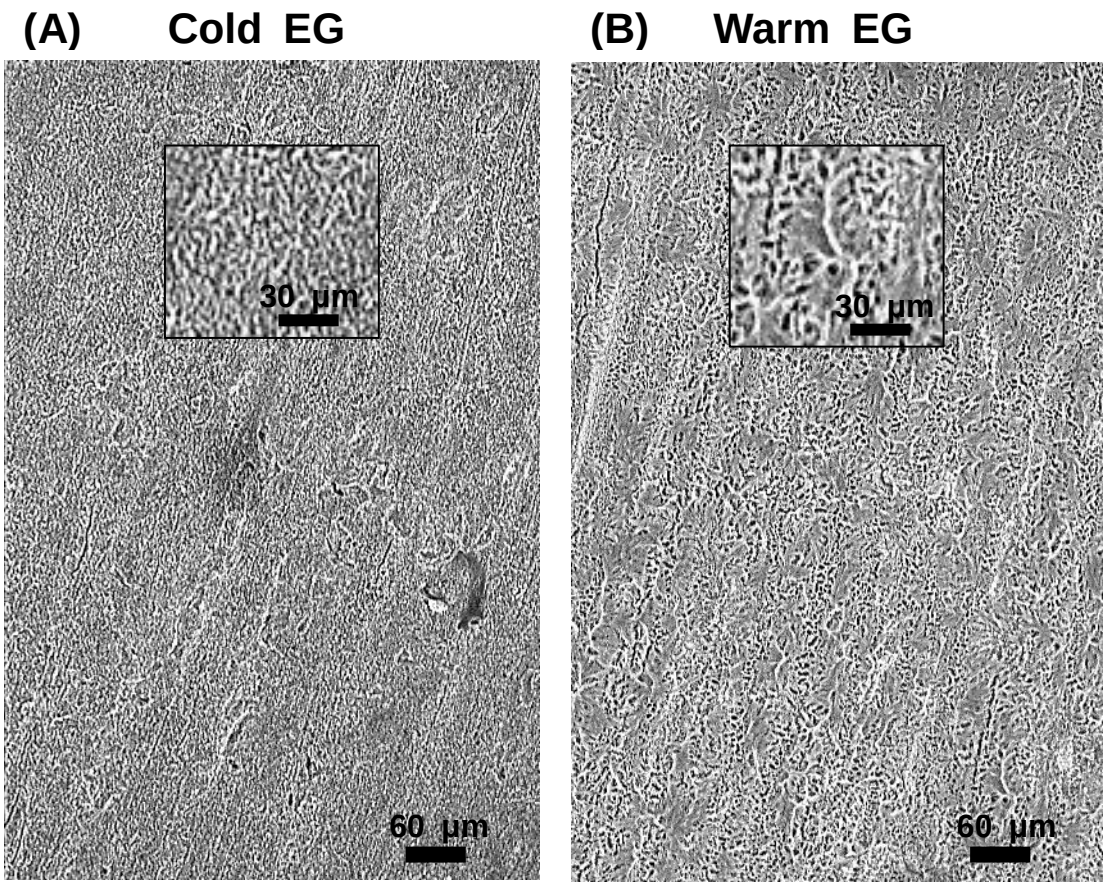

Figure 2-16. The comparison of TiO_2-NTs samples anodized in (A) cold EG electrolyte and (B) warm EG electrolyte.

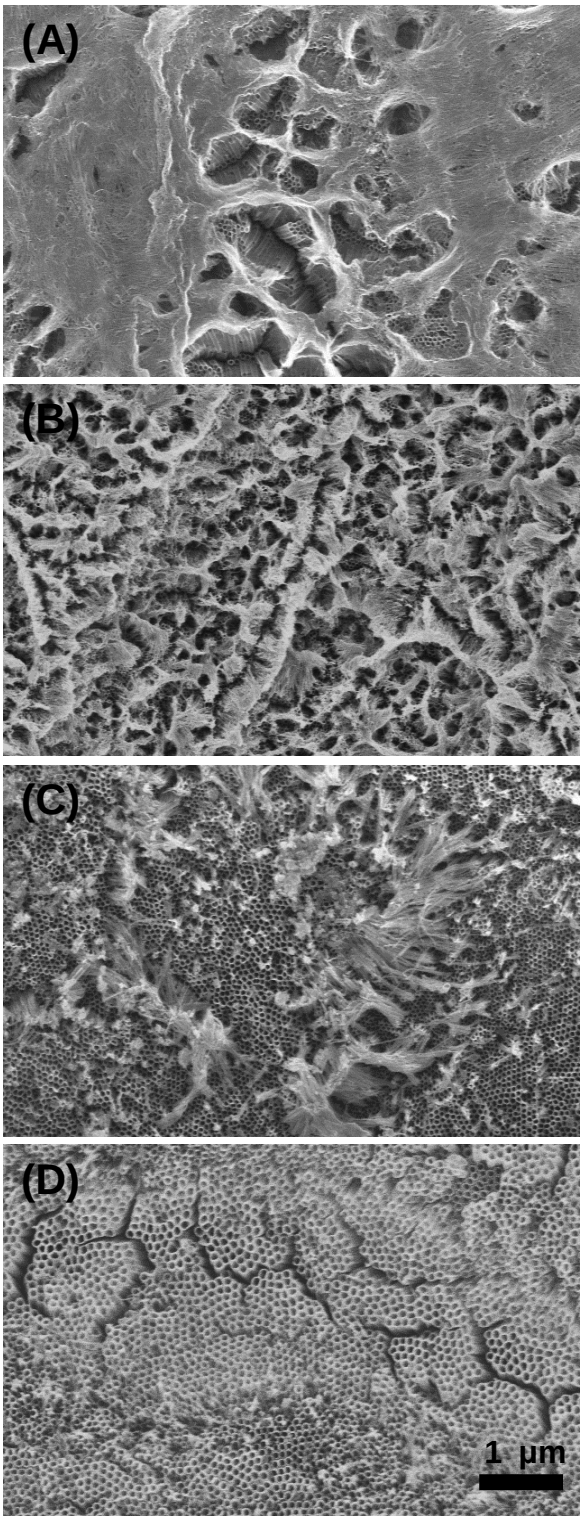

Figure 2-17. Nanograss morphology from anodization at different temperature conditions at (A) 65 º, (B) 40 º, (C) 25 º, and (D) 1 ºC.

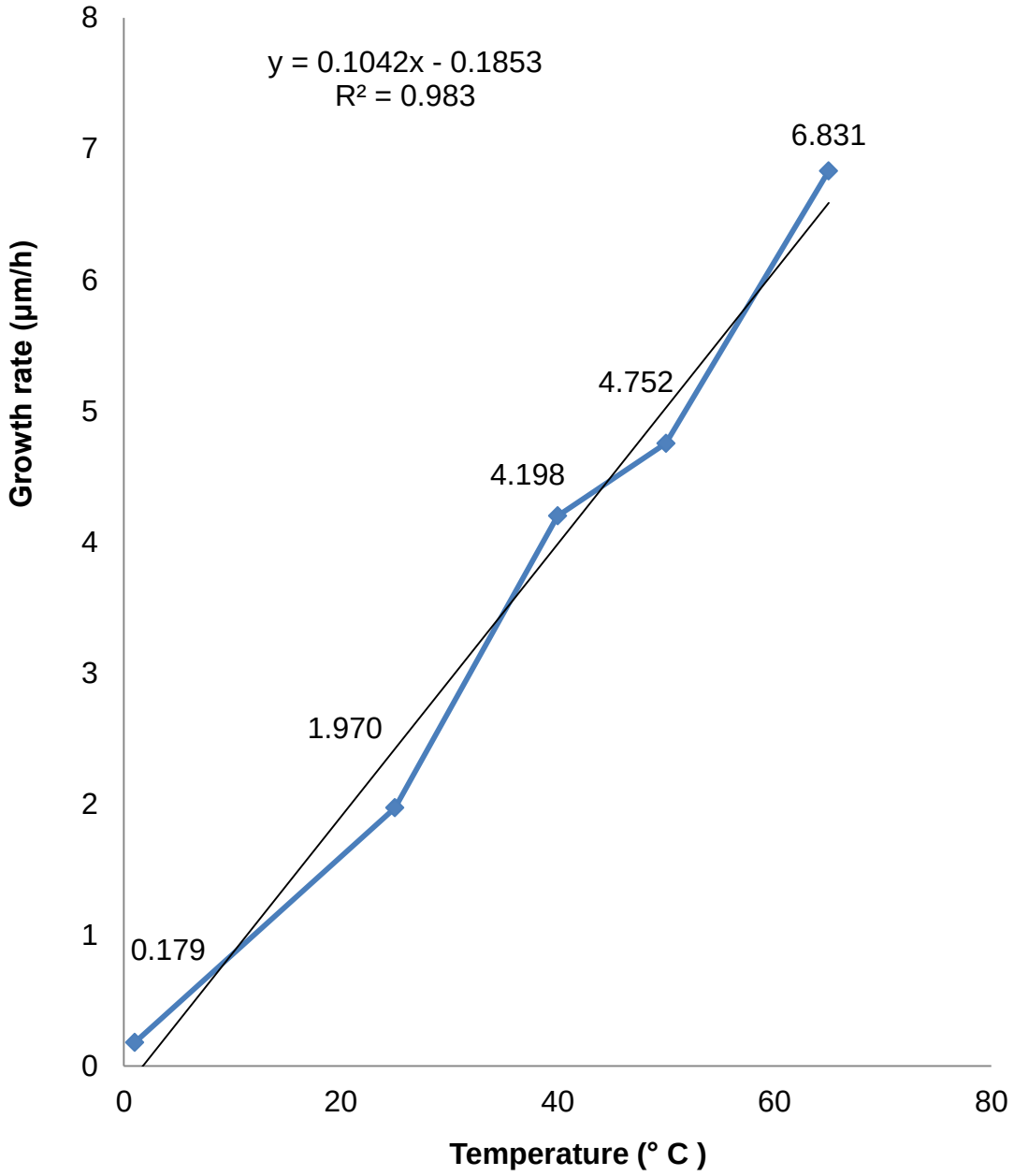

Figure 2-18. The rate of nanotube growth under different electrolyte temperature conditions.

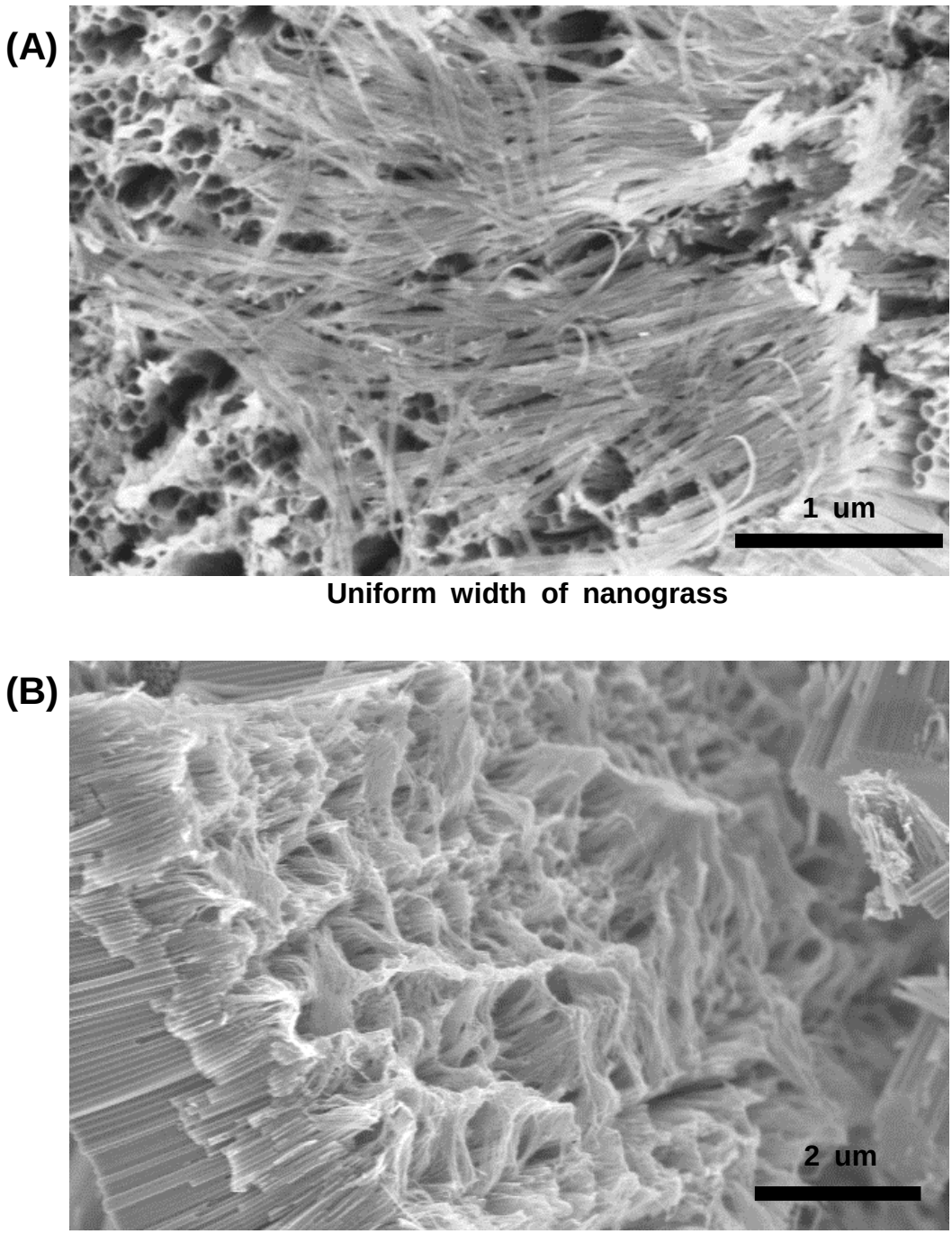

Figure 2-19. Nanograss morphology from (A) top view and (B) lateral view (anodized in 30 volts, 1 h, and 25 ºC of EG electrolyte).

Individual nanograss from one nanotube was gathered to make a bundle-shape terminal region of nanograss. The terminal part is shown as a white line at lower magnification (Figure 2-16 and 2-17) because of its relatively higher density. The lateral view shows that the white line has the regularity of big linearized white lines (Figure 2-19, right).

A single nanograss can be observed in Figure 2-20. The SEM image measured the width of single nanograss, 36.3 nm. This width is generally observed through other SEM analysis.

2.7.3 Nanolace

A thin layer is observed on the nanotube surface and is called nanolace (Figure 2-21).[34] This nanolace is considered the initial titanium oxide layer of nanotube growth steps (Figure 2-2) even though this structure has not been studied well so far. This nanostructure has potential for large anatase networks. Moreover, nanograss is observed under the nanolace, thus it is supported that nanolace is the top layer of the titanium oxide layer. More nanolace is observed from anodization using hydrofluoric acid polished Ti foil (0.5 % HF for 5 seconds). The reason why HF treated TiO_2-NTs has more nanolace structure is because of the surface condition at the beginning of anodization. Generally Ti foil is polished using sandpaper. Even though the polishing process heads in one direction, there is a lot of valley-shaped scratches. The nanolace structure generated on this tough TiO_2-NTs surface might be easily peeled off by small and weak physical shock during the washing process. HF treatment, however, does not rough up the surface of Ti foil. Therefore the nanolace on this Ti foil can remain on the nanotubes longer.

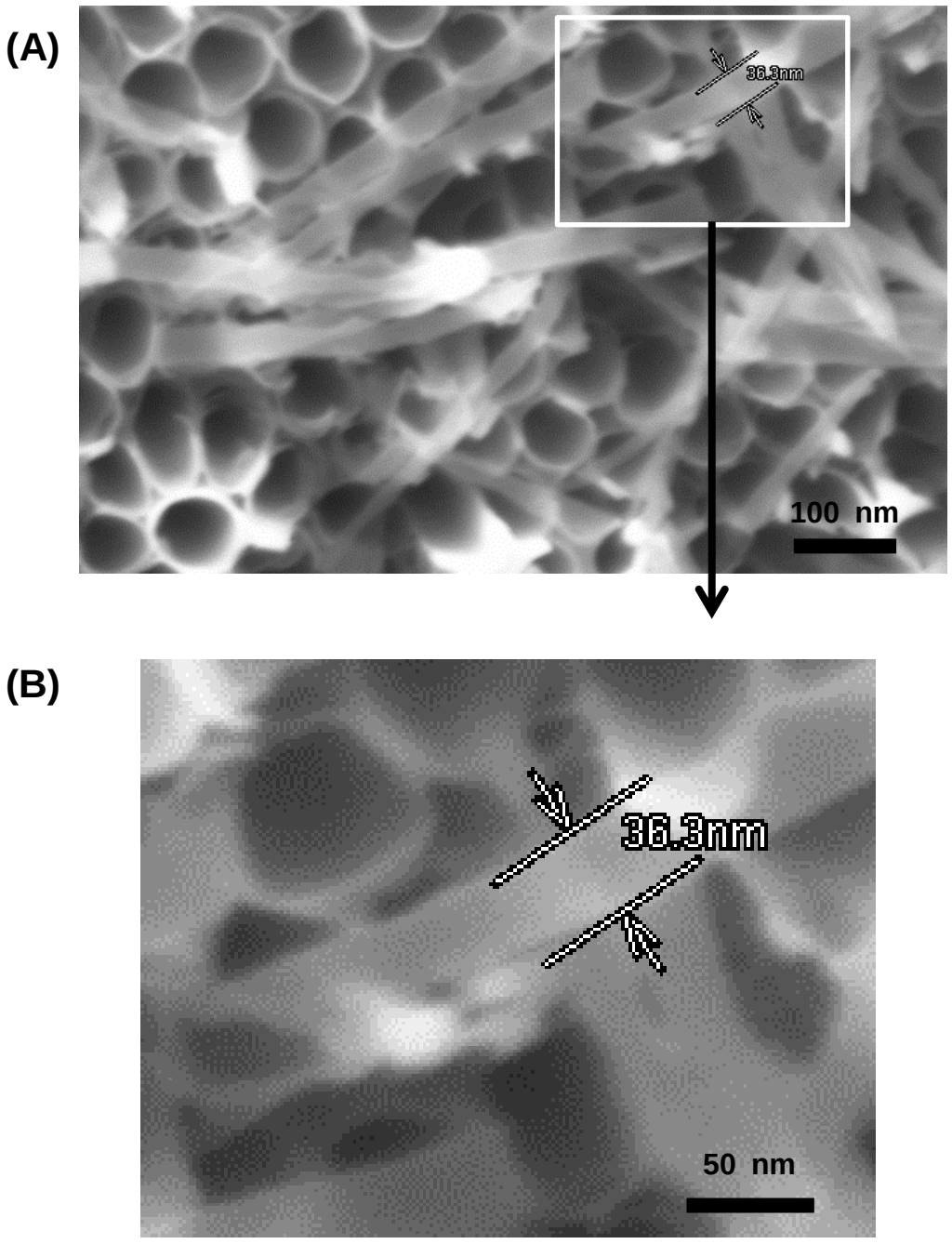

Figure 2-20. High magnification of SEM image of nanograss (A) (upper) and zoom-in image for single nanograss (B) (lower).

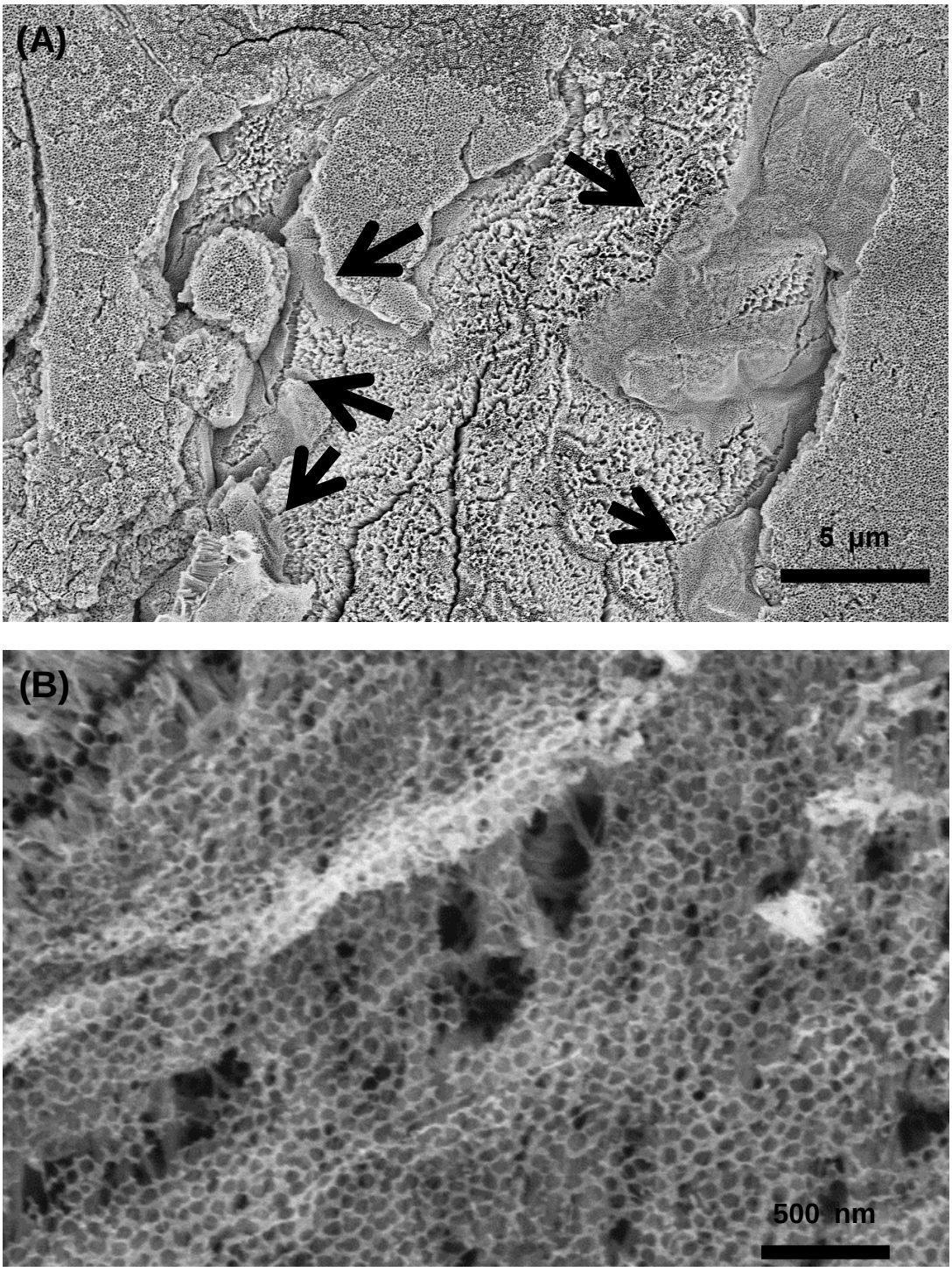

Figure 2-21. The SEM image of nanolace at lower magnification (A) (upper) and higher magnification (B) (lower).

2.8 Conclusion

TiO_2-NTs anodization by electrochemical method shows nicely self-organized nanotube structures. The nanotube morphologies of diameters and lengths are regularly changed by EG concentration and applied voltage. However, the reused electrolyte is corrossive and damages Ti foil and nanotube layers. Moreover, the diameter and length of TiO_2-NTs are smaller and shorter, less than half the size when anodized in the 13 h reused electrolyte. From the 1^{st} to the 4^{th} anodization does not show any corrossive damage on the TiO_2-NTs surface. A quick calculation of this phenomena supports that 100 ml of electrolyte is good for 2 h use with 0.5 cm $\times$ 1 cm size of Ti foil. Although the details of the corrossive mechanism requires additional study, it has been confirmed that fluoride content in TiO_2-NTs is decreased and pH is increased with the later anodization.

Still, the nanograss is thought to be the remnant structure of etching the nanotubes. However, the length of nanograss is similar among nanotubes, and this suggests an unknown mechanism of nanograss growth. Moreover, individual nanograsses are not etched much but show smooth and uniform shape in SEM images; this extended length contributes to increase the whole surface area of TiO_2-NTs. In addition, it has been confirmed that the growth of nanograss can be controlled by temperature: high temperature for longer nanograss.

Nanolace is a rarely studied structure. At the beginning of anodization, the initial layer of oxide is separated and remains during the anodization process. This kind of net shape anatase structure has potential applications.

CHAPTER 3

DEVELOPMENT OF TUBERCULOSIS DETECTABLE TITANIUM DIOXIDE NANOTUBES SENSING PLATFORM

3.1 Introduction

Volatile organic compounds (VOCs) are compounds that easily vaporize at ambient temperature. VOCs come from a variety of sources including industrial processing, environmental pollution (i.e., automobiles and factories), house hold chemicals, and most recently research has focused on VOCs derived from diseases that affect the human body.[35, 36] Disease-specific VOCs can be considered biomarkers for diagnostics and have the potential to be utilized in noninvasive rapid testing and point of care (POC). Several diseases have associated volatile biomarkers such as asthma,[37-39] lung cancer,[40-44] breast cancer,[45-47] diabetes,[48] and tuberculosis (TB). TB is of particular interest as no highly sensitive and specific POC test is available for low resource settings.

TB is a contagious disease that mainly occurrs in the respiratory tract such as the lung. Tuberculosis is caused by infection of *Mycobacterium tuberculosis* bacteria. The route of contagion of Tuberculosis is transfer of the pathogen by touch, sneezing, and cough instead of airborne and waterborne infection.

M. tuberculosis is a heterotrophic and aerobic bacteria and gram-staining

negative bacteria that has a waxy coat on the outside surface. The scientific classification of *M. tuberculosis* is shown in Table 3-1. The proliferation rate is slower than other bacteria species. Tuberculosis slowly divides every 15-20 h compared with *Escherichia coli*, for example, which divides every 30 minutes, and this slow cell division is a main obstacle to cell-culture a TB diagnosis method.

TB causes 1.1 million deaths out of 8.8 million incidents from HIV free patients and an additional 0.35 million deaths from HIV-associated cases.[49] About 13 million (4.2 %) people in the United States are infected by TB, and most TB incidence occurs in Africa and Asia (Figure 3-1). HIV is an important factor in the lethality of TB disease because these two diseases synergetically work together. Actually, a main cause of death of HIV patients is thought to be TB infection. Two types of TB infections are reported: latent TB infection (LTBI) and active TB infection (ATBI). LTBI patients usually do not have any symptoms or pain and they cannot spread TB to other people. LTBI patients' risk of lethality is increased, however, when they are infected with HIV. Thus, newly diagnosed HIV patients should have a TB test to reduce the risk of additional illness by TB infection. In other words, active TB infected patients show various symptoms, for example continual coughing with blood in extreme cases, fever, sweats at night, weight loss, fatigue, and chills.

Even though the TB incident rate has decreased in the last 2 decades,[49] TB still widely threatens South Asia and Africa countries. Usually TB infects the lung first and then spreads out to organs such as kidney, brain, lung, and spine. About 10 % of TB carriers present symptoms of active TB infection.[50] About 90 % of LTBI patients cannot know of their infection until they get a TB test. TB is easily controlled in the initial stages

Table 3-1. Biological classification of *Mycobacterium tuberculosis*.

Kingdom	*Bacteria*
Phylum	*Actinobacteria*
Class	*Actinobacteria*
Order	*Actinomycetales*
Suborder	*Corynebacterinaea*
Family	*Mycobacteriaceae*
Genus	*Mycobacterium*
Species	*Mycobacterium Tuberculosis*

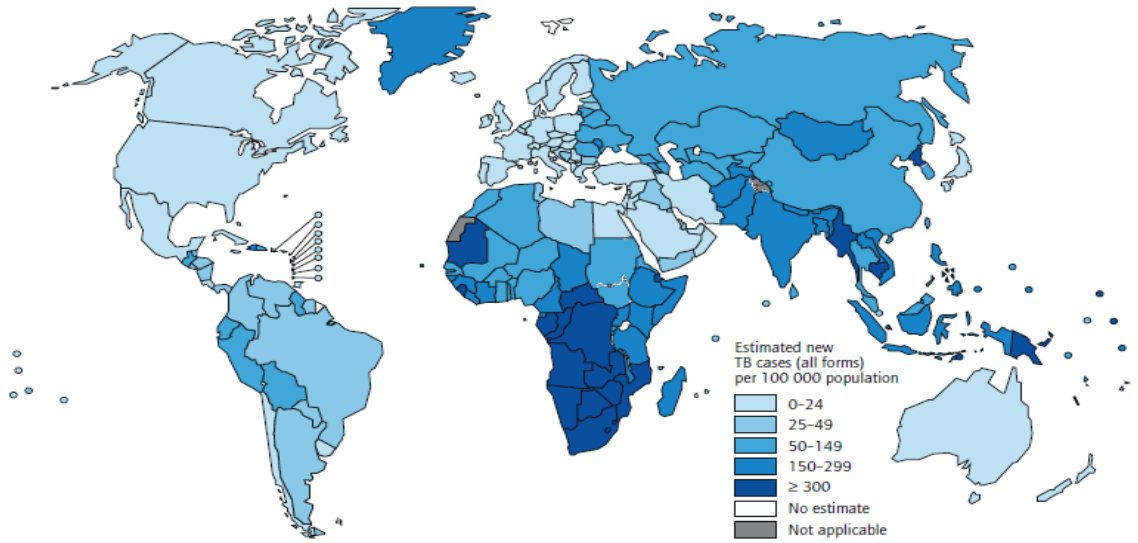

Figure 3-1. A map estimating Tuberculosis incidence in 2011. Africa and the south regions in Asia show a higher incidence rate.[49]

by antibacterial treatments, otherwise it will be lethal to patients in later stages. Thus, the diagnosis before progression of the disease is important.

Recent research has shown that various strains of the mycobacteria produce distinct gaseous volatile biomarkers that can be used as a methodology for detecting and identifying mycobacterium.[51-53] Specifically, Syhre and Chambers found that *M. tuberculosis* and *M. bovis* cultures give off four specific volatile biomarkers (methyl phenylacetate, methyl *p*-anisate, methyl nicotinate, and *o*-phenylanisole).[54] These compounds were detectable before the visual appearance of colonies *in vitro*, which could have implications in detection of latent TB infection.[55] Syhre *et al.* in a follow up publication were able to detect statistically significant differences of methyl nicotinate in the breath of smear positive TB patients when compared to healthy (smear negative) subjects.[53] Figure 3-2 shows the concept of how volatile biomarkers release between healthy humans and TB patients. Analyses in these studies were done using gas chromatography/mass spectroscopy analysis tools. While they are effective in identifying and quantifying complex gas samples, they are expensive, bulky, and not appropriate POC diagnostics. Other researchers have reported that TB detection using volatile biomarkers are found in nature. Interestingly, honeybees can distinguish specific volatile biomarkers released from TB[56] and African pouched rats can find the sputum sample of pulmonary TB patients.[57]

Conventional methods for TB detection are traditionally performed in laboratories or hospitals.[26] Table 3-2 shows many different methods of TB diagnosis. For example, the most common method for diagnosis of TB is the acid fast staining of clinical material, which is then followed by a sputum smear microscopy test. However, a

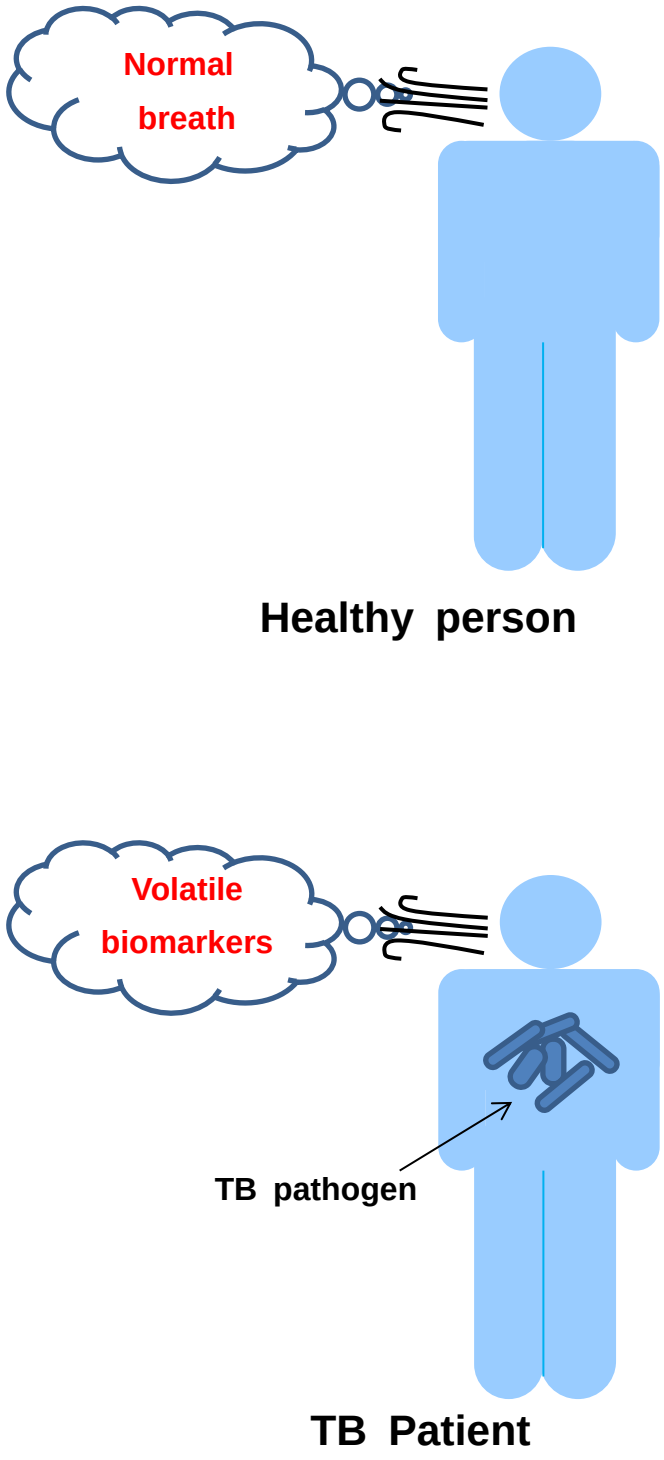

Figure 3-2. Conceptual image of the difference between healthy human and TB infected human.

Table 3-2. Various methods for TB detection.

Nonculture based	Name of methods
Antibody detection	ABP Diagnostics Focus Sure Check TB
	Advanced Diagnostics Tuberculosis Rapid Test
	American Bionostica Rapid Test for TB
	Ameritek dBest One Step TB Test
	BioMedical Products Corp TB Rapid Screen Test
	Chembio TB Stat-Pak II
	CTK Biotech TB Antibody onsite Rapid Screening Test Kit
	Hema Diagnostic Rapid 1-2-3 TB Test
	Millenium Biotechnology Immuno-Sure TB Plus
	Minerva Biotech V Scan
	Mossman Associates MycoDot
	Pacific Biotech Bioline TB
	Premier Medical Corporation First Response Rapid TB
	Princeton BioMeditech BioSign M.tuberculosis
	Silanes TB-Instantest
	Span Diagnostics TB Spot ver. 2.0
	Standard Diagnostics SD Rapid TB
	UniMED International Inc. FirstSign MTB Card Test
	Veda Lab TB Rapid Test
	Rapid Biosensor System (RBS)
Antigen detection	LAM urine test
	Antigen-based detection test
	Flow-through filter tests
Nucleic Acid Amplification (NAA)	Amplified Mycobacterium Tuberculosis Direct Test
	AMPLICO® MTB Tests
	BD ProbeTec ET® assay
	In-house PCR
	Real-time PCR
	Simplified NAT Test, TB-LAMP test
	INNO-LiPa Assays
	GenoType Assays
	PCR Sequencing
	PCR directly from AFB slides

Table 3-2. Continued.

Culture based	Name of methods
General	BACTEC460-TB®
	BACTEC MGIT 960®
	MGIT
	MB/Bact T®
	Versa Trek
	E Test
	MB redox®
	Solid culture indicator
Phase-based	FASTPlaque TB-RIFTM
	Luciperase reporter phase
Noncommercial	MODS
	Nitrate reductase assay
	Thin layer agar
	“Resa” colorimetric method

Data source: Ref [49, 58]

disadvantage with the sputum smear test is its poor sensitivity, which is estimated to be at 70 %.[59] Additionally, the sensitivity of sputum smear spectroscopy in field settings has been shown to be much lower (35 %), especially in populations that have high rates of TB and HIV coinfection.[60] Furthermore, drug susceptibility analysis of the mycobacterium cannot be determined from microscopy testing. This assessment is critical in determining the appropriate course of treatment for the patient. For this type of analysis culturing techniques are typically used.

Culturing of mycobacterium from sputum samples is a more sensitive technique. Sputum samples are collected and cultured in either solid media or liquid media looking for the presence of the mycobacterium. Drug resistance strains can be determined using this technique. However, this methodology takes time to conduct (3-4 weeks for solid cultures, and 10-14 days for liquid cultures), which makes it difficult to employ in low resource settings that are typically far from testing facilities.[61, 62] Recently, other technologies have been developed including fluorescence microscopy for smear tests (10 % more sensitive than light microscopy), LED fluorescent microscopy for inexpensive imaging equipment that can be used in the field without the need for a darkroom, rapid culturing techniques to reduce incubation time,[63] polymerase chain reaction (PCR),[62] and immunoassays. PCR techniques need sophisticated equipment and trained personnel. Immunoassays often have the same requirement and often do not have the selectivity and specificity needed for diagnosis as they can respond to families of biomarkers that are related to TB specific biomarkers. Despite all the improvements that have been made in TB diagnosis, no simple inexpensive POC test is available. The techniques mentioned above either focus on some sort of microscopy technique, or culture technique. In either

case, these methods require lab facilities and highly trained personnel that typically are not available in many rural or low resource areas.

Other researchers have begun looking into noninvasive analysis from breath. One example is by Draper Laboratories. This device is a differential mobility spectrometer (DMS) that analyzes volatile biomarkers present in gas. While this technology is highly sensitive, the cost of a DMS is higher when compared to other POC techniques which make it difficult for use in resource limited settings. Rapid Biosensor Systems has created a breathalyzer device for TB diagnosis in the field, however, this device is more complex to operate and requires antibodies and fluorescent analogues to interact with TB antigens, which have a shelf life and specific storage conditions.[58] The technology developed at Menssana Research, Inc. also collects volatile biomarkers from breath. While the technology is useful and has great potential, it uses portable chromatograph technology (higher cost) which is more suitable for a central lab location rather than a low resource setting POC device.

Titanium is a semiconductive metal and it has high durability and good biocompatibility, so it is widely used for bone implantation materials.[19, 29] The nanotubes structure of titanium metal, or titanium dioxide nanotubes (TiO_2-NTs), shows extremely enlarged surface area. It has a self-organized tube structure that looks like a well-packed bundle of tubes. This morphological shape is related to the amount and ratio of electron transfer per unit area of metal. Moreover, the TiO_2-NTs fabrication method is also easier and convenient than other nanotube fabrication methods. Thus, TiO_2-NTs are considered a good material for sensing mechanism research.

Titanium has a binding affinity for the hydrogen molecule. Therefore, it requires

additional metal functionalization on the TiO_2-NTs surface for selectively holding the biomarkers. Fortunately, cobalt is known as a binding material of nicotinate with organic-inorganic binding material.[64-66] In this research, this binding property is applied to selectively choose the nicotinate molecules contained in human breath from TB patients. Finally, the cobalt-nicotinate coupling mechanism leads to current change on the sensing platform of cobalt functionalized titanium dioxide nanotubes (Co-TiO_2-NTs).

The Co-TiO_2-NTs sensing platform presented here introduces a new methodology for detection of volatile biomarkers and operates on a fundamentally different mechanism than those mentioned above. The sensing platform is antibody free and label free, utilizing inorganic metal ions that bind specifically to volatile biomarkers of interest. The metals also have a long shelf life and typically are not subject to the strict storage conditions associated with antibodies. In addition, the sensing operation utilizes a simple potentiostat that can be built inexpensively and deployed in resource limited settings. The readout for the sensor is a simple current measurement that is used to indicate the presence of the volatile biomarker. The device is inherently designed to be simple to use in a low resource setting environment without the need for sophisticated lab equipment or training to operate.

In this study, I tested and measured the current change by electrical reaction between Co-TiO_2-NTs and two biomarkers (methyl nicotinate and methyl *p*-anisate). Significant results were obtained from a series of tests. These results indicate that volatile biomarkers detection is a promising technique as a new TB detection method, and could help cure a lot of people in developing countries, and eventually prevent TB deaths.

3.2 Materials and methods

3.2.1 Anodization of TiO_2-NTs

TiO_2 fabrication was performed through electrolyte anodization method. The electrolyte was composed of 97 % of ethyleneglycol (Reagent grade, Aqua Solution, USA), 0.5 wt% of ammonium fluoride (98 %, Sigma Aldrich, USA), and 3 % of DI water (18.2 MΩ quality, Siemens, Germany) in this study. Titanium foil (ESPI metal, USA) was cut as regular size (10 mm × 15 mm × 0.2 mm) and polished using 150-grit and 1,500-grit sand papers continuously. The sample was rinsed with flowed DI water for couple of seconds to remove dust. Then it was soaked in 1:1 mixture of acetone and isopropyl alcohol (VWR, USA) for 10 minutes in ultrasonic bath (Branson, USA) to remove organic contamination on the surface. After the alcohol compounds were removed, 2-3 mm of the top part of the foil was cut about half length of width, and fold perpendicularly to height. This folded tip was used as a connection part to a copper alligator clip. Titanium was connected with anode and platinum was connected with cathode, and the distance between the two metals was around 2-3 cm. Nanotubes were anodized under 30 volts (E3647A, Agilent, USA) for 1 h with stirring at 70 rpm using a 1 inch magnetic bar. After anodization, samples were rinsed in 50 ml of DI water containing beaker for 5 seconds in ultrasonication bath, and annealed in pure oxygen gas for 2 h at 500 °C with 0.5 °C/m ramp rate.

3.2.2 Cobalt functionalization

To decorate cobalt ions on nanotube surface, the TiO_2-NTs samples were warmed in a 110 °C vacuum oven (414004-580 Symphony vacuum oven, VWR, USA)

first. The warm samples were soaked in 0.5 wt% of Cobalt (II) Chloride anhydrous ($CoCl_2$, 99.7 %, Alfa Aesar, USA) dissolved in 100 ml of ethanol (200 proof, Decon Labs, USA) and incubated in ultrasonication bath for 30 minutes. After the reaction, the samples were gently rinsed by ethanol and dried up in a 110 ° C vacuum oven. The nanotubes fabrication was observed using Hitachi S-4800 scanning electron microscope (SEM). The cobalt content was confirmed by energy dispersive X-ray (EDX) and X-ray photoelectron spectroscopy (XPS).

3.2.3 Measurement of mimics of biomarkers

3.2.3.1 Prepare different chemicals as negative controls

As negative controls, 5 chemical mimics of main volatile biomarkers from human breath were chosen to compare with nicotinate and anisate: ethanol (SIGMA-ALDRICH, USA), methanol (SIGMA-ALDRICH, USA), acetone (ACS grade, VWR, USA), benzene (VWR, USA), and phenol (ACS grade, J. T. Baker, USA).[67, 68] All undiluted chemical solutions were placed as 10 ml in 50 ml containers that were connected with nitrogen gas tank and a sensing chamber.

3.2.3.2 Prepare mimics of volatile biomarkers for CV scan

To test the binding affinity between cobalt and volatile biomarkers, the cyclic voltametric scan was performed using biomarker solution and cobalt chloride solution. Two chemical mimics of biomarkers were prepared: 2.5 mM of methyl nicotinate (nicotinate, $C_7H_7NO_2$, 99 %, CAS: 93-60-7, Alfa Aesar, USA) and 2.5 mM of *p*-anisic acid methyl ester (anisate, $CH_3OC_6H_4COOCH_3$, CAS: 121-98-2, Tokyo Kasei Kogyo,

Japan) in DI water. The reason for the low concentration of anisate was its poor solubility in water at room temperature. The cyclic voltametric scan software was applied from potentiostats (Reference 600^{TM}, GAMRY, USA). The cycle began from 0 V to - 2.0 V on reduction area, and then went up to 1 volt and back to 0 volt with 10 millivolts *per* second.

3.2.3.3 Prepare mimics of volatile biomarkers for potentiostatic scan

Two chemical mimics of biomarkers were prepared: 100 mM and 10 mM of nicotinate and 2.5 mM of anisate in DI water.

3.2.3.4 Design of measurement circuit

Each biomarker solution was filled up to 200 ml in 250 ml side armed flasks, and capped with one-hole air tight rubber stopper. Pure nitrogen gas flowed through all measurements with 150 mass of standard cubic centimeter per minute (SCCM) (Figure 3-3). A plastic rod was placed at the bottom of the flask to generate extra bubbles for higher diffusivity of biomarker molecules. After each test, tygon tubing was washed with water to remove any possibility of chemical contamination. A hand-made volatile biomarkers detection chamber was designed using 50 ml centrifuge tube (VWR, USA) and located in a Faraday cage (16 inches × 16 inches × 30 inches covered with metal mesh). Nanotubes sensor sample was cooled down to room temperature before the test. Nanotube (front side) and titanium metal (back side, polished) were connected with potentiostats. Potentioststic scan program was used to measure current change when different biomarkers were introduced. All measurements in this experiment were triplicated and averaged.

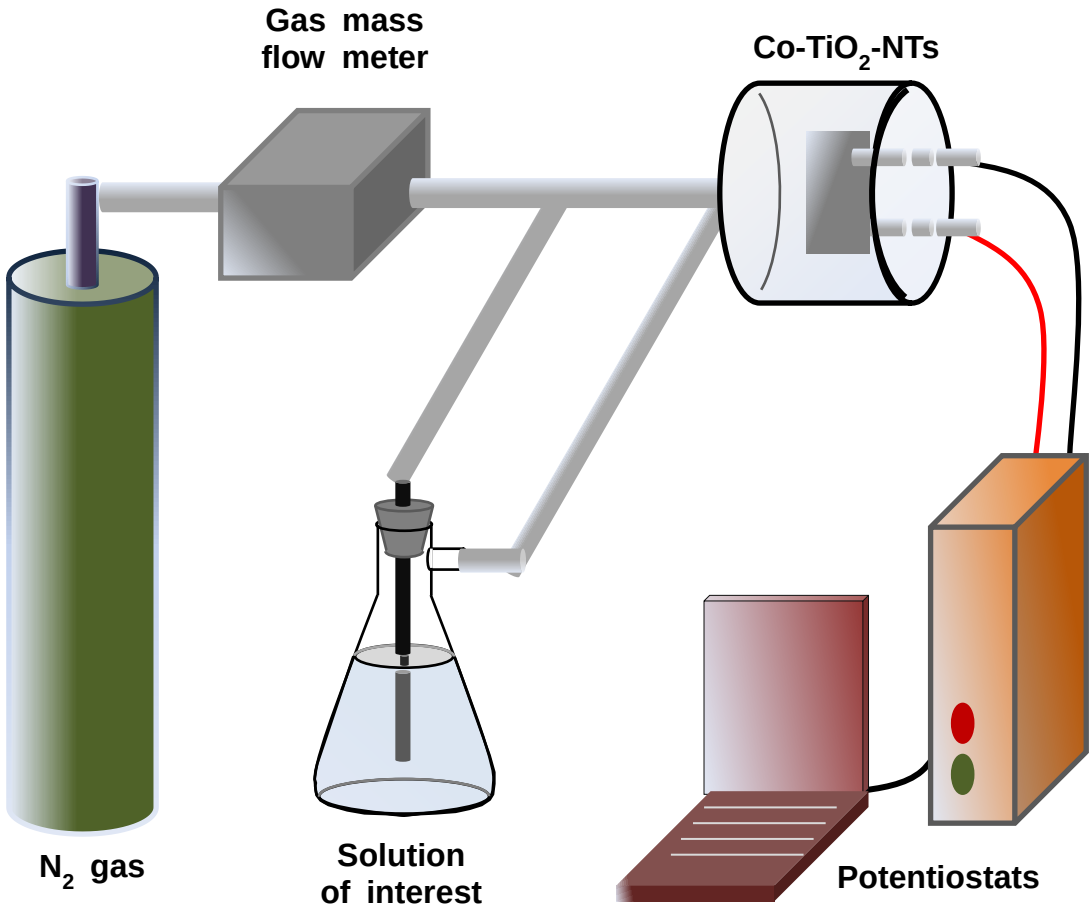

Figure 3-3. Concept of gas detection circuit system. All tubing is sealed to prevent air contamination from ambient air and three-way valves the control the gas flow. Pure nitrogen gas flowed 150 SCCM through Tygon tubing to the detection chamber (right upper side), and then the gas is passed through water and biomarker in order (middle). The sensor located in the hand-made chamber and contact gases. The chamber is linked with potentiostats to detect current change.

3.2.3.5 Design of current measurement gas chamber

Figure 3-4 shows an overall set-up of the volatile biomarkers detection chamber. To obtain more reasonable and elaborate results, a hand-made chamber was designed with a small volume (50 cc). The chamber was sealed except one inlet and two nail-size outlet holes. The outlet holes are as small as possible to minimize inlet of ambient air from outside preventing air contamination. The details of the handmade chamber are drawn in Figure 3-5.

3.2.3.6 Current measurement of nicotinate and anisate

The fixed voltages of potentiostatic scan were -0.5 V for nicotinate and -0.8 V for anisate. These potentials were decided by cyclic voltametric scan results. After set up of all solution and nanotubes, nitrogen gas flowed into the sample chamber until the plot of the potentiostatic scan was flattened. Then the gas was passed with water bubbling. At last, only pure nitrogen gas flowed again. After drying the Co-TiO_2-NTs samples for a while, these steps were repeated using biomarker solutions and the results were compared. All data plots were obtained every 0.1 seconds and re-plotted. Each run was continued until the peak was on the plateau phase.

3.2.3.7 Main volatile organic compounds

Five main volatile organic compounds were tested to compare with nicotinate and anisate: ethanol, methanol, acetone, benzene, and isopropanol using Co-TiO_2-NTs. The water bubbling step was omitted because these organic solutions cannot be dissolved in water. The processes were performed in hood due to some chemicals' toxicity.

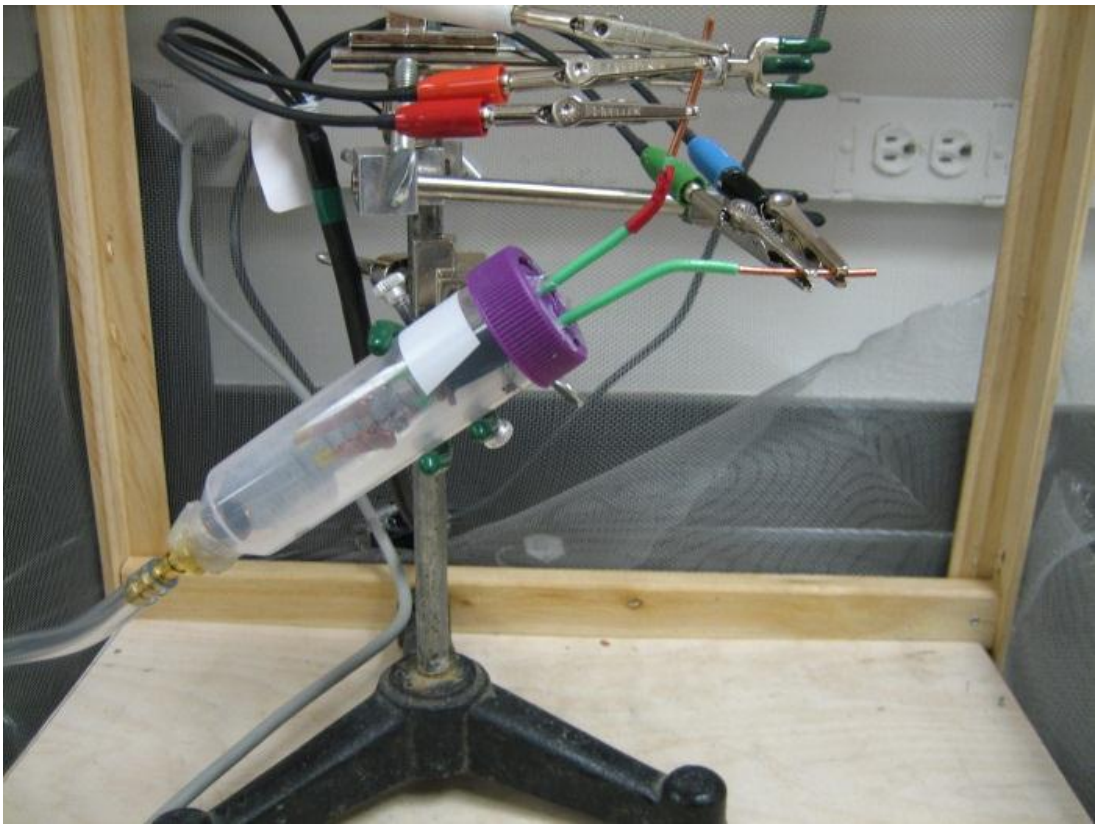

Figure 3-4. The setup of volatile biomarker detection chamber in a Faraday cage covered with metal mesh to prevent electric noise from outside.

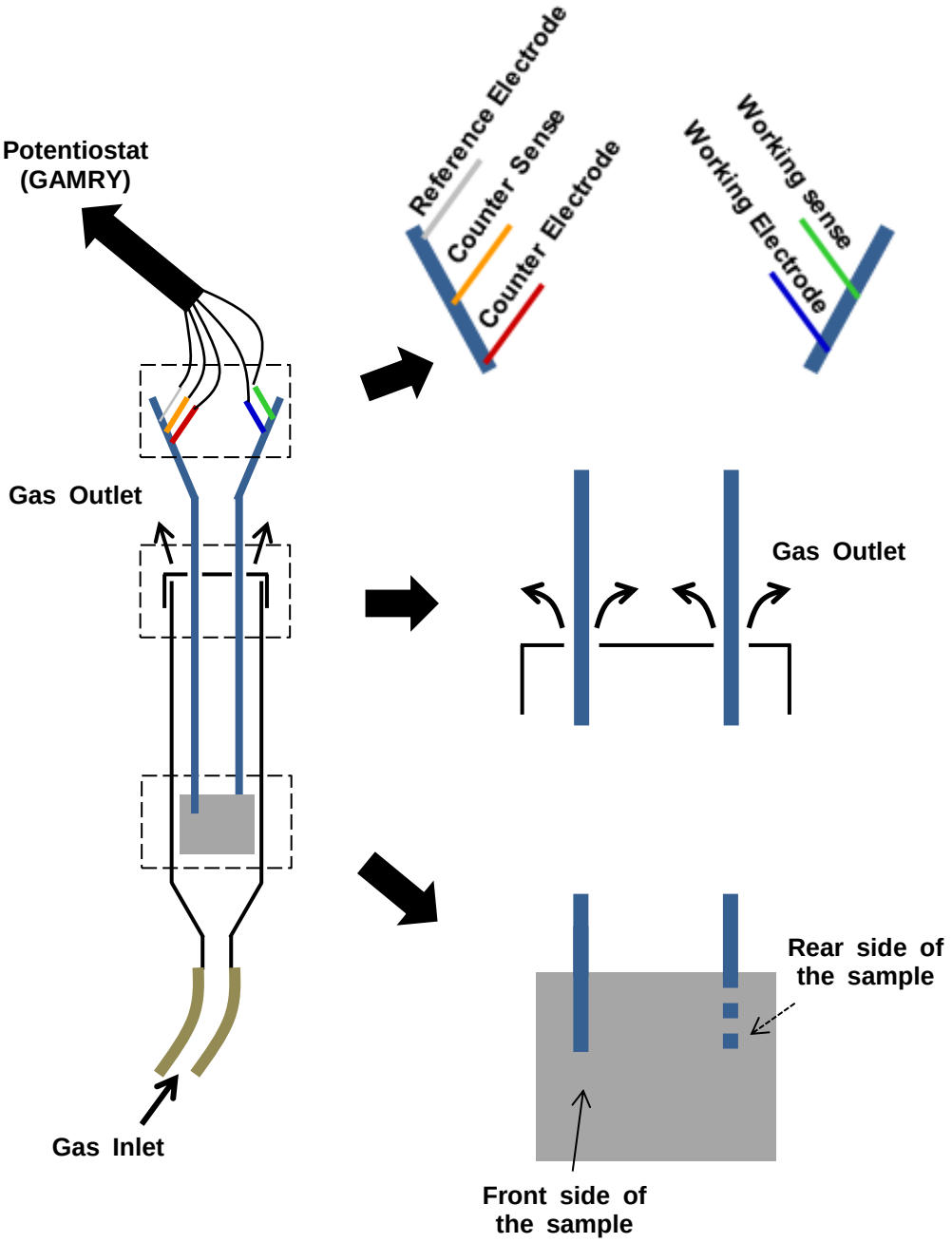

Figure 3-5. A detailed conceptual image of the handmade volatile biomarker detection chamber.

Measurements were performed under two voltages (-0.5 volts and -0.8 volts) and then organized after the biggest and smallest data were removed.

3.2.3.8 Negative controls applied different voltage for anisate (-0.2 volts)

Inappropriate potential was applied to test whether the voltage is a critical factor in the relationship between Co-TiO_2-NTs and biomarkers in a potentiostatic scan. The potential of -0.2 volts which has not been considered for potentiostatic scan of anisate was tested. Water and 2.5 mM of anisate solution were tested and compared. Measurements were performed as in the biomarkers case.

3.2.3.9 Negative controls without cobalt functionalized samples (-0.8 volts)

Without cobalt loaded TiO_2-NTs were tested to know whether cobalt metal is necessary to detect biomarkers at appropriate potential (-0.8 volts). Thus, bare TiO_2-NTs samples were tested with water and 2.5 mM of anisate solution.

3.3 Results and discussion

3.3.1 Cyclic voltametric scan test

The purpose of the CV test is to confirm the binding between biomarkers and cobalt. Therefore, 2.5 mM of cobalt was scanned first. Then 2.5 mM of biomarkers were added for the next scan. The plots of $CoCl_2$ (red) in Figure 3-6 show oxidation peaks and reduction peaks clearly, but the plots of $CoCl_2$/biomarkers show that oxidation peaks are removed and overall plots become thinner. The changed plot shapes imply that cobalt ion is bound to biomarkers and interrupted its reduction/oxidation reaction.

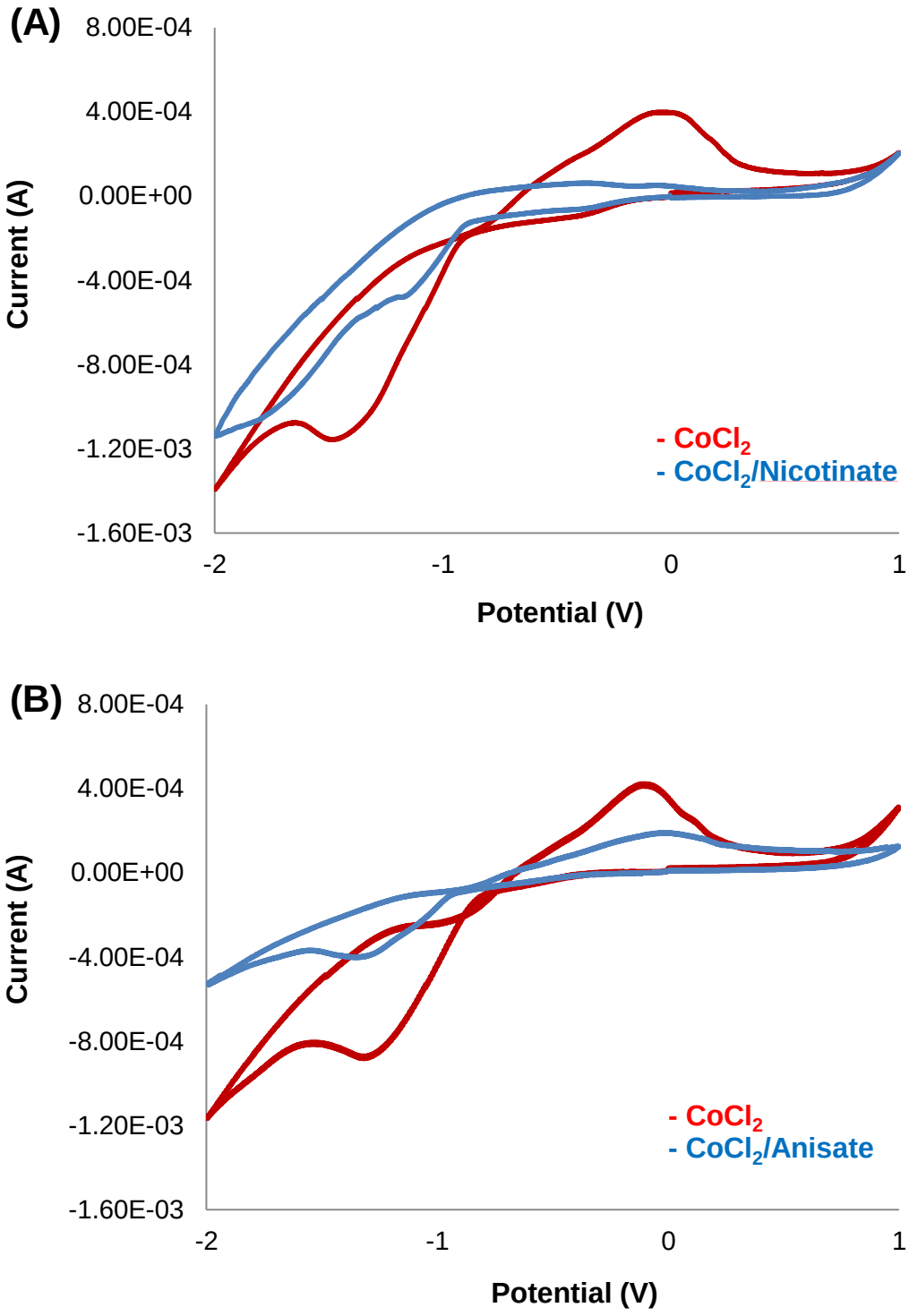

Figure 3-6. The results of cyclic voltametric scans of $CoCl_2$ alone and $CoCl_2$/biomarkers mixture. Nicotinate (A) (upper) and anisate (B) (lower) are tested and compared. All solutions are prepared at 2.5 mM concentration.

3.3.2 Preparation of Co-TiO_2-NTs

3.3.2.1 Anodization and crystallization

Amorphous TiO_2-NTs are anodized by electrolyte method in this research. The anodized TiO_2-NTs samples were annealed under oxygen rich circumstance to generate additional hydroxide groups on titanium surfaces like Ti-OH. Also, high temperature annealing is an essential step for crystallization of amorphous of titanium nanotubes. The phase change of titanium is well studied and the anatase phase is generated at $500\,^{\circ}C$ with minimal crystallization of rutile.

UV-VIS spectrophotometer profiles of the TiO_2-NTs samples show the difference of absorbance between before and after annealing at $500\,^{\circ}C$. The absorbance was increased to around 380 nm, which is the characteristic of anatase. The absorbance at 250 nm was decreased about 60 % on oxygen annealed samples and it represents the structure of nanotubes crystallized; the plots are expanded to the UV area (Figure 3-7).

3.3.2.2 Cobalt functionalization on nanotubes and EDX analysis

Cobalt is known as a binding metal with nicotinate. Decoration of cobalt metal ion on TiO_2-NTs is performed by functionalization method. Under high energy from ultrasonic wave, cobalt molecules are exchanged with hydrogen groups on TiO_2-NTs. Thus, the number of hydroxyl group is one of the factors deciding the amount of cobalt functionalization. Figure 3-8 shows an EDX spectrum of cobalt loaded TiO_2-NTs sample.

Table 3-3 is an example of raw data of EDX analysis. Even though the nanotube is anodized using pure Ti foil, a small amount of impurities are contained such as C, Si, Cu, and Cl. In addition, cobalt (II) chloride shows better functionalized concentration

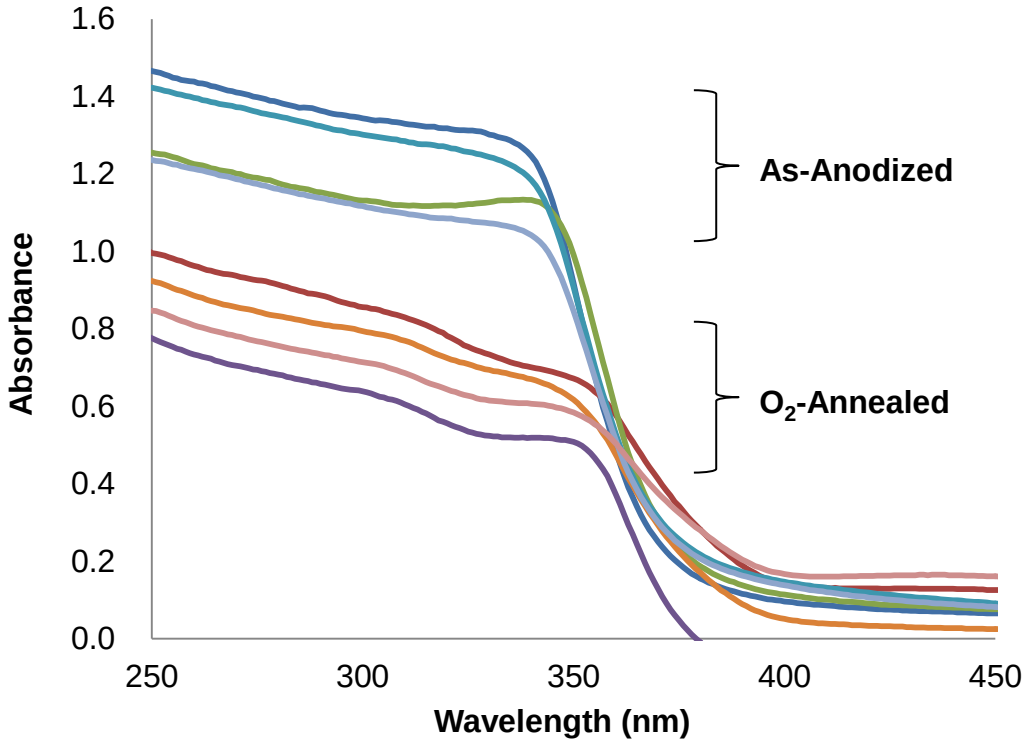

Figure 3-7. The UV-VIS patterns of as-anodized samples and oxygen annealed samples.

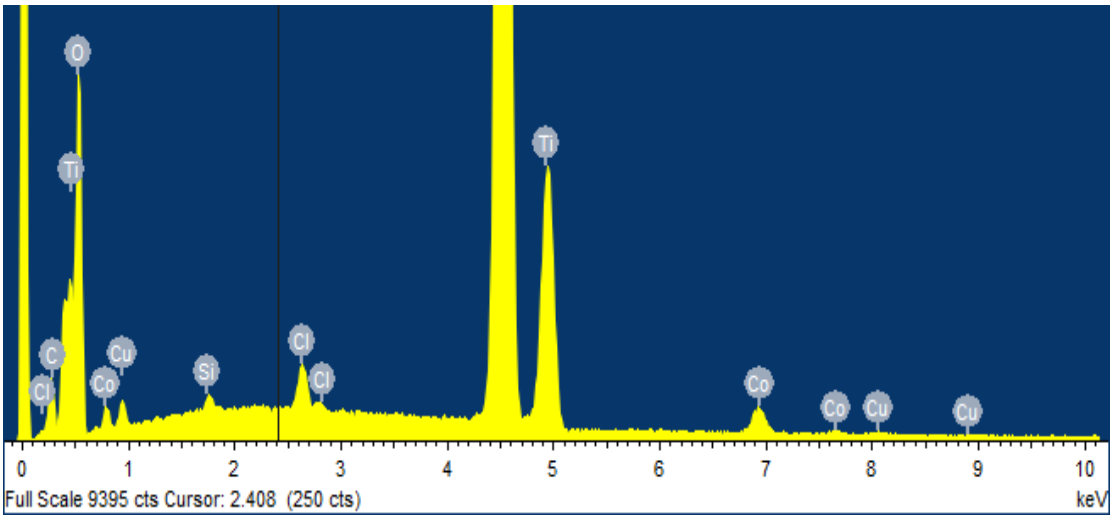

Figure 3-8. An example of the spectrum of EDX analysis of Co-TiO_2-NTs.

Table 3-3. An example of the result of EDX analysis of Co-TiO_2-NTs.

Elements	**Weight%**
C K	0.96
Si K	1.64
Cl K	0.16
Ti L	52.46
Co L	2.43
Cu L	1.78
O	40.57
Totals	100.00

compared with cobalt nitrate because $CoCl_2$ contains higher cobalt molar concentration than other cobalt compound mimics. Also, the EDX profile result indicates that ethanol is better than acetone for functionalization efficiency (Table 3-4). The average data of EDX analysis from samples is 1.88 wt%, 53.98 wt%, and 39.91 wt% for cobalt, titanium and oxygen, respectively.

3.3.2.3 XRD analysis of Co-TiO_2-NTs

Similarly, the XPS analysis Co-TiO_2-NT shows 5.91 at%, 16.17 at%, and 48.36 at% for cobalt, titanium, and oxygen, respectively. This atomic percent is comparatively increased more than EDX analysis. It might be caused by focusing on the cobalt-rich area on the surface of the uneven cobalt metal distribution. The binding energy difference between $Co2p_{3/2}$ (780.6 eV) and $Co2p_{1/2}$ (796.5 eV) is 15.9 eV, and it represents the existence of cobalt (Figure 3-9).

3.3.2.4 Current measurement

Figure 3-10 shows a conceptual image of binding between cobalt and volatile biomarkers that causes current change. The strong covalent binding mechanism of cobalt-nicotinate is already studied and reported.[66] In this sensing experiment, however, the bonding seems not to be as strong because the current signal is reduced under less concentration of biomarker inlet. It is thought that cobalt and nicotinate make weak polarcovalent bonds because of the difference in their electronegativity, 1.88 for cobalt and 3.04 for nitrogen. This weak bond is thought to be easily broken and released out of the biomarkers. In experiment, it is observed that the current changes of biomarkers are

Table 3-4. Triplicated and averaged wt% of main components in Co-TiO_2-NTs.

		$CoCl_2$	**$Co(NO_3)_2$**	**Bare TiO_2-NTs**
EtOH	**Ti**	53.98	53.83	56.10
	Co	1.88	0.39	0.00
	O	39.91	43.09	37.11
Acetone	**Ti**	53.66	52.09	
	Co	1.50	1.37	
	O	41.86	42.95	

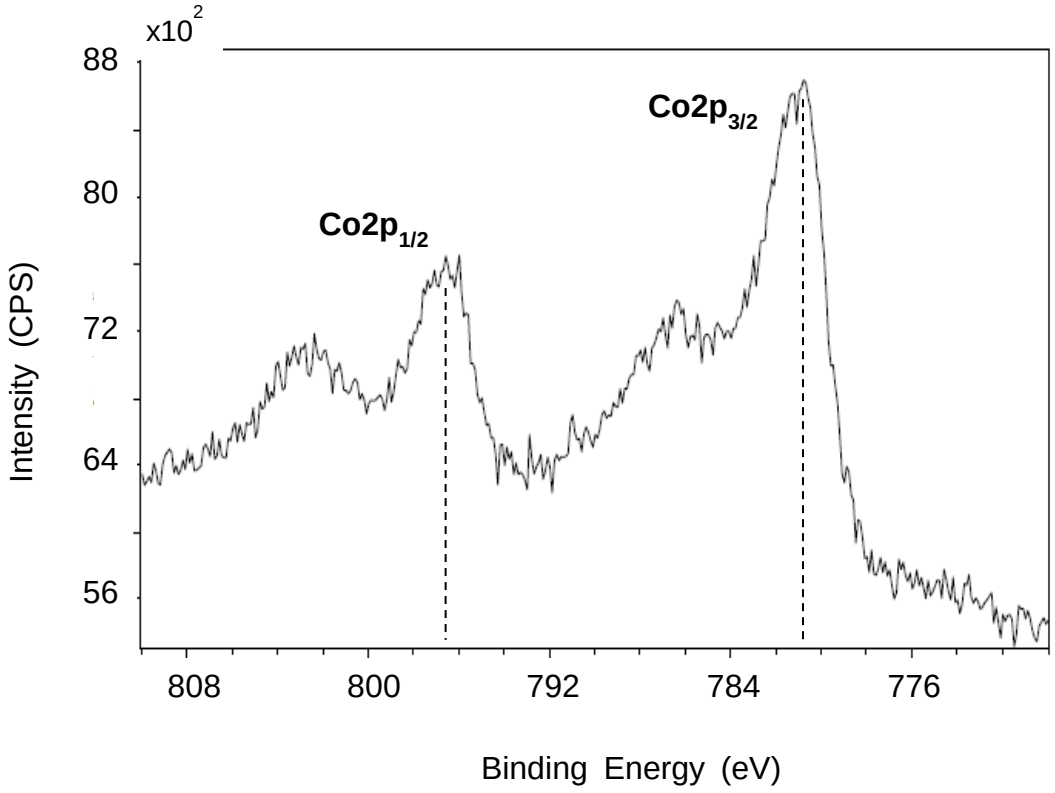

Figure 3-9. XPS result of cobalt functionalized TiO_2-NT. Difference binding energy of $Co2p_{3/2}$ (780.6 eV) and $Co2p_{1/2}$ (796.5 eV) is 15.9 eV.

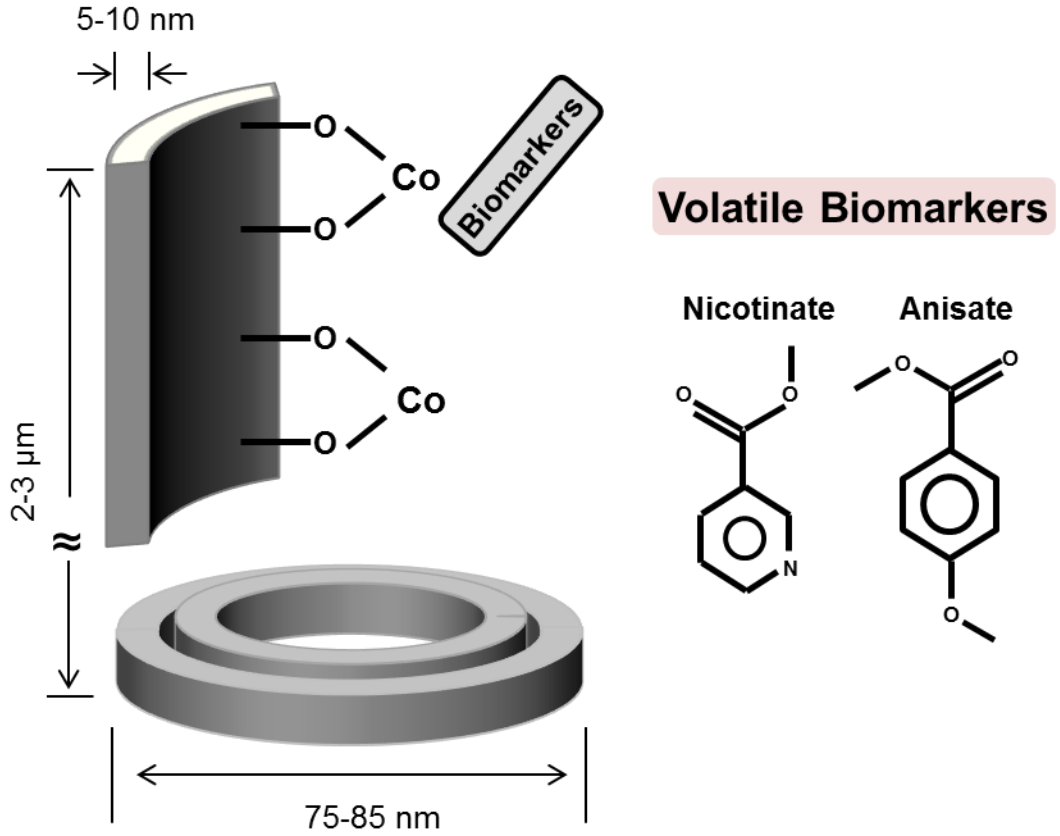

Figure 3-10. A conceptual image of TiO_2-NTs characteristics and binding of cobalt and nicotinate molecule. Cobalt and nitrogen on nicotinate make a polar covalent bond because the electronegativity of cobalt is 1.88 and nitrogen is 3.04 (1.16 difference of electronegativity). This bond is easily released when the VOCs concentration is less.

reduced after quitting the gas flow. Therefore, it is reasonable that the current of nicotinate is reduced when the VOCs concentration is less, and it also implies a TB sensor is reusable. Although the characteristic and mechanism of cobalt-anisate reaction is still being studied by me, the Co-TiO_2-NTs sensor detects anisate similarly to nicotinate detection.

3.3.3 Preparation of volatile biomarkers

3.3.3.1 Requirements of biomarker preparation

There are several necessary factors for efficient biomarker detection experiments using chemical mimics of human exhaled breath. First, nonreactive pure nitrogen gas is required to remove unexpected signals from contamination from other gases and chemicals contained in normal air. Second, water is better than PBS in this experiment. Biomarkers are dissolved in water and diffused and bubbles help to increase diffusivity. PBS, even though it is really similar to human body fluid, contains some chemicals which may react to the Co-TiO_2-NTs. Therefore, water is needed to remove the possibility of contamination. Third, a powdered form of biomarker chemicals should be dissolved in water because this sensing system will analyze the human breath as a sample moisturized from the lung. It is known that water and titanium have some binding affinity. The current change from water is considered as a threshold to calculate extra current signals caused by biomarkers. Last, bubbling is an essential factor to increase the diffusivity of dissolved biomarkers because the vapor pressures of biomarkers are smaller than water: 3.9×10^{-3} atm (400 Pa) for nicotinate, 2.1×10^{-5} atm (2.1 Pa) for anisate, 2.302×10^{-2} atm (2,333 Pa) for water at 20 °C (Table 3-5).

Table 3-5. Vapor pressures of compounds at 20 ºC.

Compounds	**Vapor pressure at 20 ºC**
Nicotinate	3.9×10^{-3} atm (400 Pa)
Anisate	2.1×10^{-5} atm (2.1 Pa)
Water	2.302×10^{-2} atm (2,333 Pa)

3.3.3.2 Biomarkers concentration determination

As Syhre and Chambers reported, about 10-100 times larger concentration of nicotinate is released from *M. tuberculosis* than anisate.[33] Therefore, 100 mM of nicotinate and 2.5 mM of anisate solutions were prepared in the following range because: 1) 2.5 mM is the maximum solubility of anisate in water; 643 mg/l at 20 °C; and 2) 40 times (2.5/100 mM) is reasonably included in the range of 10-100 times release ratio of nicotinate and anisate from pathogen. Interestingly, 2.5 mM of anisate solution (2.1 Pa) has a stronger smell than 100 mM of nicotinate solution (400 Pa) as judged by coworkers in my group.

3.3.3.3 Affinity of water molecule with TiO_2-NTs

Titanium nanotubes are known as having strong binding affinity with water molecules.[69] Thus, the nanotubes need to distinguish the current changes by water and biomarkers. So, three phases of measurements were read: nitrogen gas phase (N_2), moist nitrogen gas phase (H_2O), and moist biomarker containing nitrogen gas phase (nicotinate or anisate).

3.3.4 Results analysis

3.3.4.1 Equation to calculate the relative difference

The potentiostatic scan plot in this experiment consists of a nitrogen gas only region (N_2), vapor of biomarker or water region, and nitrogen gas only region, again (N_2). The signal from the N_2 region indicates the basic conditions of TiO_2-NTs sample such as sensitive as a baseline. Therefore, the current signal from the biomarker region should be

converted to a relative value depending on the baseline. Thus, the current between biomarker and baseline is divided by baseline and this is the relative difference:

$$\boldsymbol{Relative\ difference} = \left|\frac{\boldsymbol{Maximum\ current - Baseline\ (N_2\ gas)}}{\boldsymbol{Baseline\ (N_2\ gas)}}\right| \qquad (3.1)$$

In this test, negative voltage is applied because of the results from the cyclic voltametric scan. Therefore, the measured current should be negative. Sometimes, however, the potential is really close to zero and expanded to the positive area for a little while. Because current is inverse proportion to resistance from ohm's law, V = IR, it implies resistance is extremely high at that moment. The opposite sign of baseline makes negative value of the calculated relative difference. Thus, the whole equation is converted to the absolute value to prevent change of the sign and this does not affect the amount of relative difference.

3.3.4.2 Calculate the relative difference: water

It is known that TiO_2-NTs have sensitivity to water molecules. Therefore, the relative difference for water is another guideline or baseline for volatile biomarkers' relative differences. In Figure 3-11, averaged relative difference of water is -1.16E-08 and this value will be compared with volatile biomarkers. The relative difference calculation of these values is:

$$\boldsymbol{Relative\ difference} = \left|\frac{(\boldsymbol{-1.16E-08}) - (\boldsymbol{-7.09E-11})}{(\boldsymbol{7.09E-11})}\right| = \mathbf{1.63E+02} \qquad (3.2)$$

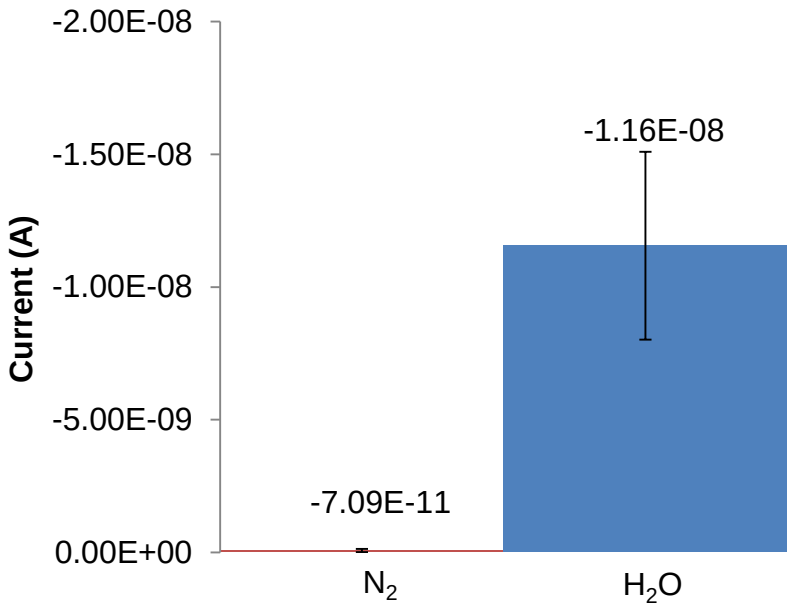

Figure 3-11. The potentiostatic scan result of nitrogen gas and water vapor.

Therefore the final relative difference is 163, and it means that the Co-TiO_2-NTs sample has 163 times larger sensitivity for water than nitrogen gas.

3.3.4.3 Calculate the relative difference: bare TiO_2-NTs

At first, bare TiO_2-NTs are tested to know whether the cobalt ion is necessary to detect biomarkers at -0.8 V. The strongest signals are -68.9 uA for anisate -53.9 uA for water vapor and 65 fA for the baseline (Figure 3-12, A). Therefore, the relative differences are 8.09E+05 for water vapor and 1.06E+06 for anisate. These two values from bare TiO_2-NTs are really close with 1.3 times difference and this ratio supports that copper is necessary to detect anisate (Figure 3-12, B).

3.3.4.4 Calculate the relative difference: inappropriate potential

In the same vein, Co-TiO_2-NTs are tested to know whether potential is a critical factor in detecting biomarkers. The potential to detect anisate is determined as -0.8 volts, so inappropriate voltage (-0.2 V) is chosen and applied in this test. The strongest signals are -808.9 pA for water vapor, -693.7 pA for anisate and 74.5 pA for the baseline (Figure 3-13, A). Therefore the relative differences are 11.9 for water vapor and 10.4 for anisate.

These two values from bare TiO_2-NTs are really close with 1.15 times difference and this ratio supports that voltage is a critical point to detect anisate (Figure 3-13, B).

3.3.4.5 Calculate the relative difference: five main chemicals of breath

Next, mimics of 5 major VOCs contained from healthy human breath are measured and compared with nicotinate and anisate using Co-TiO_2-NTs samples (Figure

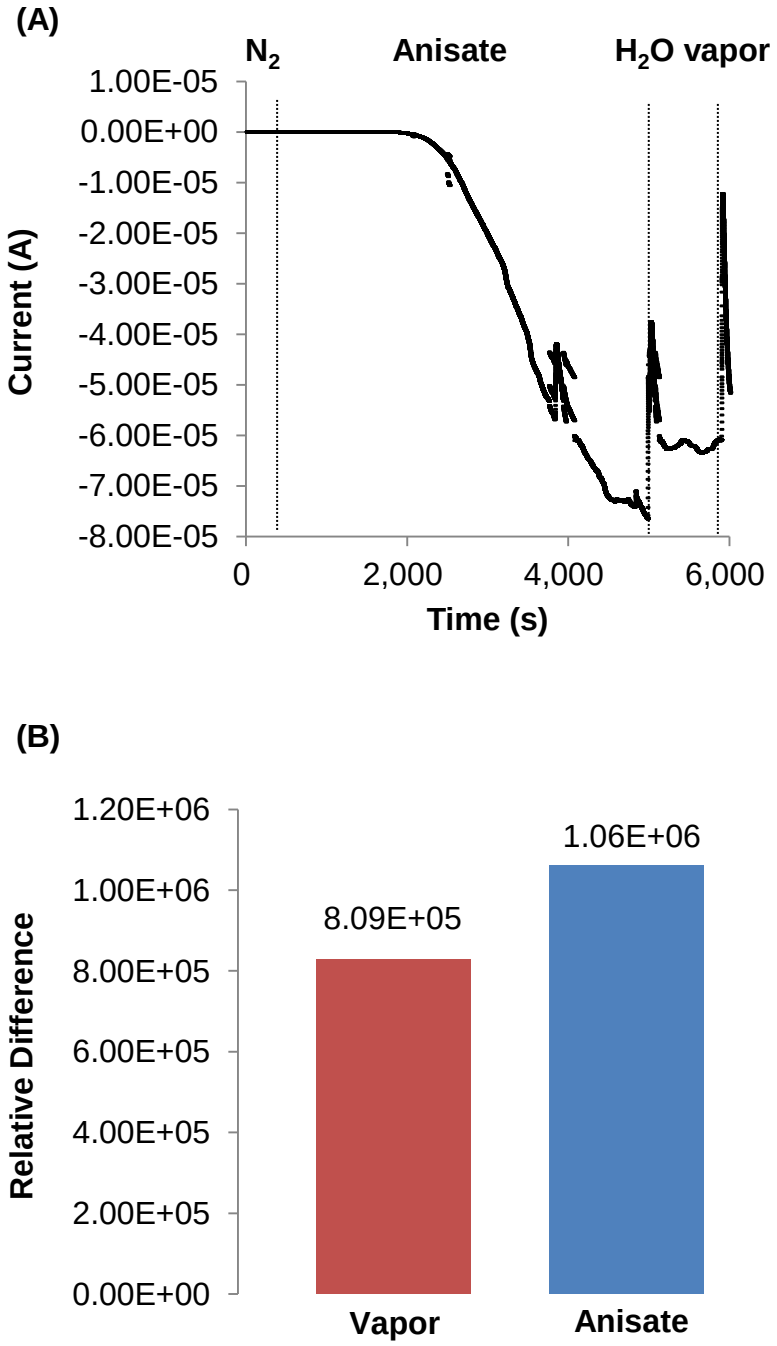

Figure 3-12. The plot of potentiostatic scan to compare water vapor and anisate vapor using bare TiO_2-NTs sample under -0.8 V. (A) The raw plot of potentiostatic scan and (B) the bar graph of the relative differences of vapor and anisate.

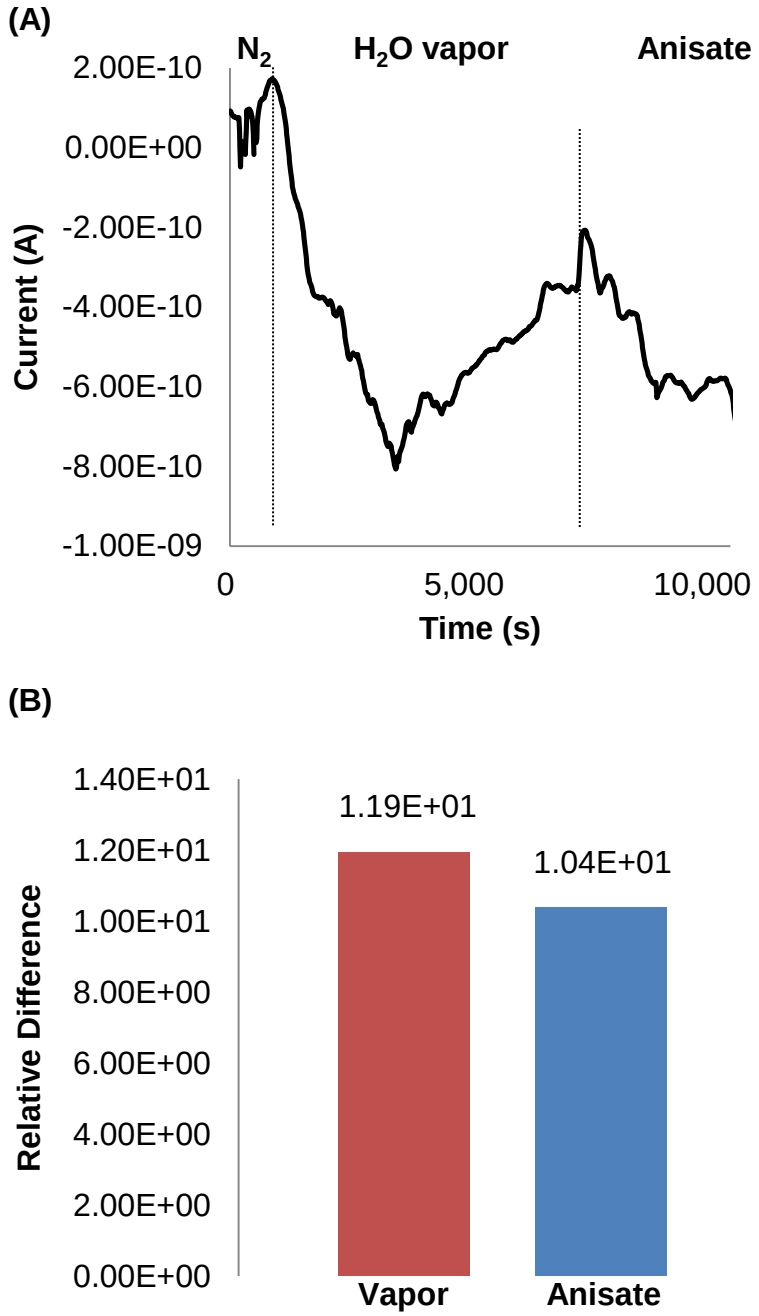

Figure 3-13. The plot of potentiostatic scan to compare water vapor and anisate vapor using Co-TiO_2-NTs sample under -0.2 V, which is inappropriate voltage. (A) The raw plot of potentiostatic scan and (B) the bar graph of the relative differences of vapor and anisate.

3-14, left five bars). Reliable data among 6 trials (3 results from-0.5 volts and 3 results from -0.8 volts) are selected and their relative differences calculated and error bars as shown. The relative differences of VOCs are 4.81E-02, 1.31E+00, 5.51E-01, 3.32E-02, 6.52E+00 for acetone, methanol, ethanol, phenol, and benzene, respectively. Even though benzene shows a little higher than others, these five chemicals seems no significant binding affinity to cobalt. In other words, the 5 major chemicals from normal people could not be detected by Co-TiO_2-NTs.

3.3.4.6 Calculate the relative difference: nicotinate and anisate

The plots of volatile biomarkers show large relative difference values which are 9.19E+02, 3.03E+05, and 7.61E+06 for 10 mM and 100 mM for nicotinate and 2.5 mM of anisate, respectively (Figure 3-14, right three bars). Interestingly, the concentration and vapor pressure of anisate is only 2.5 mM and 2.1 Pa which is smaller than nicotinate at 100 mM and 400 Pa. But the relative difference of anisate is larger than the nicotinate sample. Some possibilities could be that 1) the difference of molecular structure in the chemicals and 2) nicotinate molecule is difficult to bind with cobalt due to its higher vapor pressure.

3.4 Conclusions

Tuberculosis is not a dangerous disease if it is found at an early stage. In other words, its lethality is dramatically increased if there is no cure and process until later stages. Early diagnosis of TB is such an important issue because it prevents unnecessary pain and danger from TB. So far, many different kinds of TB diagnosis methods have

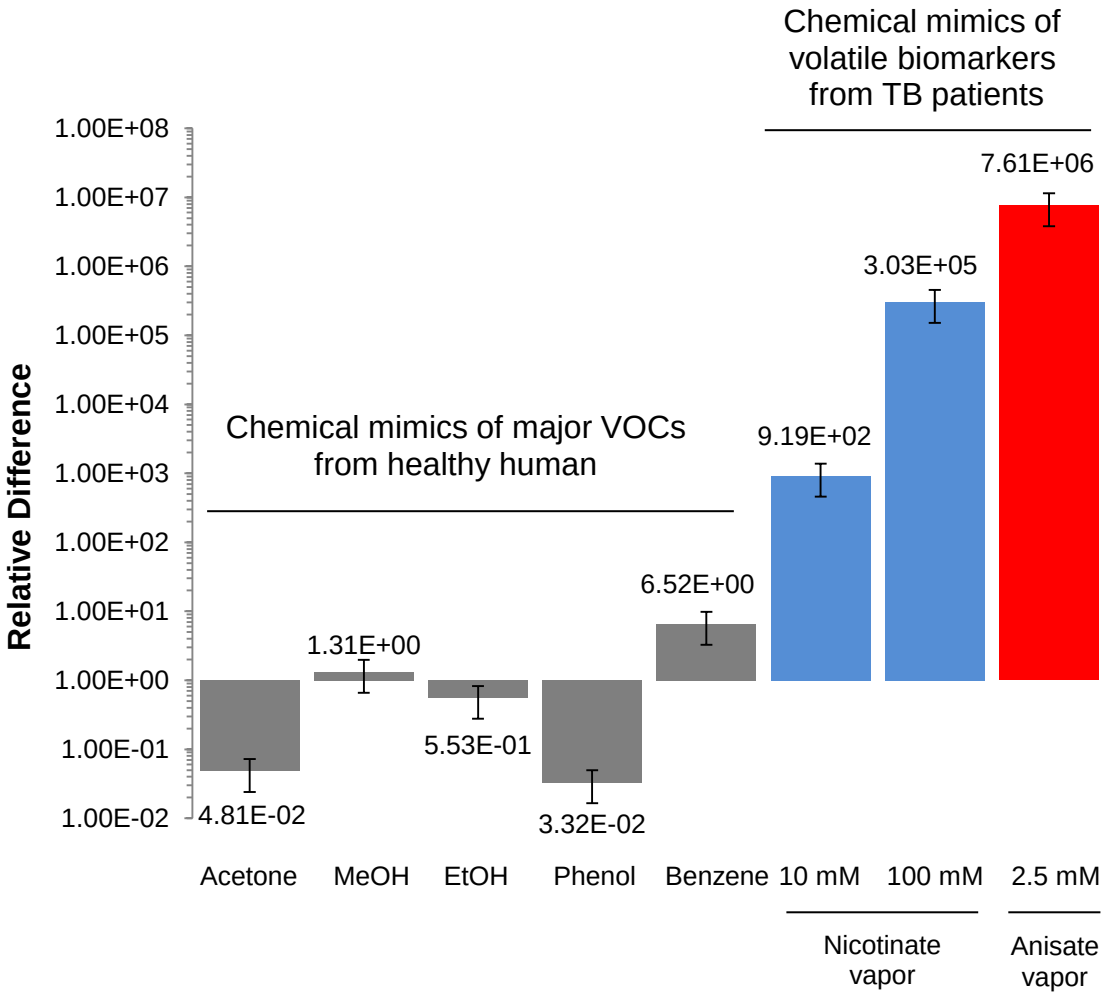

Figure 3-14. The relative differences of 5 major volatile organic compounds that mimic chemicals (left five bars); 10 mM and 100 mM of nicotinate and 2.5 mM of anisate solution (right three bars)

been developed, but most of them need days to weeks preparation time or expensive machines and labor. For these reasons, a new diagnosis tool for TB that is cheaper, faster, and easier is required. In this study, a new detection method of specific volatile biomarkers of Tuberculosis has been suggested to develop faster detection with lower cost POC; my research used cobalt loaded TiO_2-NTs and potentiostatic scan to detect TB.

First, cobalt metal has been functionalized on the TiO_2-NTs surface (Co-TiO_2-NTs). The amount of cobalt was confirmed around 2 wt% by EDX analysis. Cobalt chloride dissolved in ethanol showed better cobalt loading amounts compared to that dissolved in acetone.

Second, two types of control sets have been tested: 1) no cobalt functionalized TiO_2-NTs with appropriate voltage (-0.8 V for anisate) and 2) inappropriate voltage applied to Co-TiO_2-NTs (-0.2 V for anisate). The necessity of cobalt metal functionalization was confirmed from the first test and the requirement of the critical voltage was checked in the second test.

Third, tests were simulated using chemical mimics with nitrogen gas instead of real TB patients' breath in this research. The largest sensing power is 0.3 million for nicotinate and 7.6 million for anisate, respectively, compared with nitrogen gas as a baseline. These enormous current changes seem enough to detect the target VOCs signal from exhaled breath of TB patients. The sensitivity for water is about 160, so that the sensitivity of anisate and nicotinate is greater than water.

This newly tried quick noninvasive point-of-care VOCs sensor research is valuable work because it will make possible quick TB detection and cure patients in the early stages in developing countries. There are some details to be improved to get more

accurate, sensitive, and elaborate detection results in further studies: response time, optimal temperature, specificity for target VOCs, filtration of nontarget VOCs, *et cetera*.

CHAPTER 4

GLUTHATIONE MEASUREMENT USING TITANIUM DIOXIDE NANOTUBES SENSOR FOR DIAGNOSIS OF OXIDATIVE STRESS

4.1 Introduction

Living organisms sustain their lives through metabolism. Metabolism is the general name of chemical transformations within cells. Various byproducts, such as H_2O_2 or reactive oxygen species (ROS), are generated as a result of metabolism. These byproducts are usually strong electron acceptor and have their own function at normal status. The overproduced ROS, however, are removed in order to maintain stable homeostasis of host cells. When the homeostasis is broken by overproduced ROS, it results in oxidation damage to deoxyribonucleic acids (DNA), ribonucleic acids (RNA), phospholipids, enzymes, and proteins causing malfunction of the cell cycle and these lead to cell necrosis.[70, 71] The incidence of high concentration of ROS in cells is called oxidative stress. There are several endogenous and exogenous factors which cause oxidative stress. Cigarette smoke, as an exogenous factor, contains a huge amount of free radicals and breaks down antioxidants such as vitamin C and E.[73, 73] Other examples of oxidative stress initiation are UV,[74-76] lack of methionine,[77] virus or bacterial

infections,[78-80] tissue injury from various factors such as burn or surgery,[81, 82] alcohol,[83-85] physical exercise,[86] and high altitude (hypoxia).[87]

Endogenous factors, for example, are mitochondria, endoplasmic reticulum, NADPH oxidase (NOX) complex, and peroxisome system, and they produce ROS during the reduction of oxygen.[88-90] The oxidative stress in the human body is an important cue of acute diseases such as brain stroke, hyperoxia, and hypertension and chronic diseases such as diabetes and cancer.

Excess ROS is removed by antioxidant molecules such as superoxide dismutase (SOD),[91] glutathione sulfhydryl (GSH),[92, 93] melatonin,[94, 95] vitamin E (tocopherols and tocotrienols),[96-98] vitamin C (ascorbic acid),[99-101] and catalase. The antioxidants are grouped in two categories that contain a thiol group (GSH and thioredoxin) as electron donor and a nonthiol group (vitamins and polyphenols) as a radical chain blocker.[102] Among them, GSH (γ-glutamyl-$_{L}$-cysteinyl-glycine) is one of the most significant molecules to keep intracellular homeostasis at a redox state.[102] GSH is a tripeptide protein that is composed of three kinds of amino acids: glutamate, glycine, and cysteine (as shown in Figure 4-1).[103] GSH is ubiquitous in microorganisms, plants, and animals.[104] As a strong antioxidant, the reduced form of GSH has the ability to donate electrons to ROS and free radicals to remove their toxicity of oxidation capability. Two oxidized GSH molecules become one GSSG (glutathione disulfide) linked with a thiol group (–SH) located on cysteine residue of GSH. Thus, the amount of sulfide in the human body is a limiting element of the synthesis of GSH. The concentration of GSH in healthy people is reported to be 0.684-2.52 mM in blood,[105] 1-10 mM in whole body, and ~10 mM in liver.[104] It is known that 90 % of GSH and 10 % of GSSG exists in a normal human body,

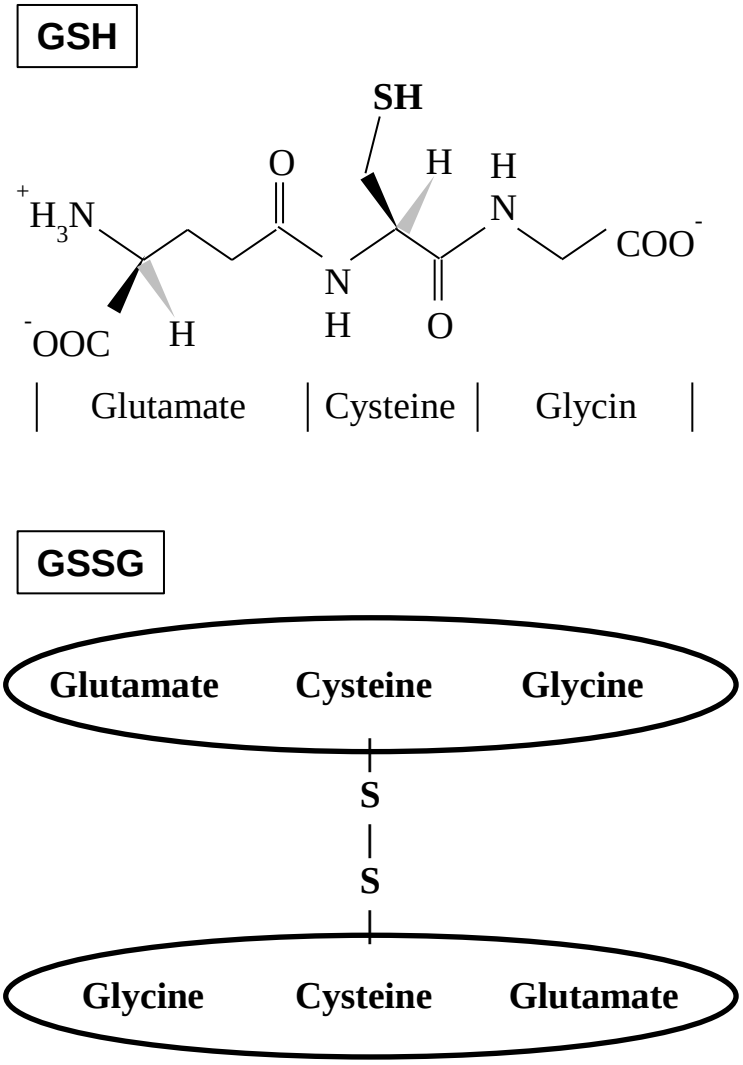

Figure 4-1. GSH and GSSG chemical formula structures. Reduced form GSH (left) has one thiol group at cysteine residue and carboxyl groups at each ends. One GSSG (right) is composed of two oxidized GSHs linked with disulfide bond. The γ-glutamyl residue in GSH is known as a binding site with copper ion.

so the ratio of GSH/GSSG can indicate the level of oxidative stress.[104] Therefore, homeostatic GHS level is an important guideline of detoxification and protection against oxidative stress.

Copper (II) is widely used for the cell physiologic process and cell homeostasis[71, 106-108] and its binding mechanism and affinity with GSH has been reported.[109, 110] It is also found that the binding of copper and GSH makes two tetragonal structures in the appropriate pH solution.[71] Therefore, the copper-glutathione coupling mechanism is regarded as a promising candidate for GSH selective detection platform.

Since the oxidative stress is considered as a potential factor causing many diseases from acute to chronic ones, the measurement of the ratio of GSH/GSSG levels in the body are an indicator of oxidative stress and a real-time diagnosis and point-of-care detection tool. In other words, higher GSSG concentration means that higher amounts of ROS are removed. Therefore, the relative concentration of GSH and GSSG and the ratio of GSH/GSSG in the body can indicate the risk of oxidative stress. Workers in critical and limited circumstance such as airplane pilots, astronauts, submarine crews, and soldiers especially need to monitor their vital signs for safety. Therefore, the research and development of GSH detectable specific biosensing platform using safe material as a point-of-care type kit is a detection method in high demand.

Titanium dioxide nanotubes (TiO_2-NTs) have high surface area as a structural property and therefore are considered a good material for a sensing platform because 1) the extremely enlarged surface area of nanotubes increases the signal changes and 2) titanium is usually applied as a biomaterial with a lack of allergenicity.[111] In this study, I

combined these beneficial characteristics; copper ions are functionalized on the TiO_2-NTs (Cu-TiO_2-NTs) to selectively detect glutathione molecules.

In the present study I established a hypothesis that copper functionalized TiO_2-NTs can selectively bind with glutathione molecules and I examined the binding affinity using cyclic voltametry (CV) test with a potential window of -300 mV to 300 mV for copper. So far this kind of experiment has not been tried, it is not in the literature, and in that respect my study is worthy of development.

4.2 Materials and methods

4.2.1 Preparation of TiO_2-NTs and copper functionalization

A 10 mm × 10 mm size of titanium foil was cut, polished, and rinsed in isopropanol in ultrasonic bath for 5 minutes. Electrolyte for anodization was prepared with 0.5 w/v% of ammonium fluoride (NH_4F, Alfa Aesar, USA) dissolved in 3 % DI water in ethylene glycol (EG, $C_2H_6O_2$, Alfa Aesar, USA). Platinum coil served as a cathode and titanium foil served as an anode side in an EG solution applying 30 volts of direct current (DC) for 1h. Nanotube fabricated titanium samples were rinsed in deionized water for 5 seconds in an ultrasonic bath then dried in a 110 °C chamber at least 1 day. Samples were annealed under an oxygen rich circumstance to crystalize the anatase structure from amorphous TiO_2 at 500 °C for 2 h.

For metal functionalization, anatase nanotube samples dipped in three different copper salt solutions were prepared using 0.32 g of $CuSO_4$ $5H_2O$ in 50 ml of DI water and 0.41 g of $Cu(NO_3)_2$ $5H_2O$ and 0.2 g of $CuCl_2$ in 50 ml of ethanol. All metal salt was purchased from Alfa Aesar, USA. These samples in solution were incubated in an

ultrasonic bath for 30 minutes. Samples were rinsed in DI water with 3 seconds of ultrasonication then dried in a 110 °C chamber for 1 day. The morphologies of nanotubes were observed using scanning electron microscopes (SEM, Hitachi S-4800) with various magnifications from 10,000 times to 500,000 times. The amount of functionalized copper on TiO_2-NTs was analyzed using an energy dispersed X-ray spectroscope (EDX, Oxford Ins., UK).

4.2.2 Preparation of GSH and GSSG

Molecular weight of GSH (CAS: 70-18-8, Sigma Aldrich, USA) and GSSG (CAS: 27025-41-8, Sigma Aldrich, USA) are 307.32 g/mol and 612.63 g/mol, respectively. These compounds were dissolved as 100 mM in DI water for stock solution and diluted as 1 mM for tests.

4.2.3 CV measurements

CV software was adapted from Reference 600^{TM}, GAMRY system. A platinum wire served as a counter electrode and an Ag/AgCl electrode served as a reference electrode, and a copper decorated TiO_2-NTs sample, with a working electrode, was connected. Potential windows were from -300 millivolts to 300 millivolts with 10 millivolts *per* second of scan rate. Current plots of CV were obtained from pure 30 ml of DI water, GSH, and GSSG, in turn. All equipment in the CV tests was rinsed using DI water after every reading for stringency. Measured current data were converted to current density ($A \cdot cm^{-2}$) for comparison. The minimum values of current density at the moment of -300 mV were displayed using bar graphs with reverse order of the Y-axis for

convenience. All multiple data were averaged with error bars.

4.2.4 Preliminary test using real saliva and CV test

For quick and brief preliminary test for real saliva, a method of saliva sample preparation was established:

1. Do not eat anything 2 h before from sampling to prevent any possibility of contamination such as chemicals and spices.
2. Clean mouth more than 3 times gargling using tap water.
3. Prepare 50 ml of DI water in disposal cup.
4. Keep whole (50 ml) water in mouth and sit calmly for 30 seconds.
5. Spit the fluid back into the cup trying to minimize bubbles in the mouth.
6. Filter the fluid using 0.2 μm pore size syringe filter.
7. Measure as soon as possible.

Prepared saliva sample was measured through CV using the same method. Bare TiO_2-NTs and Cu-TiO_2-NTs samples were used and compared for the saliva sample and DI only sample.

4.2.5 GSH dose-dependent CV tests

Four different concentrations (0, 0.1, 1, and 10 mM) of GSH solutions were prepared to measure the pattern of current increase by GSH concentration change. Cu-TiO_2-NTs samples were prepared in different batches, so the amount of loaded copper was 1.32 wt%, which is less than the 5.4 wt% for previous tests. The potential window was narrowed as -200 mV to 0 mV for testing convenience. All values at the moment of

-200 mV were obtained, averaged, and plotted for comparison.

4.3 Results and discussions

4.3.1 Functionalization test of copper

The three different copper salts, $CuSO_4$, $Cu(NO_3)_2$, and $CuCl_2$, were used for depositing on the TiO_2-NTs surface. The shapes of copper on the surface of nanotubes are different depending on the kind of copper salt. Through the SEM image (Figure 4-2), the structure of copper sulfate shows needle shapes of around 500 micrometers length on TiO_2-NTs surface with 5.46 wt% of copper content by EDX analysis (Table 4-1). Comparatively, the shapes of functionalized copper nitrate are a mass of tiny particles distributed on the nanotube surface with 1.56 wt% copper contents. Copper chloride are 100 nanometers diameter particles spread on the nanotube surface with 0.97 wt% copper contents. Because the EDX cannot analyze the whole sample area of 1 cm × 1 cm, the most reasonable regions were selected and analyzed. By these results, copper sulfate is considered as the best candidate of functionalization material because of its increased surface area by needle shape, the highest amount of copper loading, and more even and wide distribution of copper on TiO_2-NTs surface than others in the SEM image analysis.

4.3.2 CV tests for glutathione chemicals

The redox potential of GSH/GSSG exists roughly between -350 mV and 40 mV range according to a literature search.[112-115] Not only the oxidation of GSH, but the oxidation of copper is an issue for CV tests because their redox potentials affect oxidation status. showed needle shape, fine mud shape, and particle shape from $CuSO_4$, $Cu(NO_3)_2$,

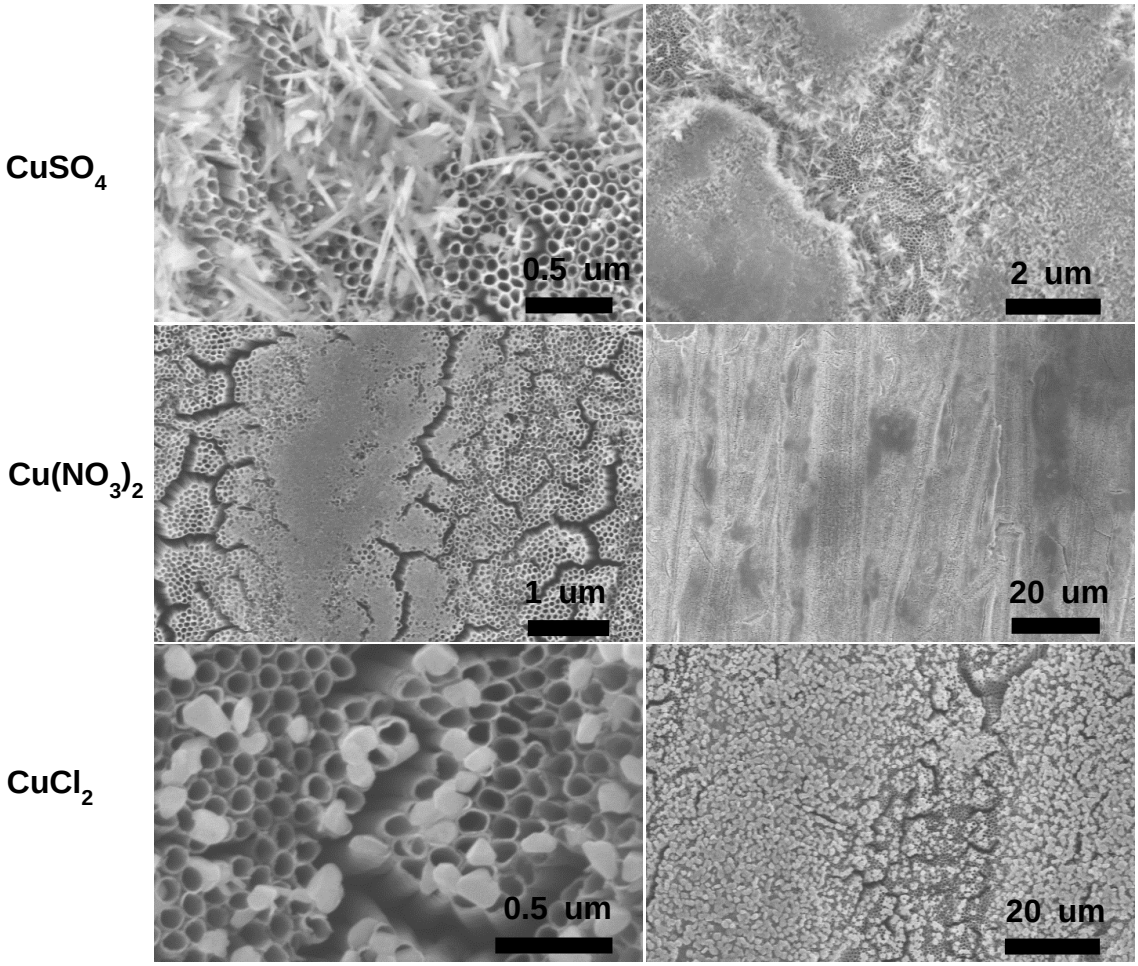

Figure 4-2. TiO_2-NTs samples after functionalization with $CuSO_4$, $Cu(NO_3)_2$, $CuCl_2$, and $CoCl_2$. Functionalization was performed using solution of 0.24 g, 0.28 g, and 0.2 g of $CuSO_4$, $Cu(NO_3)_2$, and $CuCl_2$ dissolved in 50 ml of ethanol, respectively, then incubated in ultrasonic bath for 30 minutes. SEM images were taken at higher magnification (left) and lower magnification (right) for comparison. The morphology of functionalization

Table 4-1. EDX results of functionalization of each copper salt.

Compounds	**Elements**	**wt%**
$CuSO_4$	S	1.23
	Ti	54.01
	Cu	**5.46**
	O	39.30
$Cu(NO_3)_2$	Ti	58.22
	Cu	**1.56**
	O	39.72
$CuCl_2$	Ti	58.74
	Cu	**0.97**
	O	39.86

and $CuCl_2$, respectively.

In reality, the current density values at -0.3 V are continuously decreased after every cycle (Figure 4-3). However, the redox potential is not considered a problem because the purpose of this study is to analyze the binding pattern between copper and GSH/GSSG molecules. Therefore, measured currents from the first cycle of CV are enough for evaluative purposes. Thus, the reduction or oxidation of GSH after the first cycle of CV tests need not be considered. After testing several voltage windows, the potential range for CV were determined between -0.3 volts and 0.3 volts. The reduction/oxidation issue in this study will be improved in a future study.

Concentration of GSH solution for the experiment was determined as 1 mM since the concentration of GSH in blood is between 0.68-2.52 mM.[105] GSSG solution is prepared as 1 mM for a convenient comparison even though it is known to exist as ~10 % of GSH concentration at homeostasis.

4.3.2.1 Glutathione binding with bare TiO_2-NTs

In Figure 4-4, current density values at the moment of -300 mV of CV were compared. The current densities were -17 $\mu A/cm^2$ and -31.3 $\mu A/cm^2$ for GSH and GSSG for bare TiO_2-NTs. Table 4-2 shows that the ratio of measured current of GSSG/GSH from nonfunctionalized TiO_2-NTs samples was 1.87 (-3.13E-05 / -1.7E-05, 4.1).

$$\frac{GSSG_{Bare}}{GSH_{Bare}} = \frac{\text{-3.13E-05}}{\text{-1.7E-05}} = 1.87 \qquad (4.1)$$

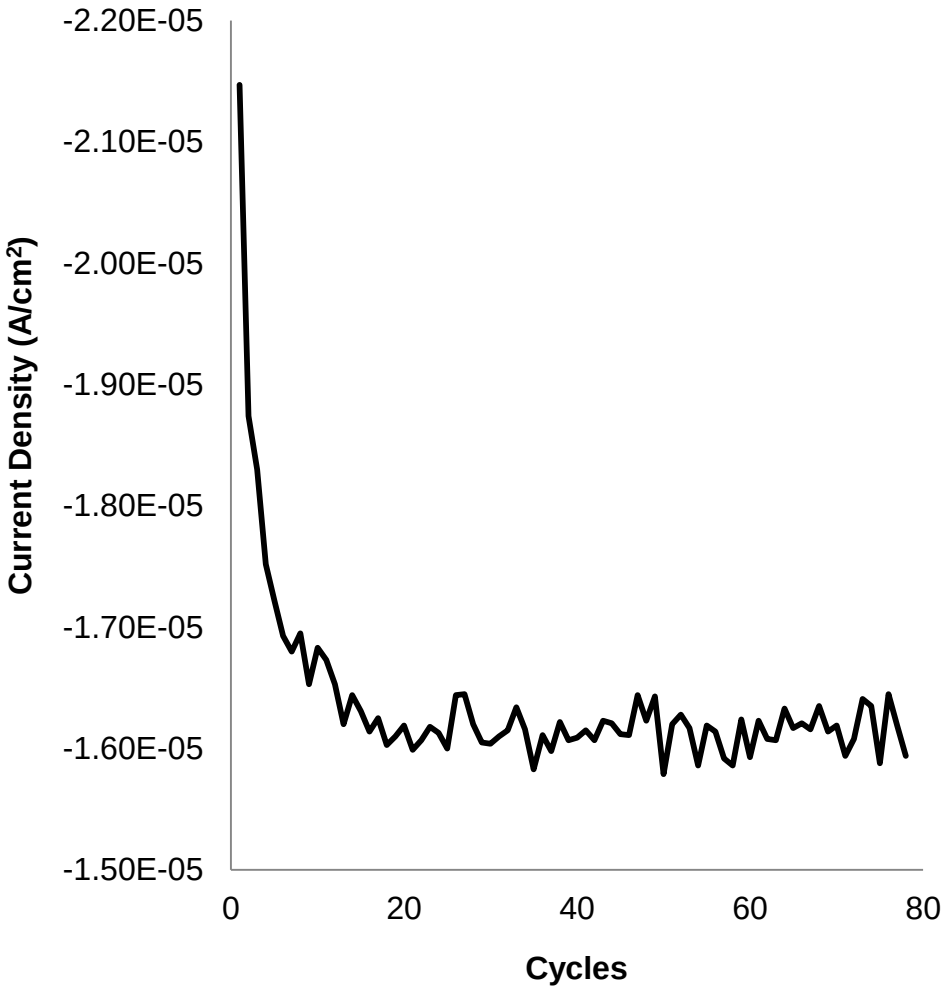

Figure 4-3. The current density at -0.3 V from multiple cycles of CV. The current signal is decreased as cycles go by. It is dramatically decreased from the 1st cycle to the 7th cycle and stable after the 8th cycle of CV.

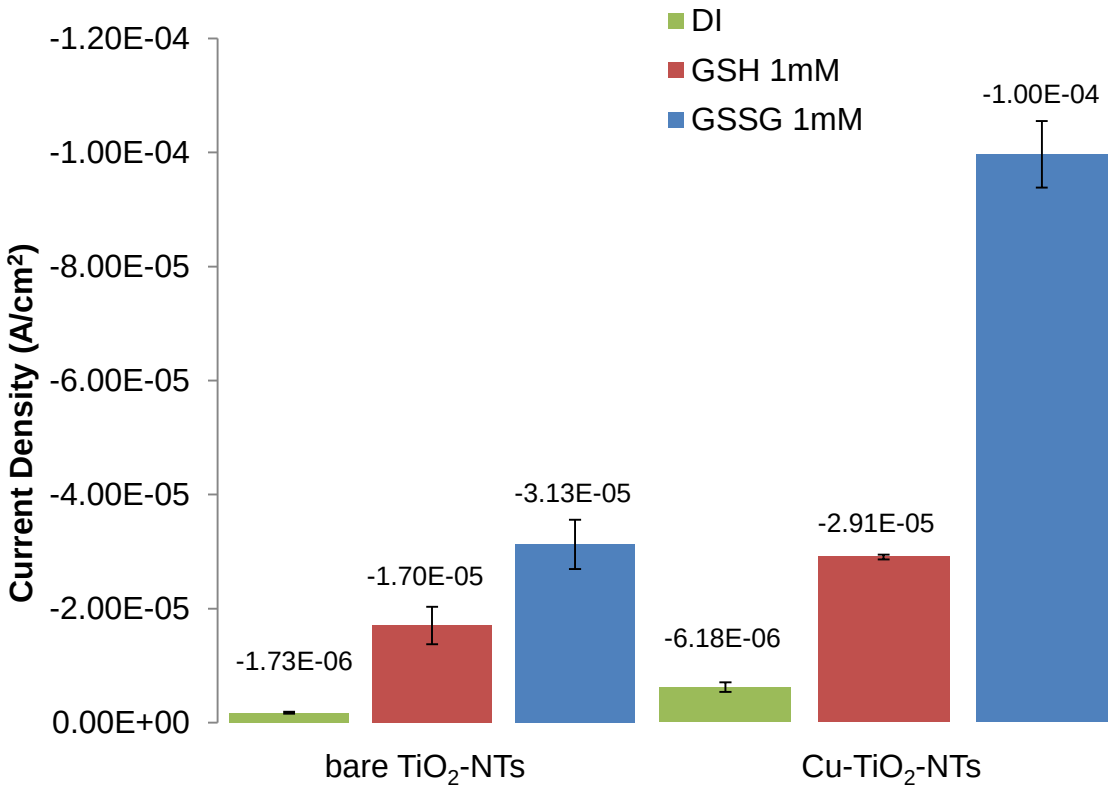

Figure 4-4. CV measurements of GSH and GSSG using $CuSO_4$ functionalized TiO_2-NTs. Range of cyclic voltametric scan is from -300 mV to 300 mV with 10 mV/s of scan rate. All values recorded the minimum current at the moment of -300 millivolts of CV and converted to current density. Left three bars are current density from bare TiO_2-NTs and right bars are Cu-TiO_2-NTs. From left to right, DI, 1 mM of GSH, and 1 mM of GSSG are displayed, respectively.

Table 4-2. The ratio of CV results of bare TiO_2-NTs samples in 1 mM of GSSG and GSH solution.

Glutathiones	**Ratio**
$GSSG_{Bare}$ / GSH_{Bare}	1.87

4.3.2.2 Glutathione binding with Cu-TiO_2-NTs

As compared with the results of bare TiO_2-NTs, copper loaded TiO_2-NTs show higher signal than without copper samples. The current densities were -29.1 μA/cm^2 and -100 μA/cm^2 for GSH and GSSG for Cu-TiO_2-NTs. The GSSG/GSH ratio is 3.43 (-1.00E-04 / -2.91E-05, 4.2); that is larger than bare TiO_2-NTs and it indicates the selectivity of copper for glutathione (Table 4-3).

$$\frac{GSSG_{Cu}}{GSH_{Cu}} = \frac{\text{-1.00E-04}}{\text{-2.91E-05}} = 3.43 \qquad (4.2)$$

It has been known that a carboxyl group at gamma-glutamate residue of GSH is the binding site of copper,[109] thus it is expected that GSSG should show about 2 times higher binding affinity than GSH for copper.

4.3.2.3 GSSG signal strength to copper

Interestingly, the ratio of GSSG current at copper present and absent shows 3.19 (-1.00E-04 / -3.13E-05, 4.3). The measured current of GSSG between without-copper and with-copper shows more than 3 times difference and it implies that copper plays a role in increasing current for GSSG. Although the ratio of signals from GSH without and with copper is 1.71 (-2.91E-05 / -1.70E-05, 4.4), GSSG shows different current ratio pattern with immobilized copper (Table 4-4).

Table 4-3. The ratio of CV results of Cu-TiO_2-NTs samples in 1 mM of GSSG and GSH solution.

Glutathiones	**Ratio**
$GSSG_{Cu}$ / GSH_{Cu}	3.43

Table 4-4. Comparison of the ratios of measured currents between Cu-TiO_2-NTs with GSH and bare TiO_2-NTs with GSH solution, and Cu-TiO_2-NTs with GSSG and bare TiO_2-NTs with GSSG solution.

Glutathiones	**Ratio**
$GSSG_{Cu}$ / $GSSG_{Bare}$	3.19
GSH_{Cu} / GSH_{Bare}	1.71

$$\frac{GSSG_{Cu}}{GSSG_{Bare}} = \frac{-1.00E-04}{-3.13E-05} = 3.19 \quad (4.3)$$

$$\frac{GSH_{Cu}}{GSH_{Bare}} = \frac{-2.91E-05}{-1.70E-05} = 1.71 \quad (4.4)$$

In addition, the molar ratio of glutathione to copper is roughly 100:7 in this study since the immobilized copper (~5 wt%) is calculated as ~70 μM and dissolved glutathione is 1 mM. Therefore, the substrate (glutathione) is more than enough to saturate the binding capacity of copper.

The increase of the overall current density when copper is deposited on the TiO_2-NTs surface further supports that copper metal has a binding affinity for glutathione molecules. The currents of DI from bare TiO_2-NTs and Cu-TiO_2-NTs show not a small difference, which might be affected by unexpected contamination of experimental equipment during several tests (Figure 4-4). But this small error does not affect to other big current values.

4.3.3 Preliminary CV test of real saliva

Because the method of saliva sample preparation has not been well established for GSH sensing experiment, a brief method was designed for this preliminary test. Since it is commonly known that saliva is secreted at 1.5 liters *per* day, it could be assumed that 500 μl of saliva is contained in the prepared sample in this experiment (1500 ml / 24 h / 60 m = 1.04 ml/m = 0.5 ml *per* 30 s). Thus, the dilution factor of saliva is expected to be 0.01 (0.5 ml saliva / 50 ml DI water).

The results finally tell us that the Cu-TiO_2-NTs sample shows higher signal than bare TiO_2-NTs, for real saliva. The measured currents are -1.38E-05 and -3.11E-05 from bare TiO_2-NTs and Cu-TiO_2-NTs, respectively (Figure 4-5). The ratio of Cu-TiO_2-NTs and bare TiO_2-NTs for saliva sample is 2.25 (-3.11E-05 / -1.38E-05, 4.5).

$$\frac{\text{Saliva}_{Cu}}{\text{Saliva}_{Bare}} = \frac{\text{-3.11E-05}}{\text{-1.38E-05}} = 2.25 \qquad (4.5)$$

To quickly estimate the concentration of glutathione in a real saliva sample, the measured currents from bare TiO_2-NTs for GSH and saliva samples are compared, because GHS is expected to have the most portions of glutathione molecules in saliva, not GSSG. The currents are -29.1 μA and -13.8 μA for GSH and saliva, respectively (Table 4-5), and the measured current from saliva is about half that from 1 mM of GSH. Because the saliva sample is 100 times diluted, the theoretical concentration could be 0.01 mM because of 1 mM of GSH in body fluid. The ionic strength of normal saliva is presumed as 0.01-0.05 mM after 100 times dilution.[116] Therefore, the saliva sample may contain less than 0.1 mM of chemicals by these calculations, but the actual current measurement shows half current strength of 1 mM GSH. From this result, additional unknown chemical reactions seem to have possibly occurred in the real saliva sample and it also needs further study.

4.3.4 GSH dose dependent current changing pattern

Figure 4-6 shows that the pattern of current density changing is affected by the concentration of substrate, GSH or GSSG, in this experiment. From all CV results, the

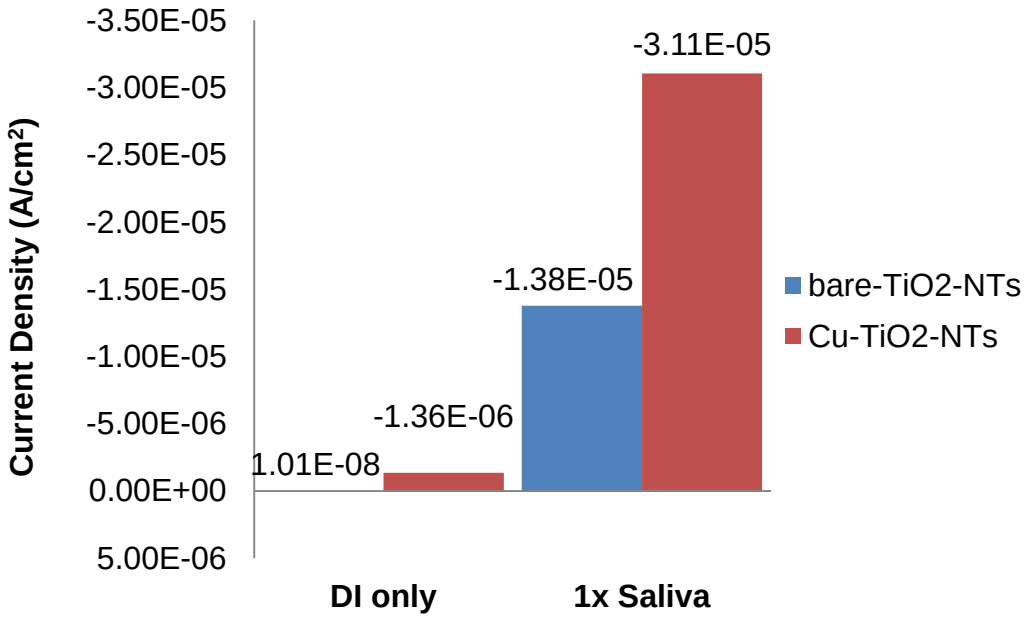

Figure 4-5. CV measurement of real saliva sample (1:100 diluted with DI water). Current value was obtained at the moment of -300 mV of the first cycle for each CV scan. Signal shows 2.25 times difference between bare and copper loaded TiO_2-NTs. Left two bars express the measured currents from DI water and right two bars are for 1 / 100 diluted real saliva sample. Blue bars are the value of bare TiO_2-NTs and red bars are the value of Cu-TiO_2-NTs.

Table 4-5. The ratio of measured currents between Cu-TiO_2-NTs and bare TiO_2-NTs using real saliva (1 / 100 diluted in water) sample.

Glutathiones	**Ratio**
$Saliva_{Cu}$ / $Saliva_{Bare}$	2.25

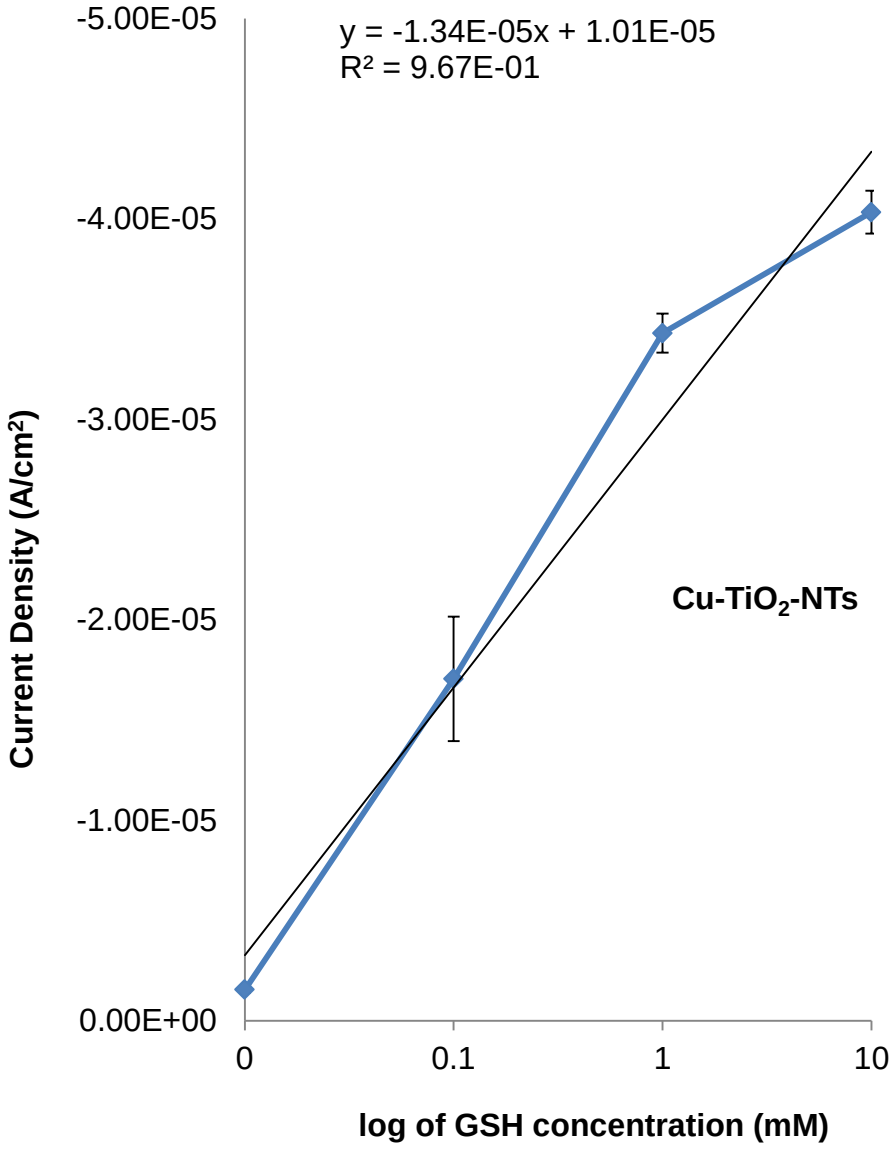

Figure 4-6. The pattern of current density depending on concentration of GSH. The signals were obtained and plotted at the moment of -200 mV from all CV cycles. The signal is linearly increased for the X-axis of the logarithmic scale of GSH concentration from 0 to 10 mM.

current density values were obtained at the moment of -200 mV and plotted for comparison. The concentration of substrate (X-axis) has a proportionally increased current density (Y-axis).

The plot of the Cu-TiO_2-NTs sample from the new batch (1.32 wt% of copper loaded) shows -1.34E-05 of slope with 0.967 of R^2 value. These results support that the current signal is proportional to the logarithmic increase of GSH concentration.

4.4 Conclusions

In this work, we have examined the binding affinity between copper and reduced and oxidized glutathione. First, we have observed the different appearance of copper salts ($CuCl_2$, $CuSO_4$, and $Cu(NO_3)_2$) for metal functionalization on TiO_2-NTs using the same protocol. Nanostructure of copper sulfate was considered to be beneficial to the sensing mechanism in comparison to copper chloride and copper nitrate for three reasons: highest amount (5.4 wt%), needle shape for enlarged surface area, and most equal distribution on the whole sample area.

Second, we have presented the sensing response of metal and glutathione molecules. Definitely, copper metal shows a higher binding for GSSG and GSH than nonmetal loaded TiO_2-NTs. The measured current density for GSSG of Cu-TiO_2-NTs was -100 μA and this current was 3.43 times larger than GSH of Cu-TiO_2-NTs and 3.14 imes larger than GSSG of bare TiO_2-NTs. These results supported that copper pulls the glutathione selectively.

As a result, we have confirmed the possibility of the glutathione sensing platform using TiO_2-NTs system. Future studeis will focus on finding a better potential

window for CV tests for more stable current detection, exploring better metal candidates for sensing, improving the questionable binding strength of immobilization of metals, and refining the sample preparation method for the real saliva test. After improving these points, the glutathione detectable sensing platform will be established for detecting oxidative stress with individual point-of-care tools and alerting people of potential risks or problems.

CHAPTER 5

FUTURE STUDIES

5.1 Organic/inorganic binding mechanism

The binding mechanism between functionalized metal on TiO_2-NTs and biomarkers needs to be studied in order to clearly understand the weak binding process of biomarkers in humid air.

5.2 Improvement of sensitivity for breath analyzer sensing platform

Other metal candidates for functionalization are required in order to study and improve the selective detection of specific biomarkers. Nickel, chromium, copper, and zinc are considered as the next metal-organic compound binding materials to be studied. Also, the functionalization method should be studied to control the amount of metal loaded, so there is less damage on TiO_2-NTs.

REFERENCES

1. Iijima, S., Helical Microtubules of Graphitic Carbon. *Nature* **1991,** *354*, 56-58

2. McAlpine, M. C.; Ahmed, H.; Wang, D.; Heath, J. R., Highly Ordered Nanowire Arrays on Plastic Substrates for Ultrasensitive Flexible Chemical Sensors. *Nature Materials* **2007,** *6*, 379-384

3. Lieber, C. M., One-Dimensional Nanostructures: Chemistry, Physics & Applications. *Solid State Communications* **1998,** *107*, 607-616

4. Zhang, Y. X.; Li, G. H.; Jin, Y. X.; Zhang, Y.; Zhang, J.; Zhang, L. D., Hydrothermal Synthesis and Photoluminescence of TiO_2 Nanowires. *Chemical Physics Letters* **2002,** *365* (3–4), 300-304

5. Li, D.; Xia, Y., Fabrication of Titania Nanofibers by Electrospinning. *Nano Letters* **2003,** *3* (4), 555-560

6. Wen, B.; Liu, C.; Liu, Y., Controllable Synthesis of One-dimensional Single-crystalline TiO_2 Nanostructures. *Chemistry Letters* **2005,** *34* (3), 396-397

7. Xie, R.-C.; Shang, J., Morphological Control in Solvothermal Synthesis of Titanium Oxide. *J Mater Sci* **2007,** *42* (16), 6583-6589

8. Yoshida, R.; Suzuki, Y.; Yoshikawa, S., Syntheses of TiO_2(B) Nanowires and TiO_2 Anatase Nanowires by Hydrothermal and Post-heat Treatments. *Journal of Solid State Chemistry* **2005,** *178* (7), 2179-2185

9. Daoud, W. A.; Pang, G. K. H., Direct Synthesis of Nanowires with Anatase and TiO_2-B Structures at near Ambient Conditions. *The Journal of Physical Chemistry B* **2006,** *110* (51), 25746-25750

10. Amin, S. S.; Nichllas, A. W.; Xu, T. T., A Facile Approach to Synthesize Single-crystalline Rutile TiO_2 One-dimensional Nanostructures. *Nanotechnology* **2007,** *18* (44), 1-5

11. Ideta, T.; Yamazaki, M.; Kudou, S.; Higashida, M.; Mori, S.; Kaneda, T.; Nakazawa, M., Investigation of Radio Frequency Heating of Dental Implants Made of Titanium in 1.5 Tesla and 3.0 Tesla Magnetic Resonance Procedure: Measurement of the

Temperature by Using Tissue-equivalent Phantom. *Nihon Hoshasen Gijutsu Gakkai zasshi* **2013,** *69* (5), 521-528

12. Mobilio, N.; Stefanoni, F.; Contiero, P.; Mollica, F.; Catapano, S., Experimental and Numeric Stress Analysis of Titanium and Zirconia One-piece Dental Implants. *The International Journal of Oral & Maxillofacial Implants* **2013,** *28* (3)

13. Farsinezhad, S.; Mohammadpour, A.; Dalrymple, A. N.; Geisinger, J.; Kar, P.; Brett, M. J.; Shankar, K., Transparent Anodic TiO_2 Nanotube Arrays on Plastic Substrates for Disposable Biosensors and Flexible Electronics. *Journal of Nanoscience and Nanotechnology* **2013,** *13* (4), 2885-2891

14. Kwen, H. D.; Yang, H. S.; Lee, I. H.; Choi, S. H., Fabrication of Non-enzymatic Biosensor Based on Metallic Catalyst-TiO_2 Hollow Sphere Nanocomposite for Determining Biomolecules. *Journal of Nanoscience and Nanotechnology* **2012,** *12* (7), 5216-5221

15. Zhang, X.; Wang, H.; Yang, C.; Du, D.; Lin, Y., Preparation, Characterization of Fe_3O_4 at TiO_2 Magnetic Nanoparticles and Their Application for Immunoassay of Biomarker of Exposure to Organophosphorus Pesticides. *Biosensors & Bioelectronics* **2013,** *41*, 669-674

16. Zong, X. L.; Wu, C. S.; Wu, X. L.; Lu, Y. F.; Wang, P., A Non-labeled DNA Biosensor Based on Light Addressable Potentiometric Sensor Modified with TiO_2 Thin Film. *Journal of Zhejiang University. Science. B* **2009,** *10* (11), 860-866

17. Gao, Z. D.; Guan, F. F.; Li, C. Y.; Liu, H. F.; Song, Y. Y., Signal-amplified Platform for Electrochemical Immunosensor Based on TiO_2 Nanotube Arrays Using a HRP Tagged Antibody-Au Nanoparticles as Probe. *Biosensors & Bioelectronics* **2013,** *41*, 771-775

18. Marchand, R.; Brohan, L.; Tournoux, M., TiO_2(B) A New Form of Titanium Dioxide and The Potassium Octatitanate $K_2Ti_8O_{17}$. *Materials Research Bulletin* **1980,** *15* (8), 1129-1133

19. Roy, P.; Berger, S.; Schmuki, P., TiO_2 Nanotubes: Synthesis and Applications. *Angewandte Chemie International Edition* **2011,** *50* (13), 2904-2939

20. Santos, C. X. C.; Anjos, E. I.; Augusto, O., Uric Acid Oxidation by Peroxynitrite: Multiple Reactions, Free Radical Formation, and Amplification of Lipid Oxidation. *Archives of Biochemistry and Biophysics* **1999,** *372* (2), 285-294

21. Vu, N. H.; Le, H. V.; Cao, T. M.; Pham, V. V.; Le, H. M.; Nguyen-Manh, D., Anatase-Ruitle Phase Transformation of Titanium Dioxide Bulk Material: A DFT + U approach. *Journal of Physics: Condensed Matter* **2013,** *24* (40), 1-10

22. Jiang, Z.; Yang, F.; Luo, N.; Chu, B. T. T.; Sun, D.; Shi, H.; Xiao, T.; Edwards, P. P., Solvothermal Synthesis of N-doped TiO_2 Nanotubes for Visible-light-responsive Photocatalysis. *Chemical Communications* **2008,** *0* (47), 6372-6374

23. Macak, J. M.; Sirotna, K.; Schmuki, P., Self-organized Porous Titanium Oxide Prepared in Na_2SO_4/NaF Electrolytes. *Electrochimica Acta* **2005,** *50* (18), 3679-3684

24. Yan, J.; Zhou, F., TiO_2 Nanotubes: Structure Optimization for Solar Cells. *Journal of Materials Chemistry* **2011,** *21* (26), 9406-9418

25. Beranek, R.; Hildebrand, H.; Schmuki, P., Self-organized Porous Titanium Oxide Prepared in H_2SO_4/HF Electrolytes. *Electrochemical Solid-State Letter* **2003,** *6* (3), B12-B14

26. Yasuda, K.; Schmuki, P., Control of Morphology and Composition of Self-organized Zirconium Titanate Nanotubes Formed in $(NH_4)_2SO_4/NH_4F$ Electrolytes. *Electrochimica Acta* **2007,** *52* (12), 4053-4061

27. Macak, J. M.; Hildebrand, H.; Marten-Jahns, U.; Schmuki, P., Mechanistic, Aspects and Growth of Large Diameter Self-organized TiO_2 Nanotubes. *Journal of Electroanalytical Chemistry* **2008,** *621*, 254-266

28. Albu, S. P.; Ghicov, A.; Aldabergenova, S.; Drechsel, P.; LeClere, D. T., G. E.; Macak, J. M.; Schmuki, P., Formation of Double-walled TiO_2 Nanotubes and Robust Anatase Membranes. *Advanced Matererial* **2008,** *20* (21), 4135-4139

29. Raja, K. S.; Misra, M.; Paramguru, K., Formation of Self-ordered Nano-tubular Structure of Anodic Oxide Layer on Titanium. *Electrochimica Acta* **2005,** *51* (1), 154-165

30. Alatraktchi, F. A. a.; Zhang, Y.; Noori, J. S.; Angelidaki, I., Surface Area Expansion of Electrodes with Grass-like Nanostructures and Gold Nanoparticles to Enhance Electricity Generation in Microbial Fuel Cells. *Bioresource Technology* **2012,** *123* (0), 177-183

31. Kim, D.; Chicov, A.; Schmuki, P., TiO_2 Nanotube arrays: Elimination of Disordered Top Layers ("Nnograss") for Improved Photoconversion Efficiency in Dye-sensitized Solar Cells. *Electrochemistry Communications* **2008,** *10*, 1835-1838

32. Wang, Y.; Guo, M.; Zhang, M.; Wang, X., Facile Syntehsis of SnO_2 Nanograss Array Films by Hydrothermal Methods. *Thin Solid Films* **2010,** *518*, 5098-5103

33. Vaenas, n.; Stergiopoulos, T.; Kontos, A. G.; Likodimos, V.; Boukos, N.; Falaras, P., Sensitizer Activated Solar Cells Based on Self-organized TiO_2 Nanotubes. *Microelectronic Engineering* **2012,** *90*, 62-65

34. Albu, S. P.; Kim, D.; Schmuki, P., Growth of Aligned TiO_2 Bamboo-type Nanotubes and Highly Ordered Nanolace. *Angewandte Chemie International Edition* **2008,** *40* (10), 1916-1919

35. Buckley, T. J.; Payne-Sturges, D.; Kim, S. R.; Weaver, V. *VOC Exposure in an Industry-Impacted Community*; The Johns Hopkins Bloomberg School of Public Health: 2005; p 95

36. Jung, J. H.; Choi, B. W.; Kim, M. H.; Baek, S. O.; Lee, G. W.; Shon, B. H., The Characteristics of The Appearance and Health Risks of Volatile Organic Compounds in Industrial (Pohang, Ulsan) and Non-industrial (Gyeongju) Areas. *Environmental Health and Toxicology* **2012,** *27*, e2012012

37. Montuschi, P.; Corradi, M.; Ciabattoni, G.; Nightingale, J.; Kharitonov, S. A.; Barnes, P. J., Increased 8-isoprostane, A Marker of Oxidative Stress, in Exhaled Condensate of Asthma Patients. *Am J Respir Crit Care Med* **1999,** *160* (1), 216-220

38. Olopade, C. O.; Zakkar, M.; Swedler, W. I.; Rubinstein, I., Exhaled Pentane Levels in Acute Asthma. *Chest* **1997,** *111* (4), 862-865

39. Paredi, P.; Kharitonov, S. A.; Barnes, P. J., Elevation of Exhaled Ethane Concentration in Asthma. *American Journal of Respiratory and Critical Care Medicine* **2000,** *162* (4), 1450-1454

40. Mazzone, P. J., Exhaled Breath Volatile Organic Compound Biomarkers in Lung Cancer. *Journal of Breath Research* **2012,** *6*, 1-8

41. Mazzone, P. J.; Hammel, J.; Dweik, R.; Na, J.; Czich, C.; Laskowski, D.; Mekhail, T., Diagnosis of Lung Cancer by The Analysis of Exhaled Breath with A Colorimetric Sensor Array. *Thorax* **2007,** *62* (7), 565-568

42. Phillips, M.; Gleeson, K.; Hughes, J. M.; Greenberg, J.; Cataneo, R. N.; Baker, L.; McVay, W. P., Volatile Organic Compounds in Breath as Markers of Lung Cancer: A Cross-sectional Study. *Lancet* **1999,** *353* (9168), 1930-1933

43. Westhoff, M.; Litterst, P.; Freitag, L.; Urfer, W.; Bader, S.; Baumbach, J. I., Ion Mobility Spectrometry for The Detection of Volatile Organic Compounds in Exhaled Breath of Patients with Lung Cancer: Results of A Pilot Study. *Thorax* **2009,** *64* (9), 744-748

44. Zilberman, Y.; Tisch, U.; Pisula, W.; Feng, X.; Mullen, K.; Haick, H., Spongelike Structures of Hexa-peri-hexabenzocoronene Derivatives Enhance The Sensitivity of Chemiresistive Carbon Nanotubes to Nonpolar Volatile Organic Compounds of Cancer. *Langmuir: the ACS Journal of Surfaces And Colloids* **2009,** *25* (9), 5411-5416

45. Phillips, M.; Cataneo, R. N.; Ditkoff, B. A.; Fisher, P.; Greenberg, J.; Gunawardena, R.; Kwon, C. S.; Rahbari-Oskoui, F.; Wong, C., Volatile Markers of Breast Cancer in The Breath. *The Breast Journal* **2003,** *9* (3), 184-191

46. Phillips, M.; Cataneo, R. N.; Ditkoff, B. A.; Fisher, P.; Greenberg, J.; Gunawardena, R.; Kwon, C. S.; Tietje, O.; Wong, C., Prediction of Breast Cancer Using Volatile Biomarkers in The Breath. *Breast Cancer Res Treat* **2006,** *99* (1), 19-21

47. Phillips, M.; Cataneo, R. N.; Saunders, C.; Hope, P.; Schmitt, P.; Wai, J., Volatile Biomarkers in The Breath of Women with Breast Cancer. *Journal of Breath Research* **2010,** *4* (2), 1-8

48. Novak, B. J.; Blake, D. R.; Meinardi, S.; Rowland, F. S.; Pontello, A.; Cooper, D. M.; Galassetti, P. R., Exhaled Methyl Nitrate as a Noninvasive Marker of Hyperglycemia in Type 1 Diabetes. *Proceedings of the National Academy of Sciences* **2007,** *104* (40), 15613-15618

49. WHO *Global Tuberculosis Controll 2011*; World Health Organization: Global Tuberculosis Control, Geneva, Switzerland., 2011, 1-258

50. Konstantinos, A., Testing for Tuberculosis. *Australian Prescriber* **2010,** *22* (1), 1-7

51. Phillips, M.; Cataneo, R. N.; Condos, R.; Ring Erickson, G. A.; Greenberg, J.; La Bombardi, V.; Munawar, M. I.; Tietje, O., Volatile Biomarkers of Pulmonary Tuberculosis in The Breath. *Tuberculosis (Edinb)* **2007,** *87* (1), 44-52

52. Phillips, M.; Basa-Dalay, V.; Blais, J.; Bothamley, G.; Chaturvedi, A.; Modi, K. D.; Pandya, M.; Natividad, M. P.; Patel, U.; Ramraje, N. N.; Schmitt, P.; Udwadia, Z. F., Point-of-care Breath Test for Biomarkers of Active Pulmonary Tuberculosis. *Tuberculosis (Edinb)* **2012,** *92* (4), 314-320

53. Syhre, M.; Manning, L.; Phuanukoonnon, S.; Harino, P.; Chambers, S. T., The Scent of *Mycobacterium tuberculosis* - Part II Breath. *Tuberculosis (Edinb)* **2009,** *89* (4), 263-266

54. Syhre, M.; Chambers, S. T., The scent of *Mycobacterium tuberculosis*. *Tuberculosis (Edinburgh, Scotland)* **2008,** *88* (4), 317-323

55. Syhre, M.; Chambers, S. T., The scent of *Mycobacterium Tuberculosis*. *Tuberculosis (Edinb)* **2008,** *88* (4), 317-323

56. Suckling, D. M.; Sagar, R. L., Honeybees *Apis mellifera* can Detect The Scent of *Mycobacterium tuberculosis*. *Tuberculosis (Edinb)* **2011,** *91* (4), 327-328

57. Weetjens, B. J.; Mgode, G. F.; Machang'u, R. S.; Kazwala, R.; Mfinanga, G.; Lwilla, F.; Cox, C.; Jubitana, M.; Kanyagha, H.; Mtandu, R.; Kahwa, A.; Mwessongo, J.; Makingi, G.; Mfaume, S.; Van Steenberge, J.; Beyene, N. W.; Billet, M.; Verhagen, R., African Pouched Rats for The Detection of Pulmonary Tuberculosis in Sputum Samples. *The International Journal of Tuberculosis and Lung Disease: The Official Journal of the International Union Against Tuberculosis and Lung Disease* **2009,** *13* (6), 737-743

58. Camilleri, D., New Screening Solution offers Hope in the Battle Against TB. In *Rapid Biosensor Systems Ltd Babraham Hall, Babraham, Cambridge, CB2 4AT*, Systems, R. B., Ed. 2008; p 4

59. Steingart, K. R.; Henry, M.; Ng, V.; Hopewell, P. C.; Ramsay, A.; Cunningham, J.; Urbanczik, R.; Perkins, M.; Aziz, M. A.; Pai, M., Fluorescence Versus Conventional Sputum Smear Microscopy for Tuberculosis: A Systematic Review. *Lancet Infect Dis* **2006,** *6* (9), 570-581

60. Corbett, E. L.; Watt, C. J.; Walker, N.; Maher, D.; Williams, B. G.; Raviglione, M. C.; Dye, C., The growing Burden of Tuberculosis: Global Trends and Interactions with The HIV Epidemic. *Arch Intern Med* **2003,** *163* (9), 1009-1021

61. Aceti, A. A.; Zanetti, S.; Mura, m. S.; Sechi, L. A.; Turrini, F.; Saba, F.; Babudieri, S.; Mannu, F.; Fadda, G. F., Identification of HIV Patients with Active Pulmonary Tuberculosis Using Urine Based Polymerase Chain Reaction Assay. *Thorax* **1999,** *54*, 145-146

62. Zhou, L.; He, X.; He, D.; Wang, K.; Qin, D., Biosensing Technologies for *Mycobacterium tuberculosis* Detection: Status and New Developments. *Clinical and Developmental Immunology* **2011,** *2011*, 1-8

63. Dorman, S. E., New Diagnostic Tests for Tuberculosis: Bench, Bedside, and Beyond. *Clinical Infectious Diseases* **2010,** *50* (Supplement 3), S173-S177

64. Aschauer, U.; He, Y.; Cheng, H.; Li, S.-C.; Diebold, U.; Selloni, A., Influence of Subsurface Defects on the Surface Reactivity of TiO_2: Water on Anatase (101). *The Journal of Physical Chemistry C* **2009,** *114* (2), 1278-1284

65. Jia, H.-B.; Yu, J.-H.; Xu, J.-Q.; Ye, L.; Ding, H.; Jing, W.-J.; Wang, T.-G.; Xu, J.-N.; Li, Z.-C., Hydrothermal Synthesis and Characterization of A Novel Supramolecular Network Compound of $Co(NIA)_2(H_2O)_4$ with Molecular Ladder Hydrogen Bond Chains (NIA=nicotinate). *Journal of Molecular Structure* **2002,** *641*, 1-5

66. Liu, Y.; Ma, B.; Zhao, X.; Deng, Y.; Zhang, H.; Wang, Z., The Decomposition of $Co(NIA)_2(H_2O)_4$ in Nitrogen Atmosphere. *Thermochimica Acta* **2005,** *433*, 1-3

67. Fenske, J. D.; Paulson, S. E., Human Breath Emissions of VOCs. *Journal of the Air & Waste Management Association* **1999,** *49*, 1-5

68. Phillips, M.; Herrera, J.; Krishnan, S.; Zain, M.; Greenberg, J.; Cataneo, R. N., Variation in Volatile Organic Compounds in The Breath of Normal Humans. *Journal of Chromatography B: Biomedical Sciences and Applications* **1999,** *729* (1–2), 75-88

69. Cheong, C.-G.; Escalante-Semerena, J. C.; Rayment, I., The Three-Dimensional Structures of Nicotinate Mononucleotide:5,6-Dimethylbenzimidazole Phosphoibosylrans-fease (CobT) from Salmonella typhimurium Complexed with 5,6-Dimethybenzimidazole and Its Reaction Products Determined to 1.9 Å Resolution. *Biochemistry* **1999,** *38*, 1-11

70. Finkel, T.; Holbrook, N. J., Oxidants, Oxidative Stress and The Biology of Ageing. *Nature* **2000,** *408* (6809), 239-247

71. Formicka-Kozlowska, G.; Kozlowski, H.; Zezowska-Trzebiatowska, B., Metal-glutathione Interaction in Aqueous Solution: Nickel(II), Cobalt(II) and Copper(II) Complexes with Oxidized Glutathione. *Acta Biochimica Polonica* **1979,** *26* (3), 239-248

72. Cross, C. E.; Halliwell, B.; Borish, E. T. In *Oxygen Radicals and Human Disease*, Ann Intern Med, 1987; pp 526-545

73. Kidd, P. M. L., S.A., The Free Radical Oxidant Toxins of Polluted Air. In *Antioxidant Adaptation and Its Role in Free Radical Pathology*, Biocurrents: San Leandro, CA, 1985; pp 69-103

74. El-Sonbaty, S. M.; El-Hadedy, D. E., Combined Effect of Cadmium, Lead, and UV Rays on *Bacillus cereus* using Comet Assay and Oxidative Stress Parameters. *Environmental Science and Pollution Research International* **2012**

75. Lee, C. W.; Ko, H. H.; Chai, C. Y.; Chen, W. T.; Lin, C. C.; Yen, F. L., Effect of *Artocarpus communis* Extract on UVB Irradiation-Induced Oxidative Stress and Inflammation in Hairless Mice. *International Journal of Molecular Sciences* **2013,** *14* (2), 3860-3873

76. Singh, V. P.; Srivastava, P. K.; Prasad, S. M., Differential Effect of UV-B Radiation on Growth, Oxidative Stress and Ascorbate-glutathione Cycle in Two Cyanobacteria Under Copper Toxicity. *Plant Physiology and Biochemistry: PPB / Societe Francaise de Physiologie Vegetale* **2012,** *61*, 61-70

77. Ko, K.; Yang, H.; Noureddin, M.; Iglesia-Ara, A.; Xia, M.; Wagner, C.; Luka, Z.; Mato, J. M.; Lu, S. C., Changes in S-adenosylmethionine and GSH Homeostasis During Endotoxemia in Mice. *Laboratory Investigation; A Journal of Technical Methods and Pathology* **2008,** *88* (10), 1121-1129

78. Bilgin, R.; Yalcin, M. S.; Yucebilgic, G.; Koltas, I. S.; Yazar, S., Oxidative Stress in *Vivax malaria*. *The Korean Journal of Aarasitology* **2012,** *50* (4), 375-377

79. Grant, S. S.; Hung, D. T., Persistent Bacterial Infections, Antibiotic Tolerance, and The Oxidative Stress Response. *Virulence* **2013,** *4* (4), 273-283

80. Lee, J.; Koh, K.; Kim, Y. E.; Ahn, J. H.; Kim, S., Up-regulation of Nrf_2 Expression by Human Cytomegalovirus Infection Protects Host Cells from Oxidative Stress. *The Journal of General Virology* **2013**, 1-35

81. Chung, B. H.; Lim, S. W.; Doh, K. C.; Piao, S. G.; Heo, S. B.; Yang, C. W., Human Adipose Tissue Derived Mesenchymal Stem Cells Aggravate Chronic Cyclosporin Nephrotoxicity by The Induction of Oxidative Stress. *PLoS One* **2013,** *8* (3), e59693

82. Nassar, M. A.; Eldien, H. M.; Tawab, H. S.; Saleem, T. H.; Omar, H. M.; Nassar, A. Y.; Hussein, M. R., Time-dependent Morphological And Biochemical Changes Following Cutaneous Thermal Burn Injury and Their Modulation by Copper Nicotinate Complex: An Animal Model. *Ultrastructural Pathology* **2012,** *36* (5), 343-355

83. Costa-Matos, L.; Batista, P.; Monteiro, N.; Henriques, P.; Girao, F.; Carvalho, A., Hfe Mutations and Iron Overload in Patients with Alcoholic Liver Disease. *Arquivos de Gastroenterologia* **2013,** *50* (1), 35-41

84. Hakenewerth, A. M.; Millikan, R. C.; Rusyn, I.; Herring, A. H.; Weissler, M. C.; Funkhouser, W. K.; North, K. E.; Barnholtz-Sloan, J. S.; Olshan, A. F., Effects of Polymorphisms in Alcohol Metabolism and Oxidative Stress Genes on Survival from Head and Neck Cancer. *Cancer Epidemiology* **2013,** *37* (4), 479-491

85. Sid, B.; Verrax, J.; Calderon, P. B., Role of AMPK Activation in Oxidative Cell Damage: Implications for Alcohol-induced Liver Disease. *Biochemical Pharmacology* **2013,** *86* (2), 200-209

86. Ji, L. L., Oxidative Stress During Exercise: Implication of Antioxidant Nutrients. *Free Radical biology & Medicine* **1995,** *18* (6), 1079-1086

87. Askew, E. W., Work at High Altitude and Oxidative Stress: Antioxidant Nutrients. *Toxicology* **2002,** *180* (2), 107-119

88. Muller, F., The Nature and Mechanism of Superoxide Production by The Electron Transport Chain: Its Relevance to Aging. *Journal of American Aging Association* **2000,** *23* (4), 227-253

89. Han, D.; Willams, E.; Cadenas, E., Mitochondrial respiratory Chain-dependent Generation of Superoxide Anion and Its Release into The Intermembrane Space. *Biochemistry Journal* **2001,** *15* (353), 411-416

90. Li, X.; Fang, P.; Mai, J.; Choi, E. T.; Wang, H.; Yang, X.-F., Targeting Mitochondrial Reactive Oxygen Species as Novel Therapy for Inflammatory Diseases and Cancers. *Journal of Hematology & Oncology* **2013,** *6* (19), 1-19

91. Bannister, J. V.; Bannister, W. H.; Rotilio, G., Aspects of The Structure, Function, and Applications of Superoxide Dismutas. *Critical Reviews in Biochemistry and Molecular Biology* **1987,** *22* (2), 111-180

92. Hassan, I.; Sajad, P.; Majid, S.; Hassan, T., Serum Antioxidant Status in Patients with Systemic Sclerosis. *Indian journal of Dermatology* **2013,** *58* (3), 239

93. Machado, A. A.; Hoff, M. L.; Klein, R. D.; Cardozo, J. G.; Giacomin, M. M.; Pinho, G. L.; Bianchini, A., Biomarkers of Waterborne Copper Exposure in The Guppy *Poecilia vivipara* Acclimated to Salt Water. *Aquat Toxicol* **2013,** *29*, 60-69

94. Bai, J.; Dong, L.; Song, Z.; Ge, H.; Cai, X.; Wang, G.; Liu, P., The role of Melatonin as an Antioxidant in Human Lens Epithelial Cells. *Free Radical Research* **2013,** *47* (8), 635-642

95. Umosen, A. J.; Ambali, S. F.; Ayo, J. O.; Mohammed, B.; Uchendu, C., Alleviating Effects of Melatonin on Oxidative Changes in The Testes and Pituitary Glands Evoked by Subacute Chlorpyrifos Administration in Wistar rats. *Asian Pacific Journal of Tropical Biomedicine* **2012,** *2* (8), 645-50

96. Lee, K. S.; Yuen, K. H.; Ng, W. K., Deposition of Tocopherol and Tocotrienol in The Tissues of Red Hybrid Tilapia, *Oreochromis sp*., Fed Vitamin E-free Diets Supplemented with Different Plant Oils. *Fish Physiology and Biochemistry* **2013**

97. Lee, S. J.; Kim, S. Y.; Min, H., Effects of Vitamin C and E Supplementation on Oxidative Stress and Liver Toxicity in Rats Fed a Low-fat Ethanol Diet. *Nutrition Research and Practice* **2013,** *7* (2), 109-14

98. Ma, P.; Wu, Y.; Zeng, Q.; Gan, Y.; Chen, J.; Ye, X.; Yang, X., Oxidative Damage Induced by Chlorpyrifos in The Hepatic and Renal Tissue of Kunming Mice and The Antioxidant Role of Vitamin E. *Food Chem Toxicol* **2013,** *26*, 177-183

99. Meister, A., Glutathione-Ascorbic Acid Antioxidant System in Animals. *The Journal of Biological Chemistry* **1994,** *269* (13), 9397-9400

100. Wells, W. W.; Xu, D. P.; Yang, Y.; Rocque, P. A., Mammalian Thioltransferase (glutaredoxin) and Portein Disulfide Isomerase have Dehydroascorbate Reductase Acticity. *Journal of Biological Chemistry* **1990,** *265*, 15361-15364

101. Padayatty, S. J.; Katz, A.; Wang, Y.; Eck, P.; Kown, O.; Lee, J.-H.; Chen, S.; Corpe, C.; Dutta, A.; Dutta, S. K.; Levine, M., Vitamin C as an Antioxidant: Evaluation of Its Role in Disease Prevention. *Journal of American College of Nutrition* **2003,** *22* (1), 18-35

102. Filomeni, G.; Rotilo, G.; Ciriolo, M. R., Disulfide Relays and Phosphorylative Cascades: Partners in Redox-mediated Signaling Pathways. *Cell Death and Differentiation* **2005,** *12*, 1555-1563

103. Heller, J.; Meyer, A. J.; Tudzynski, P., Redox-sensitivie GFP2: Use of The Genetically Encoded Biosensor of The Redox Status in The Filamentous Fungus *Botrytis cinerea*. *Molecular Plant Pathology* **2012,** *13* (8), 935-947

104. Kidd, P. M., Glutathione: Systemic Protectant Against Oxidative and Free Radical Damage. *Alternative Medicine Review* **1997,** *2* (3), 155-176

105. Michelet, F.; Gueguen, R.; Leroy, P.; Wellman, M.; Nicolas, A.; Siest, G., Blood and Plasma Glutathione Measured in Healthy Subjects by HPLC: Relation to Sex, Aging, Biological Variables, and Life Habits. *Clinical Chemistry* **1995,** *41* (10), 1509-1517

106. Hatori, Y.; Clasen, S.; Hasan, N. M.; Barry, A. N.; Lutsenko, S., Functional Partnership of The Copper Export Machinery and Glutathione Balance in Human Cells. *Journal of Biological Chemistry* **2012,** *287* (32), 26678-26687

107. Jouini, M.; Lapluye, G.; Huet, J.; Julien, R.; Ferradini, C., Catalytic Activity of A Copper(II)-oxidized Glutathione Complex on Aqueous Superoxide Ion Dismutation. *Journal of Inorganic Biochemistry* **1986,** *26* (4), 269-280

108. Marzano, C.; Pellei, M.; Tisato, F.; Santini, C., Copper Complexes as Anticancer Agents. *Anti-Cancer Agents in Medicinal Chemistry* **2009,** *9*, 185-211

109. Pederson, J.; Steinhkuhler, C.; Weser, U.; Rotilio, G., Copper-glutathione Complexes Under Physiological Conditions: Structures in Solution Different from The Solid State Coordination. *Biomaterials* **1996,** *9* (1), 3-9

110. Freedman, J. H.; Ciriolo, M. R.; Peisach, J., The Role of Glutathione in Copper Metabolism and Toxicity. *The Journal of Biological Chemistry* **1988,** *264* (10), 5598-5605

111. Kang, E. H.; Park, S. B.; Kim, H. I.; Kwon, Y. H., Corrosion-related Changes on Ti-based Orthodontic Brackets in Acetic NaF Solutions: Surface Morphology, Microhardness, and Element Release. *Dent Mater J* **2008,** *27* (4), 555-560

112. Aslund, F.; Berndt, K. D.; Holmgren, A., Redox Potentials of Glutaredoxins and Other Thiol-Disulfide Oxidoreductases of the Thioredoxin Superfamily Determined by Direct Protein-Protein Redox Equilibria. *The Journal of Biological Chemistry* **1997,** *272* (49), 30780-30786

113. Kirlin, W. G.; Cai, J.; Thompson, S. A.; Diaz, D.; Kavanagh, T. J.; Jones, D. P., Glutathione Redox Potential in Response to Differentiation And Enzyme Inducers. *Free Radical Biology and Medicine* **1999,** *27* (11–12), 1208-1218

114. Millis, K. K.; Weaver, K. H.; Rabenstein, D. L., Oxidation/reduction Potential of Glutathione. *The Journal of Organic Chemistry* **1993,** *58* (15), 4144-4146

115. Rost, J.; Rapoport, S., Reduction-potential of Glutathione. *Nature* **1964,** *201* (4915), 185

116. Yao, J. W.; Xiao, Y.; Lin, F., Effect of Various pH Values, Ionic Strength, and Temperature on Papain Hydrolysis of Salivary Film. *European Journal of Oral Sciences* **2012,** *120* (2), 140-146